



National Library  
of Canada

Bibliothèque nationale  
du Canada

Canadian Theses Service

Service des thèses canadiennes

Ottawa, Canada  
K1A 0N4

## NOTICE

The quality of this microform is heavily dependent upon the quality of the original thesis submitted for microfilming. Every effort has been made to ensure the highest quality of reproduction possible.

If pages are missing, contact the university which granted the degree.

Some pages may have indistinct print especially if the original pages were typed with a poor typewriter ribbon or if the university sent us an inferior photocopy.

Previously copyrighted materials (journal articles, published tests, etc.) are not filmed.

Reproduction in full or in part of this microform is governed by the Canadian Copyright Act, R.S.C. 1970, c. C-30.

## AVIS

La qualité de cette microforme dépend grandement de la qualité de la thèse soumise au microfilmage. Nous avons tout fait pour assurer une qualité supérieure de reproduction.

S'il manque des pages, veuillez communiquer avec l'université qui a conféré le grade.

La qualité d'impression de certaines pages peut laisser à désirer, surtout si les pages originales ont été dactylographiées à l'aide d'un ruban usé ou si l'université nous a fait parvenir une photocopie de qualité inférieure.

Les documents qui font déjà l'objet d'un droit d'auteur (articles de revue, tests publiés, etc.) ne sont pas microfilmés.

La reproduction, même partielle, de cette microforme est soumise à la Loi canadienne sur le droit d'auteur, SRC 1970, c. C-30.

THE UNIVERSITY OF ALBERTA

VIBRATIONAL DYNAMICS OF THE BIFLUORIDE ION

by



VIDANAGAMAGE CHANDANA EPA

A THESIS SUBMITTED

TO THE FACULTY OF GRADUATE STUDIES AND RESEARCH

IN PARTIAL FULFILMENT OF THE REQUIREMENTS

FOR THE DEGREE OF DOCTOR OF PHILOSOPHY

DEPARTMENT OF CHEMISTRY

EDMONTON, ALBERTA

SPRING, 1988

Permission has been granted to the National Library of Canada to microfilm this thesis and to lend or sell copies of the film.

The author (copyright owner) has reserved other publication rights, and neither the thesis nor extensive extracts from it may be printed or otherwise reproduced without his/her written permission.

L'autorisation a été accordée à la Bibliothèque nationale du Canada de microfilmer cette thèse et de prêter ou de vendre des exemplaires du film.

L'auteur (titulaire du droit d'auteur) se réserve les autres droits de publication; ni la thèse ni de longs extraits de celle-ci ne doivent être imprimés ou autrement reproduits sans son autorisation écrite.

THE UNIVERSITY OF ALBERTA

RELEASE FORM

NAME OF AUTHOR Vidanagama Chandana Epa  
TITLE OF THESIS Vibrational Dynamics of the Bifluoride Ion  
DEGREE FOR WHICH THESIS WAS PRESENTED Ph. D.  
YEAR THIS DEGREE GRANTED 1988

Permission is hereby granted to the UNIVERSITY OF ALBERTA LIBRARY to reproduce single copies of this thesis and to lend or sell such copies for private, scholarly or scientific research purposes only.

The author reserves other publication rights, and neither the thesis nor extensive extracts from it may be printed or otherwise reproduced without the author's written permission.

*V. C. Epa*  
.....  
(Signed)

Permanent Address:  
20 B, Templer Road,  
Mount Lavinia  
Sri Lanka

Date *February 1, 1988* .....

Oh, how incomprehensible everything was, and actually sad, although it was also beautiful. One knew nothing. One lived and ran about the earth and rode through forests, and certain things looked so challenging and promising and nostalgic: a star in the evening, a blue harebell, a reed-green pond, the eye of a person or of a cow. And sometimes it seemed that something never seen yet long desired was about to happen, that a veil would drop from it all; but then it passed, nothing happened, the riddle remained unsolved, the secret spell remained unbroken, and in the end one grew old and looked cunning..... or wise....., and still one knew nothing perhaps, was still waiting and listening.


(from *Narcissus and Goldmund* by Hermann Hesse)

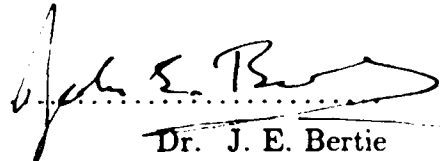
THE UNIVERSITY OF ALBERTA  
FACULTY OF GRADUATE STUDIES AND RESEARCH

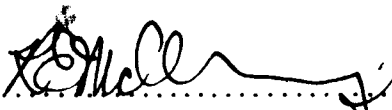
The undersigned certify that they have read, and recommend to the Faculty of Graduate Studies and Research for acceptance, a thesis entitled

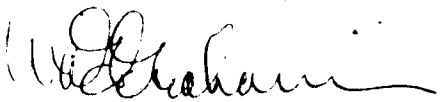
VIBRATIONAL DYNAMICS OF THE BIFLUORIDE ION

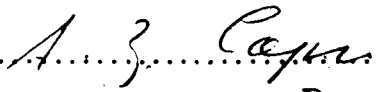
submitted by Vidanagamage Chandana Epa in partial fulfilment of the requirements for the degree of Doctor of Philosophy.

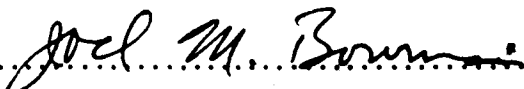
  
.....  
Supervisor Dr. W. R. Thorson

  
.....  
Dr. J. E. Bertie

  
.....  
Dr. R. E. D. McClung

  
.....  
Dr. W. A. G. Graham

  
.....  
Dr. A. Z. Capri

  
.....  
External Examiner Dr. J. M. Bowman

Date..... February 1, 1986.....

*This work is dedicated,*

*· firstly, to my parents, who have encouraged and supported me in all my endeavours,*

*and secondly, to Dr. R. A. Thiraisingham, who introduced me to the wonderful world of theoretical chemistry.*

## ABSTRACT

The initial stages of a quantitative analysis of the vibrational dynamics of the bifluoride ion,  $[\text{FHF}]^-$ , are presented in this thesis. The eventual goal is to understand the richly structured  $\text{KHF}_2(\text{s})$  IR spectrum with an isolated ion model.

710 *ab initio* data points are fitted, with a r.m.s. deviation of  $65.6 \text{ cm}^{-1}$ , to a potential surface model for the  $[\text{FHF}]^-$  ion using the prolate spheroidal coordinates  $(\xi, \eta, \phi)$  and the inter-fluorine distance,  $R$ . The solutions of the vibrational Schrödinger equation are represented in a basis set of adiabatic protonic states. The self-consistent field (SCF) method approximates each protonic state (at fixed  $R$ ) by a product of single-coordinate functions and leads to SCF equations in the  $\xi$ -coordinate (bending motion) and the  $\eta$ -coordinate (protonic stretching motion).

The quantal momentum method is used to solve these two equations numerically. The quantal momentum computed from the application of the 'classical' initial conditions to the integration of the appropriate Riccati equation is smooth and non-oscillatory. Complications posed by the singularity at the origin in the  $\xi$ -equation are overcome with a Langer transformation.

27 protonic SCF states are calculated at  $R = 3.80 - 6.40 \text{ a.u.}$  The resultant SCF energy vs.  $R$  curves give insight into the dynamical behaviour of  $[\text{FHF}]^-$ . Excitation in the anti-symmetric stretching mode ( $\nu_3$ ) should expand  $R$  while excitation of the bending mode ( $\nu_2$ ) should lead to a contraction. IR transition frequencies are estimated, giving for example,  $\nu_3 = 1536 \text{ cm}^{-1}$  and  $\nu_2 = 1341 \text{ cm}^{-1}$ . Isotope effects are computed for the systems  $[\text{FDF}]^-$  and  $[\text{F}\mu\text{F}]^-$ .

The completion of the vibrational analysis is discussed in broad outline form. Limited configuration interaction (CI) calculations are performed for the  $\pi_u$  states. The results seem to validate a 'modal' description for the lower states. The



adiabatic approximation may fail at 'avoided crossings', necessitating solution of dynamically coupled equations for the heavy particle motion. Possible extensions of this method to other problems are also discussed.

## ACKNOWLEDGEMENTS

I would like to thank my supervisor, Professor W. R. Thorson, for introducing me to this exciting research project, and guiding me throughout, especially during the writing of this thesis. It has been a greatly rewarding experience.

My thanks are due to Dr. J. H. Choi for being a source of continual moral support and much valuable advice.

The *ab initio* electronic potential surfaces that are used in this work were calculated by Dr. Mariusz Klobukowski, to whom I am also thankful for many helpful discussions.

Financial Support by the University of Alberta in the form of a Killam Memorial Pre-Doctoral Scholarship for the years 1983-1986 is gratefully acknowledged.

Finally, I would like to thank my friends and colleagues in the theoretical chemistry division, especially Dr. Gunadya Bandarage, Dr. Maria Villa, and Dr. Baltazar Aguda, for making my stay as a graduate student so enjoyable and helping me to keep a proper perspective of my work.

## TABLE OF CONTENTS

Chapter	Page
1. Introduction .....	1
A. Hydrogen-Bonded Systems and Vibrational Dynamics .....	1
B. The Bifluoride Hydrogen-Bond System .....	5
C. Previous Theoretical Work on $[\text{FHF}]^-$ .....	12
D. A Brief Outline of This Thesis .....	18
2. The Potential Energy Surface .....	22
A. Calculation of the 'ab initio' Potential Surface .....	22
B. Properties of the Potential Surface and Prolate Spheroidal Coordinates	27
C. Potential Surface Modelling .....	35
D. Summary .....	45
3. Vibrational SCF Theory .....	46
A. The Vibrational Schrödinger Equation .....	46
B. Adiabatic Description of the Proton Motion .....	47
C. SCF Mode Separation of Proton Dynamics .....	50
D. Self-Consistent Field Equations .....	53
E. Summary .....	58
4. Numerical Solution of the SCF Equations .....	59
A. General Discussion of Milne's (Quantal Momentum) Method .....	59
B. Numerical Solution of the Differential Equation for $\xi$ - Motion .....	66
1. Method of Series Solutions .....	70
2. Langer Transformation Method .....	73
C. Numerical Solution of the Differential Equation for $\eta$ - Motion .....	79
D. Calculation of the Protonic States .....	81

E. Summary .....	87
5. Discussion of the Self-Consistent Field Results .....	88
A. SCF Energy vs. R Curves .....	88
B. Frequencies of the Infra-Red Spectral Transitions .....	106
C. Isotope Effects .....	113
D. Summary .....	119
6. An Outline of Further Work .....	121
A. Configuration Interaction Calculation of Protonic Eigenstates.....	121
1. CI Expansions in SCF Functions as Basis States .....	121
2. Mathematical Formulation of the CI Scheme .....	125
B. Some Results from CI Calculations .....	127
C. Treatment of $\nu_1$ - Dynamics .....	138
1. $\nu_1$ - Dynamics in Adiabatic Approximation .....	138
2. Breakdown of Adiabatic Separation and Coupled $\nu_1$ -Dynamics .....	141
D. Future Work .....	146
1. Frequencies and Relative Intensities of IR Transitions .....	146
2. Other Potential Surfaces and H-bonded Systems .....	148
E. Summary .....	151
Bibliography .....	152
Appendix .....	159

## LIST OF TABLES

Table	Page
2. 1	Coordinate Ranges for the <i>ab initio</i> Calculations ..... 24
2. 2	Fitting $\bar{V}(z, \rho; R = 4.40)$ with a Polynomial in $(z, \rho)$ ..... 30
2. 3	Fitting Coefficients to the Potential Model $VP = CIDR - SK1$ ..... 39
5. 1	Some SCF Energies of Protonic States ..... 91
5. 2	Frequencies of the IR-Allowed Lower Transitions ..... 109
5. 3	Frequencies of the IR-Allowed Higher Transitions ..... 110
5. 4	IR Frequencies for the Isotopic Systems ..... 118
6. 1	SCF Overlap Integrals ..... 129
6. 2	Composition of the First Excited $\pi_u$ CI State ..... 133
6. 3	CI Convergence of the Five Lowest $\pi_u$ States at $R = 4.40$ a.u. .... 135

## LIST OF FIGURES

Figure	Page
1.1 Sub-cell of Crystalline $\text{KHF}_2$ .....	7
1.2 IR Transmission Spectrum of $\text{KHF}_2$ .....	9
1.3 Normal Vibrational Modes of $[\text{FHF}]^-$ .....	10
2.1 Cartesian and Polar Coordinates of the $[\text{FHF}]^-$ ion .....	26
2.2 Contour Diagram of $[\text{FHF}]^-$ <i>ab initio</i> Potential Surface at $R = 4.40$ a.u. 28	28
2.3 Contour Diagram of $[\text{FHF}]^-$ <i>ab initio</i> Potential Surface at $R = 5.80$ a.u. 33	33
2.4 Prolate Spheroidal Coordinates $(\xi, \eta, \phi)$ .....	34
2.5 Reference Energy Levels for the $[\text{FHF}]^-$ system .....	37
2.6 The Morse Potential Function .....	37
2.7 $\text{CIDR}_{\text{fit}}(\xi, \eta; R = 4.20 \text{ a.u.})$ .....	41
2.8 $\text{CIDR}_{\text{fit}}(\xi, \eta; R = 4.40 \text{ a.u.})$ .....	42
2.9 $\text{CIDR}_{\text{fit}}(\xi, \eta; R = 4.80 \text{ a.u.})$ .....	43
2.10 $\text{CIDR}_{\text{fit}}(\xi, \eta; R = 5.80 \text{ a.u.})$ .....	44
4.1 $u(\tilde{z}; R)$ vs. $\tilde{z}$ for $(3, 0, 1)_{R=4.40}$ .....	64
4.2 $q_{Rc}(\tilde{z}; R)$ vs. $\tilde{z}$ for $(3, 0, 1)_{R=4.40}$ .....	64
4.3 $k^2(x; R)$ vs. $x$ for $(0, 0, 2)_{R=4.40}$ .....	68
4.4 $\theta(x; R)$ vs. $x$ for $(0, 0, 2)_{R=4.40}$ .....	68
4.5 $q_{Rc}(x; R)$ vs. $x$ for $(0, 0, 2)_{R=4.40}$ .....	68
4.6 $k^2(x; R)$ vs. $x$ for $(0, 0, 0)_{R=4.40}$ .....	69
4.7 $q_{Rc}(x; R)$ vs. $x$ for $(0, 0, 0)_{R=4.40}$ .....	69
4.8 $k^2(\tilde{z}; R)$ vs. $\tilde{z}$ for $(0, 0, 1)_{R=4.40}$ .....	77
4.9 $q_{Rc}(\tilde{z}; R)$ vs. $\tilde{z}$ for $(0, 0, 1)_{R=4.40}$ .....	77
4.10 $k^2(\eta; R)$ vs. $\eta$ for $(0, 0, 2)_{R=4.40}$ .....	82

4.11	$k^2(\eta; R)$ vs. $\eta$ for $(0, 0, 2)_{R=4.60}$ .....	82
4.12	$q_{Re}(\eta; R)$ vs. $\eta$ for $(0, 0, 2)_{R=4.40}$ .....	83
4.13	$q_{Re}(\eta; R)$ vs. $\eta$ for $(0, 0, 2)_{R=4.60}$ .....	83
4.14	$\theta(\eta; R)$ vs. $\eta$ for $(0, 0, 2)_{R=4.40}$ .....	84
4.15	$\theta(\eta; R)$ vs. $\eta$ for $(0, 0, 2)_{R=4.60}$ .....	84
5.1	Near-degeneracy of SCF Energy Level Pairs .....	90
5.2	SCF Energy vs. $R$ for $\sigma_g$ states .....	94
5.3	SCF Energy vs. $R$ for $\sigma_u$ states .....	95
5.4	SCF Energy vs. $R$ for $\pi_u$ states .....	96
5.5	SCF Energy vs. $R$ for $\pi_g$ states .....	97
5.6	SCF Energy vs. $R$ for $\delta$ states .....	98
5.7	SCF Energy vs. $R$ for $(n', 0)$ states .....	100
5.8	SCF Energy vs. $R$ for $(0, n'')$ states .....	101
5.9	$g(\eta; R)$ in $(0, 2, 0)_R$ .....	103
5.10	$g(\eta; R)$ in $(0, 3, 0)_R$ .....	104
5.11	$f(x; R)$ vs. $x$ for $(0, 0, m)$ at $R = 4.40$ a.u. ....	105
5.12	SCF Energy vs. $R$ for $[FDF]^-$ and $[F\mu F]^-$ .....	114
5.13	$f(x; R)$ vs. $x$ for $(0, 0, 1)$ at $R = 4.40$ a.u. ....	116
5.14	$g(\eta; R)$ vs. $\eta$ for $(0, 0, 1)$ at $R = 4.40$ a.u. ....	117
6.1	Ground $\pi_u$ CI and SCF states .....	130
6.2	Avoided Crossing at $R = 4.46$ a.u. ....	132
6.3	CI Energy vs. $R$ for $\pi_u$ States .....	137
6.4	Total Vibrational States Under the Adiabatic Approximation .....	139
6.5	Avoided Crossing with $\Delta E_{split} \leq \nu_1$ .....	142

## 1. INTRODUCTION

### A. Hydrogen-Bonded Systems and Vibrational Dynamics

Hydrogen (H-) bonds have been of much interest to theoreticians and experimentalists alike for many years, with the first paper on the subject being generally attributed to Latimer and Rodebush [1] in 1920. In a H-bond the proton, normally linked by a covalent bond to one other atom, plays a bridging role linking that atom to a second atom or anion, usually a species more electronegative than H. From the standpoint of chemical theory, H-bonds are significant in several respects:

(1). Hydrogen and its isotopic variants seem to be almost unique in forming such links, possibly due to the lack of an inner shell of electrons.

(2). In contrast to the formation of normal covalent bonds, there appears to be a decrease of electron density around the hydrogen during H-bond formation.

(3). H-bond strengths are intermediate between 'normal' chemical bonds (with binding energies greater than 100 kcal/mole) and the very weak intermolecular attractions such as those produced by Van der Waals forces (with binding energies less than 1-2 kcal/mole).

(4). Effects associated with the light mass of hydrogen (such as zero-point energies) play a large role in the resulting chemistry.

These features are responsible for the characteristic effects commonly interpreted as evidence of *intermolecular* H-bond formation in the behaviour and properties of many systems, i.e. increase in melting points and boiling points, heats of vapourization, viscosities, dielectric constants, etc. The unusual properties of water as a solvent, the key role of the aqueous medium in both chemical and biological processes, and the crucial part played by hydrogen bonds in all living



organisms through H-bond linkages in the macrostructure of proteins and nucleic acids are only some of the more obvious topics to which a deeper understanding of the nature of hydrogen-bonded species is relevant, and even a superficial survey reveals a vast literature bearing on H-bonds and their properties in widely different areas of chemistry, physics, and biology.

Many review volumes and articles focus more specifically on the nature and structure of H-bonds from the perspective of theoretical and experimental physical chemistry, the most notable among them being those by Pimentel [2], Vinogradov and Linnell [3], Joesten and Schaad [4], Schuster, Zundel, and Sandorfy [5], Coulson [6], Emsley [7], Hadzi and Thompson [8], Kollman and Allen [9], and Boschke [10]. Earlier studies on H-bonded systems concentrated mainly on static properties such as crystal structures and bond enthalpies, but later more emphasis has been placed on dynamical behaviour as the key to understanding microscopic molecular properties and the function of H-bonds in kinetics as well as equilibrium states. Changes in spectroscopic and other molecular properties that accompany H-bond formation, as seen in UV/Visible, Infrared, Raman, NMR and Fluorescence spectra, Inelastic Electron Tunnelling Spectroscopy (IETS), and Inelastic Neutron Scattering (INS), give more direct information about the nature of H-bonding. These changes are quite dramatic and in some cases have been summarized phenomenologically in qualitative or semi-quantitative relationships.

This is especially true of infrared (IR) spectra, which have been studied extensively for gaseous as well as condensed phase systems. In essentially all cases formation of a H-bond (A-H...B) between A-H and B is accompanied by a decrease in frequency, exceptional broadening, and increased intensity of the IR spectral band associated with the H-stretching mode  $\nu(\text{A-H})$ . At the same time, the frequencies of the deformation modes of the system A-H...B increase as the

H-bond strength increases (cf. the reviews by Schuster et al. [5], Boschke [10], and Marechal [28]).

The most general of these phenomena are now understood in qualitative terms: the decrease in the A-H stretching frequency is due to weakening and anharmonic deformation of the original A-H covalent bond on H-bond formation [5,10], changes in intensity are due to pronounced changes in the derivatives of the bond dipole moment [5], while the broadening and the structure of the  $\nu(\text{A-H})$  band has as its primary source the anharmonic coupling [28-40] between the A...B stretching mode and A-H stretching and deformation vibrational modes. (Fermi resonances [41-43] as well as electrostatic interactions between adjacent species in a crystal [44] may also contribute in some cases.)

The earlier literature on theoretical analysis of H-bonded systems assumed that the main features of the problem can be understood by one-dimensional models where the A-H stretching motion interacts (at most) weakly with the other degrees of freedom, and the anharmonicity can be introduced as a perturbation to the essentially *harmonic* motion. In weak H-bonds these assumptions may be roughly valid, and since in many cases the spectra for such systems contain (relatively) poorly defined structure with broad bands, the observations to be accounted for usually do not justify a more detailed description. In systems with stronger hydrogen bonding however there is a wealth of spectral information which makes it clear that an one-dimensional description based on a model of the A-H 'effective potential' is not adequate and that in any case the features seen do not fit a harmonic model even in zero-order. Attempts to describe the complex structure seen in crystalline spectra have appealed to a variety of quite different ideas; for example, an important question in some cases is whether the main features of the spectrum arise from local vibrational dynamics or from coupling between neighbouring H-bonds.

Important progress in understanding vibrational spectra in moderate to strong H-bond systems has come from the idea, first proposed by Stepanov [103] in 1945, that major features of these spectra can be understood in terms of an *adiabatic* separation of the proton motions from other degrees of freedom, rather than a harmonic separation. Numerous workers (for example, Marechal, Witkowski, and co-workers [31-35,41-42], Sokolov and Savelyev [40], Coulson and Robertson [38-39], Singh and Wood [96-97], Barton and Thorson [29], Saitoh et al. [92]) subsequently investigated this concept and applied it qualitatively and later more quantitatively in models of vibrational dynamics for specific systems.

From a theoretical standpoint the problem of vibrational dynamics in moderate to strong H-bond systems is interesting because it involves systems with a few degrees of freedom which are fundamentally non-harmonic and are also non-separable to some degree. Nevertheless it may be possible to obtain an essentially quantitative description of the mechanics of such systems, with a systematic interpretation of the resulting vibrational spectra in terms of model potential surfaces. To demonstrate clearly that this is the case in at least one reasonably complex strongly H-bonded system, and to develop techniques and experience relevant to extensions to other problems, is a major overall goal of this work.

For this purpose we have selected the bifluoride ion system,  $[\text{FHF}]^-$ . Starting from an *ab initio* calculation of the electronic potential energy surface of an isolated  $[\text{FHF}]^-$  ion, we carry out the initial stages of a systematic analysis of the vibrational dynamics of the system and the resulting vibrational transitions; work completing the analysis is in progress in this laboratory, and is outlined in this thesis as a plan for further research. Based upon approximate descriptions whose validity we can justify, we can show that the dynamics can in fact be understood within a suitable 'mode description', even though these 'modes' are

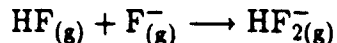
far from *harmonic* and the several degrees of freedom are not exactly separable. Success of the approach for this system offers hope that the methods developed can lead to understanding of systems which are less clearly characterized either experimentally or theoretically, and thus offer a powerful new interpretive tool for discussing H-bonded systems.

We now discuss the bifluoride H-bond system and the reasons for its use as a model problem.

## B. The Bifluoride Hydrogen-Bond System

Most 'ordinary' H-bond energies range from 3 to 8 kcal/mole [2] for water, aliphatic alcohols, carboxylic acid dimers etc. (weak H-bond) to 14 kcal/mole [104] for the bichloride ion (moderately strong H-bond). Examples of very strong H-bonds are the diacetate ion (30 kcal/mole) [106],  $\text{H}_5\text{O}_2^+$  (37 kcal/mole) [105], and the  $[\text{FHF}]^-$  system we consider here. A class of 'H-bonded' systems for which thermochemical measurements cannot give direct estimates of the enthalpy of H-bonding are those in which a proton initially on a cation is partially bonded to an anion; an example is the system triethylammonium chloride where there is no doubt based on the spectral evidence [2] that a very strong disturbance of the H in the triethylammonium cation is present, but the 'H-bond energy' cannot be separated from the dominant lattice energy term in the thermochemical information.

The bifluoride ion has one of the strongest known H-bonds. Experimental estimates of the H-bond energy for  $[\text{FHF}]^-$ , i.e. the absolute enthalpy change for the reaction



range from 37 kcal/mole by Harrell and McDaniel [11] to  $58 \pm 5$  kcal/mole by Waddington [12], and 60 kcal/mole by Dixon et al. [13]. (See also review by Tuck [14].) Heni and Illenberger [15] obtain a lower bound of 34.5 kcal/mole for  $[\text{FHF}]^-$  formed by dissociative attachment of monoenergetic electrons to  $\text{CH}_2\text{F}_2$ .

The *ab initio* electronic structure calculations for  $[\text{FHF}]^-$  which form the basis for the model potential surface used in this work (see Chapter 2) yield a value of 46.5 kcal/mole for the H-bond energy. This agrees with the more recent *ab initio* calculations by Sannigrahi and Peyerimhoff [16] giving  $40 \pm 1$  kcal/mole, and by Frisch et al. [17] giving 46.4 kcal/mole. (See Schuster et al. [5] for a review of earlier electronic structure calculations.)

Numerous X-ray diffraction and neutron diffraction experiments [18-25] on solid salts containing the  $[\text{FHF}]^-$  ion (mostly alkali metal salts  $\text{MHF}_2(\text{s})$ ), starting with Bozorth [26], in 1923 have shown conclusively that the bifluoride ion has a linear, symmetrical equilibrium geometry (point group symmetry  $D_{\infty h}$ ). (The sole exception is the anion in p-toluidinium bifluoride which has an asymmetric configuration due to its crystal environment) [27]. These studies on the bifluoride salts give a value of 2.26 Å for the bond length F...F in  $[\text{FHF}]^-$ , 0.54 Å less than the sum of the Van der Waals radii of the F atoms. This compares with 2.29 Å for the equilibrium F...F distance determined by calculations in this work. (See Chapter 5.) In crystalline  $\text{KHF}_2$ , each cation is surrounded by 8  $[\text{FHF}]^-$  closest neighbour anions, with adjacent  $[\text{FHF}]^-$  ions in a horizontal plane oriented perpendicular to each other. (See Figure 1.1).

Considerable experimental work has been done in the past on the infrared [45-61,142] as well as the Raman [48,50] and the INS [62] spectra of the  $[\text{FHF}]^-$  ion in various environments. More recently Kawaguchi and Hirota [63,141] reported observations of the fundamentals of the free  $[\text{FHF}]^-$  ion in the gas phase.

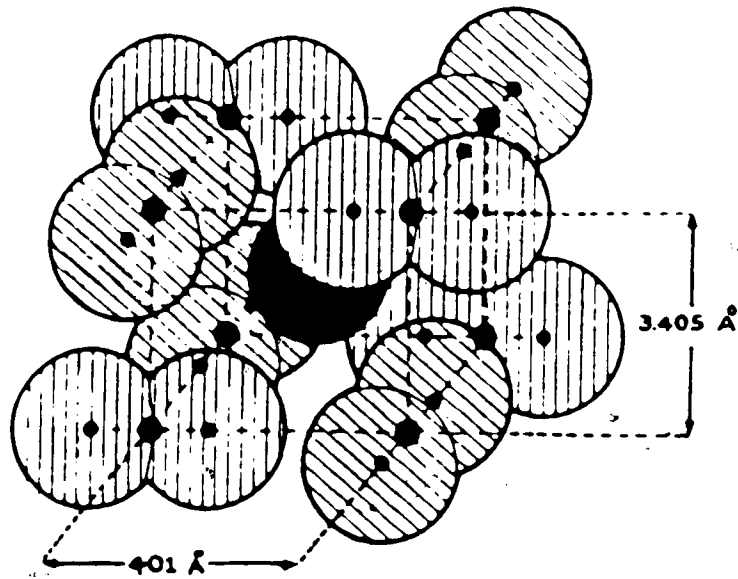


Figure 1.1 Sub-cell of Crystalline  $\text{KHF}_2$ .

(The large black sphere represents the  $\text{K}^+$  ion, while the smaller black spheres denote the positions of the nuclei in each  $[\text{FHF}]^-$  ion).

Figure 1.2 shows the IR transmission spectrum of  $\text{KHF}_2$  at 90 K obtained by Côté and Thompson [64]. This spectrum shows the broadened and complex band structure characteristic of H-bonded systems. The four vibrational degrees of freedom of this linear, symmetric triatomic system correspond essentially to the F...F symmetric stretching motion, the (doubly degenerate) 'protonic' bending motion, and the 'protonic' asymmetric stretching motion [64, 67]. In the usual spectroscopic notation, the corresponding frequencies are denoted by  $\nu_1$ ,  $\nu_2$ , and  $\nu_3$ , respectively. (Under the harmonic approximation these four degrees of freedom correspond to the normal modes shown in Figure 1.3). Côté and Thompson assigned values of 600, 1250, and 1450  $\text{cm}^{-1}$  for these three fundamentals, respectively. They also assigned most of the remaining absorption peaks at higher frequencies (using harmonic zero-order approximation) as combinations and overtones of these frequencies. Many of the assignments they made are not fundamentally in question; the problem to be solved is to account *quantitatively* for the observed frequencies and relative intensities (and perhaps fine structure of bands in some cases) over the whole region from 600 to 6000  $\text{cm}^{-1}$ .

In this research project, the primary goal is to carry out a complete quantitative analysis of the vibrational dynamics of the isolated  $[\text{FHF}]^-$  ion system, based on an *ab initio* electronic potential surface. Progress made towards such an objective is reported in this thesis. A secondary goal would be to improve the quantitative agreement of such a theory with the IR spectrum of crystalline  $\text{KHF}_2$  by minor adjustments of the potential surface parameters. An important long-term motivation of the work is to use for this analysis physical arguments that can be easily generalized so that one can utilize them to understand the non-separable, non-harmonic vibrational dynamics of H-bonded systems of all kinds within a simple, physically transparent conceptual framework. By 'physically transparent'

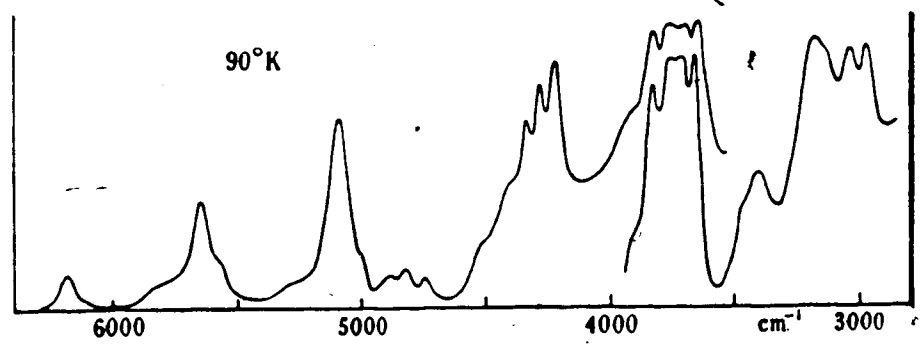
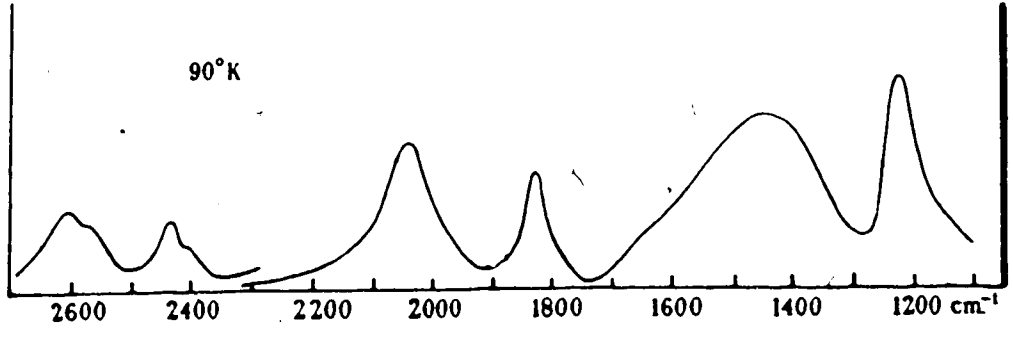


Figure 1.2 IR Transmission Spectrum of  $\text{KHF}_2$ .



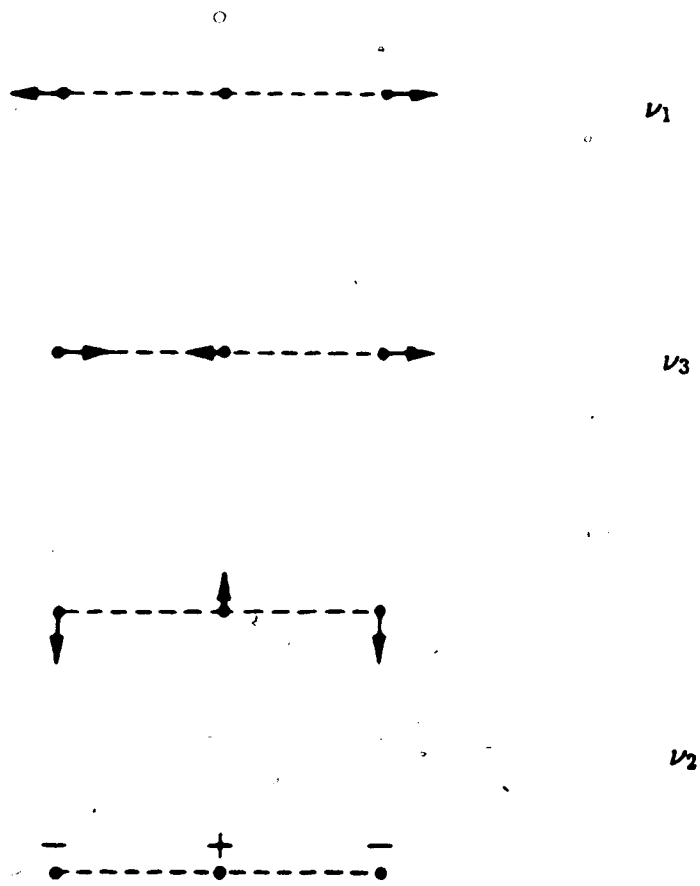


Figure 1.3 Normal Vibrational Modes of  $[\text{FHF}]^-$   
(Displacements are not to scale.)

we mean that we prefer to retain (at least in an approximate sense) a mode-type description of the vibrational motion: that is, although we may have to abandon concepts such as motion in one vibrational mode being totally independent of motion in other modes and results of such concepts such as the overtones being exact integer multiples of the fundamentals, a theory which still enables us to assign at least approximately 'good' quantum numbers to components of the total vibrational motion is by far the most helpful in understanding spectroscopic data.

It is a fundamental assumption of this work that most of the spectral features seen in crystal bifluoride spectra can be attributed to the isolated ion with relatively simple effects from the crystal environment as a 'background' perturbation.

The assumption that the species which produces the IR spectrum of  $\text{KHF}_2(\text{s})$  is  $[\text{FHF}]^-$  in at least some broad, chemical sense is strongly supported by the fact that essentially the same spectrum can be seen in many other environments, such as other crystalline bifluorides and to a lesser extent in matrix isolation spectra. Studies in such environments all lead to the conclusions that the absorbing species has  $D_{\infty h}$  symmetry, and that the fundamentals are  $\nu_2 = 1200 - 1300 \text{ cm}^{-1}$  and  $\nu_3 = 1400 - 1550 \text{ cm}^{-1}$ . Moreover X-ray crystallographic data all show that the variation in the F...F equilibrium spacing is very small and the conclusion that the H occupies the geometric center is nearly always drawn. (The sole exception is p-toluidinium bifluoride.) Also, the fact that the H-bond in this system is so strong means that it is likely that the integrity of the  $[\text{FHF}]^-$  ion is preserved in most environments.

Therefore one may justifiably argue that the IR spectra observed in  $\text{KHF}_2$  are attributable to localized vibrational transitions of a species which consists of  $[\text{FHF}]^-$  in a chemical sense (not however in the sense that it is identical

to the gas phase free ion  $[\text{FHF}]^-$ , and expect that a model based on the isolated ion might offer understanding of the vibrational dynamics of the ion as it is found in various environments. Then it is reasonable to use *ab initio* quantum chemical calculations (without any adjustable parameters) on the free ion in vacuum to generate model potential surfaces which we expect to resemble the true surface in a crystalline environment, at least in their main features.

The abundance of experimental data and the several theoretical works (although none of them analysed the vibrational dynamics in the comprehensive scale we attempt to do in this theoretical work) makes  $[\text{FHF}]^-$  a good choice for our study.

Furthermore, the linear, symmetric geometry of this ion leads to some mathematical and computational simplifications, *without* invalidating the general applicability of the physical arguments.

### C. Previous Theoretical Work on $[\text{FHF}]^-$

The Schrödinger equation describing the total vibrational dynamics in the  $[\text{FHF}]^-$  ion is given by (see Chapter 3),

$$\left[ -\frac{\hbar^2}{2\mu} \frac{\partial^2}{\partial R^2} - \frac{\hbar^2}{2m_r} \Delta_p + V(\vec{r}, R) - E \right] \Psi(\vec{r}, R) = 0 \quad (1.1)$$

where  $R$  is the F...F distance and  $\vec{r}$  is the position vector of the proton (measured from the geometric center of the F...F axis). The  $R$ -motion corresponds qualitatively to the symmetric stretching vibration with frequency  $\nu_1$ , and the 'protonic' motions to the vibrational modes with frequencies  $\nu_2$  and  $\nu_3$ .  $\mu$  and  $m_r$  are the associated reduced masses.  $\Delta_p$  is the Laplacian for  $\vec{r}$  and  $V(\vec{r}, R)$  is the poten-

tial surface for the vibrational motion, which is a non separable function of the vibrational coordinates.

The theoretical studies on  $[\text{FHF}]^-$  endeavour to obtain the solution of equation (1.1) for given  $V$  calculated by *ab initio* or empirical methods. Reduction of equation (1.1) to a 3-dimensional equation is trivial because of the cylindrical symmetry of the system. (See Chapter 3). Previous theoretical treatments summarized here have applied a number of methods to the solution or partial solution of this problem for two or more of these degrees of freedom, using potential surface models of varying complexity and quality. Earlier work mostly employed expansions in suitably chosen basis functions (usually products of harmonic oscillator functions) to solve the eigenvalue problem, while later efforts have directed attention to the use of *adiabatic* approximation or the *self-consistent field* (SCF) approximation to achieve separation of the degrees of freedom (see Chapters 3 and 4 for more detailed discussions of these separation schemes).

The earliest papers on the subject considered only the two stretching motions:  $z$ , the protonic displacement along the  $\text{F}\cdots\text{F}$  axis (corresponding to the asymmetric stretching frequency  $\nu_3$ ), and  $R$ . The emphasis in Ibers' study [98] was to obtain a potential function describing the stretching vibrations of the non-bending  $[\text{FHF}]^-$  ion. The potential constants of his simple 4-term model (containing  $z^2$ ,  $z^4$ ,  $R^2$ , and  $z^2R$ ) were adjusted so that the calculated frequencies would fit the experimental results; the vibrational eigenvalues were determined using expansions in products of harmonic oscillator (HO) functions. His study showed that the two stretching motions are coupled.

Singh and Wood [96-97] used Ibers' potential model to explore the validity of the adiabatic approximation as a scheme for separating the  $\nu_3$  and  $\nu_1$  modes for an  $\text{O-H}\cdots\text{O}$  model system: they compared the adiabatic method with

the method of direct solution by expansion in products of HO functions, and concluded that the two methods give very close agreement, within 1% for the lower eigenvalues. They also determined that in the case of  $[\text{FHF}]^-$ , the adiabatic method gave a reasonably accurate value for the isotopic shift in the equilibrium F...F distance.

Almlöf [94] performed an *ab initio* electronic calculation at the SCF level and the data was fitted with an 9-term polynomial in  $(z, R)$ . The vibrational eigenvalue problem was solved by expansion in a basis set of 160 HO product functions, (both the mixing coefficients and the Hermite exponents of the HO basis functions were variationally optimized) and the transition frequencies  $\nu_3 + n\nu_1$  were computed for  $[\text{FHF}]^-$  and  $[\text{FDF}]^-$ . Values of  $\nu_1 = 660 \text{ cm}^{-1}$  and  $\nu_3 = 1497 \text{ cm}^{-1}$  were obtained for  $[\text{FHF}]^-$ . A major source of the discrepancies between his computed frequencies (especially the upper ones) and the experimental values is the fact that the polynomial model used to fit his *ab initio* surface behaves unphysically when extrapolated to higher coordinate values (i.e. outside the domain of computed points). Also, his SCF level *ab initio* potential surface may not be very accurate at higher energies due to the neglect of electron correlation effects. Almlöf points out that with his method, (i.e. solution of the total Schrödinger equation with a basis set of HO functions) labelling the vibrational levels (in terms of  $\nu_1$  and  $\nu_3$  modes) can be done only for the lowest-lying states, for higher states the mixing between the basis functions being complete. Almlöf also estimated the isotopic shift in the equilibrium F...F distance,  $\Delta R_{eq}$ , to be  $-0.0058 \text{ \AA}$ .

Jiang and Anderson [95] fitted Almlöf's *ab initio* surface (and some empirical data) to a physical model constructed by modifying the Lippincott and Schröder form [100-101]. This model has the correct dissociation characteristics. Jiang and Anderson used the adiabatic approximation to calculate a few low-lying

proton eigenvalue curves for the non-bending  $[\text{FHF}]^-$  ion. The fundamentals  $\nu_3$  and  $\nu_1$  for the  $[\text{FHF}]^-$  and  $[\text{FDF}]^-$  as well as the isotopic shift  $\Delta R_{eq}$  were computed. ( $\nu_3$  was estimated from the vertical transition frequency at equilibrium, and  $\nu_1$  was calculated from the curvature of the protonic ground state curve using the harmonic oscillator approximation). They found values of  $\nu_1 = 694 \text{ cm}^{-1}$  and  $\nu_3 = 1490 \text{ cm}^{-1}$ . They did not examine the validity of the adiabatic separation of R- and z- motions.

Of the studies on  $[\text{FHF}]^-$  using the adiabatic method, that of Barton and Thorson [29] is the most relevant. The major objective of their study is an examination of the validity of the adiabatic approximation for the non-bending  $[\text{FHF}]^-$  ion. In their work, the 2-dimensional *ab initio* potential surface due to Almlöf (mentioned above) is used, and fitted to a globally realistic model potential of a form similar to that of Jiang and Anderson (valid in the H-bond dissociation region). They show that using the 'molecular' coordinate system (z,R), the non-adiabatic coupling matrix elements (i.e. the non-diagonal matrix elements of the operator  $(\partial/\partial R)_z$ ) do not behave physically— i.e. they do not vanish at the dissociation limit. This is overcome by defining a new heavy particle coordinate (by means of a non-linear coordinate transformation due to Thorson and Delos [99] ) which is forced to have (approximately) the correct limiting properties. The protonic eigenvalue equation is solved by numerical integration of the one-dimensional Schrödinger equation for each R. The total wave function is expanded in a basis set of adiabatic protonic states and the resultant set of coupled equations is solved to obtain the exact energies.

Barton and Thorson find that compared with these exact results, the adiabatic approximation gives transition frequencies within 1% and IR relative intensities within 10%, provided that the protonic levels are not degenerate. Frequencies computed for various overtones and combinations of  $\nu_3$  and  $\nu_1$  show

reasonable agreement with experimental results. (They obtain  $\nu_1 = 677 \text{ cm}^{-1}$  and  $\nu_3 = 1520 \text{ cm}^{-1}$ ). The major shortcoming of this work (and indeed of the all the other studies on a non-bending ion) is their assumption of separability of the protonic bending mode. As will be seen in Chapter 2, there is significant anharmonic coupling between the bending and anti-symmetric stretching modes. i.e. contrary to their assumption,  $V(\vec{r}, R) \neq V_z(z, R) + V_{xy}(x, y; R)$ , (where  $x$  and  $y$  are the Cartesian displacements perpendicular to the F...F axis).

The work of Lohr and Sloboda [93] directed attention to the problem of coupling between the protonic stretching motion  $\nu_3$  and the bending motion  $\nu_2$  (corresponding to  $z$  and  $\rho$ , respectively, in cylindrical polar coordinates). They solved the proton dynamics at the fixed value of  $R_{\text{eq}} = 4.3313 \text{ a.u.}$  (the minimum according to their *ab initio* data). The potential surface data calculations were made at the Gaussian 70 SCF 4-31G level, and were fitted to an 8-term polynomial expansion in  $z$  and  $\rho$  (the displacements of the proton along, and perpendicular to, the F...F axis respectively), and the vibrational wave function was expanded in a basis set of binary products of one-dimensional and two-dimensional HO functions. The mixing coefficients were variationally optimized leading to the diagonalization of the Hamiltonian matrix (of order 144 in this case). Associated with these methods of direct solution of the Schrödinger equation are the problems of convergence (necessitating large basis sets), and of physical interpretation of results (because of extensive mixing between basis functions). Lohr and Sloboda did not solve the F...F motion problem. They computed the transition frequencies of  $\nu_2$  and  $\nu_3$  ( $1378$  and  $1669 \text{ cm}^{-1}$ , respectively), their overtones, and combinations between them. Because they used 'vertical' transitions, their results for transitions involving  $\nu_3$  or an overtone of  $\nu_3$  are in considerable error (see Chapter 5). They do demonstrate the significant coupling which exists between anti-symmetric stretching and bending modes.

Apart from the global 3-dimensional surface  $V(\vec{r}, R)$  employed in this work, the only other work on  $[\text{FHF}]^-$  using a 3-dimensional surface is that reported recently by Janssen et al. [71]. However, their aim was not the detailed analysis of the  $[\text{FHF}]^-$  vibrational spectrum, but to demonstrate the sensitivity of the calculated vibrational frequencies to the level of theory in the *ab initio* potential surface calculation. In the vibrational calculations, the total wave function was written as a product of three one-dimensional functions of the normal coordinates of each mode. Each of these 'modal' functions was expanded in a HO function basis set, which linear combination was then variationally optimized. Vibrational modal correlation was taken into account by performing Configuration Interaction (CI) calculations using the SCF states as the basis. (See Chapter 6 for a discussion of the vibrational CI method). These vibrational calculations were done for *ab initio* potential surfaces calculated at different levels of theory (SCF, CISD, CISDT, CIDVD) and with different basis sets (from 'Double Zeta + Polarization' — DZP — to 'Triple Zeta +3 Polarization + Rydberg (or diffuse) + d on H' — TZ3P+R+d ).

Their results show significant variation among the fundamentals calculated with each *ab initio* potential. For example, at DZP-CISD level (this calculation will be denoted by JASB1 in later chapters) ,  $\nu_2 = 1449 \text{ cm}^{-1}$  and  $\nu_3 = 1698 \text{ cm}^{-1}$  while at TZ3P+R+d-CIDVD level (calculation denoted by JASB2) ,  $\nu_2 = 1363 \text{ cm}^{-1}$  and  $\nu_3 = 1427 \text{ cm}^{-1}$ . Their work shows that firstly, the inclusion of electron correlation at double excitation level is crucial for an accurate description of  $[\text{FHF}]^-$  ( while even more exhaustive treatment of electron correlation is *not* necessary ), and secondly, there is a significant dependence of the vibrational frequencies on the size of the basis set used for the electronic calculations. Janssen et al. do not compute the overtones or combination tones (apart from  $\nu_1 + \nu_3$  ). Of



course, the quartic force field with which their potential surface is fitted cannot be extrapolated far and breaks down in the dissociation region. Furthermore, using the SCF approximation to separate the F...F stretching vibration from the protonic vibrations does not explain the Franck-Condon progressions such as  $\nu_3 + n\nu_1$  observed in the spectrum as well as the adiabatic method does.

In the present work we have used a CID level calculation (see Chapter 2) for computing the global electronic surface we take as the basis for our potential  $V(\vec{r}, R)$ . In general the level of sophistication and the size of the basis used are not as complex as some of those considered by Janssen et al. but the domain covered is essentially complete and includes the dissociation region behaviour. While the point made by Janssen et al. that the vibrational frequencies do vary significantly with the level of quantum chemical computation done is an important one, (and the vibrational frequencies computed by Almlöf, Jiang and Anderson, Barton and Thorson, Lohr and Sloboda may all have significant quantitative errors in them because their *ab initio* electronic calculations did not take into account correlation effects), the focus of this work is much more directly on the question whether a reasonable global model surface is able to explain more or less completely the full system of vibrational transitions (overtones, combination tones, etc.) observed in the crystalline bifluoride system.

#### D. A Brief Outline of This Thesis

In Chapter 2, the focus of our attention will be on the *ab initio* potential energy surface of  $[\text{FHF}]^-$  (on which all the nuclear motions occur). The qualitative nature and the resultant physical implications of this (3-dimensional) potential surface will be discussed. It will be shown that the prolate spheroidal

coordinate system,  $(\xi, \eta, \phi)$ , is appropriate to describe the proton vibrational dynamics. These three coordinates along with  $R$ , the  $F\dots F$  distance will comprise the four vibrational degrees of freedom of the linear  $[FHF]^-$  ion. An analytical model for this potential surface will be presented which we claim is both physically reasonable and computationally simple. It is constructed such that the H-bond will dissociate correctly into  $HF + F^-$  fragments. The model is based solely on the *ab initio* data, and has no empirical constants whatsoever.

In Chapter 3, the adiabatic-SCF scheme is applied to the total Schrödinger equation in order to separate the vibrational modes. First, the adiabatic approximation will be used to separate the motion along the  $R$ -coordinate (essentially a  $F$  atom vibration), from the protonic vibrations. This approximation was shown conclusively to be valid for the separation of the proton stretch motion from the  $F\dots F$  motion by Barton and Thorson, so we are justified in using it here, *at least as a zero-order basis* for describing the dynamics. (However, unlike Barton and Thorson, we are now treating the bending as well as the stretching modes, and we shall see in Chapter 6 that there are situations in which this approximation does break down.) The protonic stretching motion (i.e. along the  $\eta$  coordinate) will be separated from the bending motion (along the  $\xi$  coordinate) using the SCF approximation. The underlying physical concepts and the mathematical development of the SCF method will be presented in Chapter 3.

The numerical solution of the resultant one-dimensional differential equations for the  $\xi$ - and  $\eta$ - motions are described in Chapter 4. The usual procedure in most of the previous solutions of the vibrational SCF equations has been to expand the SCF wave function in a basis set of HO functions. Such a procedure is not very efficient computationally. A method first proposed by W.E. Milne [102] will be used to solve the differential equations and determine the SCF energies.

The main advantage of this method is that we will be numerically integrating a function that is (unlike the wave function itself) *non-oscillatory*. Two methods are proposed to overcome the technical problem of the singularity in the 'effective potential' in the  $\xi$ -differential equation. Chapter 4 closes with an account of the iterative solution of the SCF equations. The resulting SCF protonic states provide a zero-order basis for a more accurate solution of the protonic motion problem.

Chapter 5 consists of the presentation and the analysis of the results of the protonic vibrational dynamics (at the SCF level). SCF energy vs. R curves will be presented for 27 different levels labelled with both the nodal quantum numbers  $(n_\xi, n_\eta, m)$  and the 'spectroscopic' quantum numbers  $(n_{\nu_2}, n_{\nu_3})$ . The complexity of these curves leads to much insight into the vibrational motion of the proton. Some of the many crossings among these SCF curves will be removed (i.e. become 'avoided crossings') when modal correlation is included (i.e. when a CI calculation is done). Vibrational frequencies will be estimated for the allowed IR transitions  $a\nu_2 + b\nu_3$  and compared with previous theoretical and experimental data. The reasonably good agreement with previous results show that the adiabatic-SCF framework provides a good description of the coupled vibrational dynamics of our system. As expected, the proton (anti-symmetric) stretching mode is much more anharmonic than the bending mode. Another noteworthy effect is that the excitation of the proton stretch tends to increase the equilibrium F...F separation, while excitation of the bending motion has the opposite effect and is somewhat less pronounced. Comparing with the systems  $[\text{FDF}]^-$  and  $[\text{F}\mu\text{F}]^-$ , several isotope effects will be also computed.

Chapters 2, 3, 4, and 5 constitute the core of this thesis. In contrast to the preceding chapters, Chapter 6 contains only a limited amount of numerical calculations. The major emphasis of this last chapter is on laying out a strategy

for completing the analysis of the total vibrational dynamics of the  $[\text{FHF}]^-$  ion. The first step in this process is obtaining the exact proton eigenvalues, i.e. doing a CI calculation among the SCF states already determined. In this chapter, the concepts behind a CI calculation and the CI technology will be discussed, and the results of limited CI among  $\pi_u$  states will be presented. These results indicate that the adiabatic-SCF separation scheme is a valid procedure for the vibrational analysis of  $[\text{FHF}]^-$ , and that the prolate spheroidal coordinates describe the protonic motion quite well.

The final phase in the vibrational analysis is the solution of the heavy particle dynamics (i.e. that associated with the symmetric stretching motion—fundamental  $\nu_1$ ). This will be discussed for both isolated adiabatic protonic energy level curves as well as for protonic curves with avoided crossings. The situation where the adiabatic approximation breaks down will be examined. Finally, some extensions of this research problem will be considered.

## 2. THE POTENTIAL ENERGY SURFACE

### A. Calculation of the 'ab initio' Potential Surface

Neglecting translational degrees of freedom of the center of mass (for an isolated ion), the Schrödinger equation for the complete [FHF]<sup>-</sup> system is,

$$[\hat{T}^N + \hat{H}^e]\Psi(\bar{r}^e, \bar{r}^N) = E\Psi(\bar{r}^e, \bar{r}^N) \quad , \quad (2.1)$$

where  $\bar{r}^N$  are the nuclear coordinates, and  $\bar{r}^e$  are the electronic coordinates measured from the rotating molecular frame;  $\hat{T}^N$  is a suitably defined kinetic energy operator for the nuclear motion and  $\hat{H}^e$  is the electronic Hamiltonian. For our purposes the 'electronic Hamiltonian' is adequately defined as the sum of electronic kinetic energies and the electrostatic potential energy of the electrons and nuclei (including the inter-nuclear repulsion energy),

$$\hat{H}^e(\bar{r}^e, \bar{r}^N) = \sum_i \frac{-1}{2m_0} \nabla_i^2 + U(\bar{r}^e, \bar{r}^N) \quad , \quad (2.2)$$

where  $m_0$  is the rest mass of the electron. Effects of an electronic reduced mass differing from  $m_0$ , mass polarization effects, and various additional terms appearing in a more rigorous formulation of the complete Hamiltonian are neglected as unimportant for the vibrational dynamics problem we consider here. The 'usual' Born-Oppenheimer approximation [68] assumes that the total wave function  $\Psi(\bar{r}^e, \bar{r}^N)$  has the form

$$\Psi(\bar{r}^e, \bar{r}^N) = \psi^N(\bar{r}^N)\psi^e(\bar{r}^e; \bar{r}^N) \quad , \quad (2.3)$$

where the electronic wave function  $\psi^e(\bar{r}^e; \bar{r}^N)$  is the solution of the electronic eigenvalue problem

$$\hat{H}^e(\bar{r}^e; \bar{r}^N)\psi^e(\bar{r}^e; \bar{r}^N) = E^e(\bar{r}^N)\psi^e(\bar{r}^e; \bar{r}^N) \quad , \quad (2.4)$$

for each nuclear configuration  $\{\bar{r}^N\}$ , and the nuclear motion (including the vibration) wave function  $\psi^N(\bar{r}^N)$  also satisfies a Schrödinger equation

$$[\hat{T}^N + E^e(\bar{r}^N)]\psi^N(\bar{r}^N) = E\psi^N(\bar{r}^N) \quad , \quad (2.5)$$

in which the electronic eigenvalue  $E^e(\bar{r}^N)$  plays the role of a potential energy surface for the nuclear motion. We make this approximation at the outset; there is no reason to believe that the very small errors resulting from this approximate separation of electronic and nuclear motions have any relevance to the vibrational dynamics of H-bonded systems. For clarity we should emphasize now that later discussion of 'the validity of an *adiabatic* separation' is not at all concerned with this approximation, but with a similar approximate separation of the *proton* vibrational motions from motions of the heavier fluorine nuclei.

Thus the first step in an *ab initio* study of vibrational dynamics in [FHF]<sup>-</sup> is calculation of the potential energy surface  $E^e(\bar{r}^N)$  for the ground electronic state. Such a calculation was performed in 1981-82 by Dr. M. Klobukowski, who is associated with Prof. S. Huzinaga's quantum chemistry research group in this Department. The calculations at each configuration  $\bar{r}^N$  were carried out at two main levels:

- (1). SCF (Self-Consistent Field) ,
- (2). SCF-CID (Self-Consistent Field + Configuration Interaction with Double replacement).

The SCF-CID level includes important electron correlation effects. For both levels a Huzinaga-Dunning [140,107] double-zeta basis set which consists of (9s,5p,1d\*/3s,2p,1d\*) basis functions on each F atom and (4s,1p\*/2s,1p\*) basis functions on the H atom were used. The SCF calculations were performed with the GAUSSIAN 80 program. Electron correlation was included by taking into account

Table 2.1

Coordinate Ranges for the *ab initio* Electronic Energy Calculations

$R$ (a.u.)	range in $z$ (a.u.)	range in $\rho$ (a.u.)
3.60	0.0 - 0.4	0.0 - 0.9
3.80	0.0 - 0.6	0.0 - 1.4
4.00	0.0 - 1.0	0.0 - 1.6
4.20	0.0 - 1.1	0.0 - 1.6
4.40	0.0 - 1.2	0.0 - 1.6
4.60	0.0 - 1.4	0.0 - 1.6
4.80	0.0 - 1.4	0.0 - 1.6
5.00	0.1 - 1.5	0.0 - 1.6
5.20	0.0 - 1.6	0.0 - 1.6
5.40	0.0 - 1.7	0.0 - 1.6
5.60	0.4 - 1.8	0.0 - 1.6
5.80	0.7 - 1.9	0.0 - 1.6
6.00	0.8 - 2.0	0.0 - 1.4
6.20	1.1 - 2.2	0.0 - 1.6
6.40	1.1 - 2.1	0.0 - 1.4
6.60	1.3 - 2.2	0.0 - 1.4
6.80	1.2 - 2.3	0.0 - 1.4
7.00	1.5 - 2.4	0.0 - 1.4
7.20	1.6 - 2.4	0.0 - 1.2

all configurations with double replacement in the CI calculation. Computations were done for 710 different nuclear configurations, with F...F separations  $R$  ranging from 3.60 a.u. to 7.20 a.u., and for a variety of proton positions  $(z, \rho)$  (c.f. Figure 2.1) at each  $R$ . Table 2.1 gives at each  $R$  the ranges of  $z$  and  $\rho$  within which (at increments of 0.2 a.u.) *ab initio* potential points were calculated. The points selected were staggered; for example, at  $R=4.40$  a.u., electronic energies were computed at (0.0,0.0), (0.0,0.2), (0.0,0.4), (0.2,0.1), (0.2,0.3), (0.4,0.0), (0.4,0.2), (0.4,0.4), but not at (0.2,0.0) or at (0.4,0.1). In this work we have taken the SCF-CID results as the basis for our model potential surface, although a parallel study for a model surface based on the much easier SCF calculations would be interesting for comparison and will be carried out in further work in this laboratory.

We may denote the resulting ground state potential energy surface by  $V(\bar{r}^N) \equiv E_0^e(\bar{r}^N)$ ; in terms of the cylindrical coordinates  $(z, \rho, R)$  shown in Figure 2.1, the equilibrium configuration of  $[\text{FHF}]^-$  (minimum of the function  $V$ ) occurs at

$$R_{\text{eq}} = 4.290513 \text{ a.u.} = 2.27 \text{ a.u.},$$

$$z_{\text{eq}} = 0.0,$$

$$\rho_{\text{eq}} = 0.0,$$

with a total energy  $E_{\text{eq}}^e = -199.886713 \text{ a.u.}$  (Hartrees).

Thus as expected,  $[\text{FHF}]^-$  has a linear, symmetric geometry at the equilibrium configuration.

*Ab initio* computations at the SCF-CID level with the same basis set were also carried out by Dr. Klobukowski for the separated sub-systems HF and  $\text{F}^-$ , with the results

$$r_{\text{eq}}^{\text{H-F}} = 1.756088 \text{ a.u.} = 0.93 \text{ \AA},$$



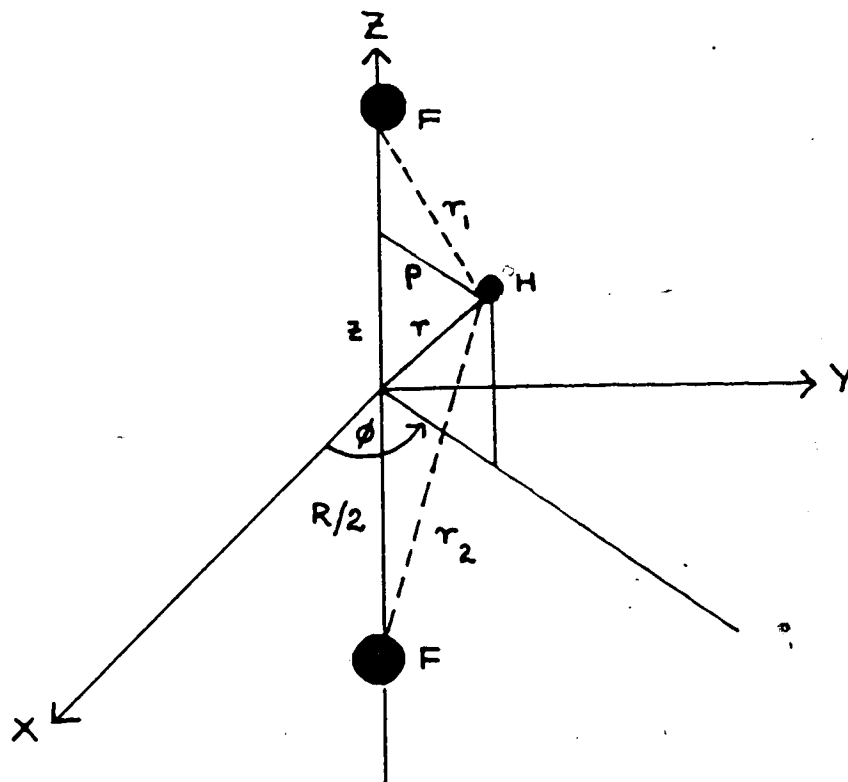
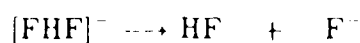


Figure 2.1 Cartesian and Polar Coordinates of the  $[\text{FHF}]^-$  ion.

$$E_{\text{eq}}^{\text{c}}(\text{H} \cdots \text{F}) = -100.223838 \text{ a.u.}, \quad \text{for HF},$$

$$\text{and for } \text{F}^-, \quad E_{\text{eq}}^{\text{c}}(\text{F}^-) = -99.588695 \text{ a.u.}$$

The calculated hydrogen-bond energy for  $[\text{FHF}]^-$ , i.e. the energy required for the process



is therefore  $\Delta E_{\text{hy}} = 0.074180 \text{ a.u.} = 16280 \text{ cm}^{-1} = 46.55 \text{ kcal/mole}$ . The estimated error of this value is  $\pm 5 \text{ kcal/mole}$ . This result agrees well with the recent calculated values of  $\Delta E_{\text{hy}} = 40 \pm 5 \text{ kcal/mole}$  and  $\Delta E_{\text{hy}} = 46.4 \text{ kcal/mole}$  reported by Peyerimhoff [16] and by Frisch et al. [17], respectively. As noted in Chapter 1, experimental estimates of  $\Delta E_{\text{hy}}$  range from 37 to 60 kcal/mole.

## B. Properties of the Potential Surface and Prolate Spheroidal Coordinates

Using the cylindrical coordinates of Figure 2.1, let us now examine sections of the *ab initio* potential surface  $V(z, \rho; R)$  for fixed values of the F...F distance  $R$ . These will provide physical insight into the vibrational dynamics. In particular, the selection of a set of dynamical coordinates adapted to the shape of the potential surface is a crucial step in the solution of the dynamics. As mentioned in Chapter 1, we plan to use the Self-Consistent Field (SCF) approximation as a zero-order separation of the proton 'bend' and 'stretch' modes. The SCF scheme is *exact* if the potential is exactly separable in the coordinates used; by considering the potential surface we may be able to choose coordinates which make the SCF approximation more accurate as a zero-order description.

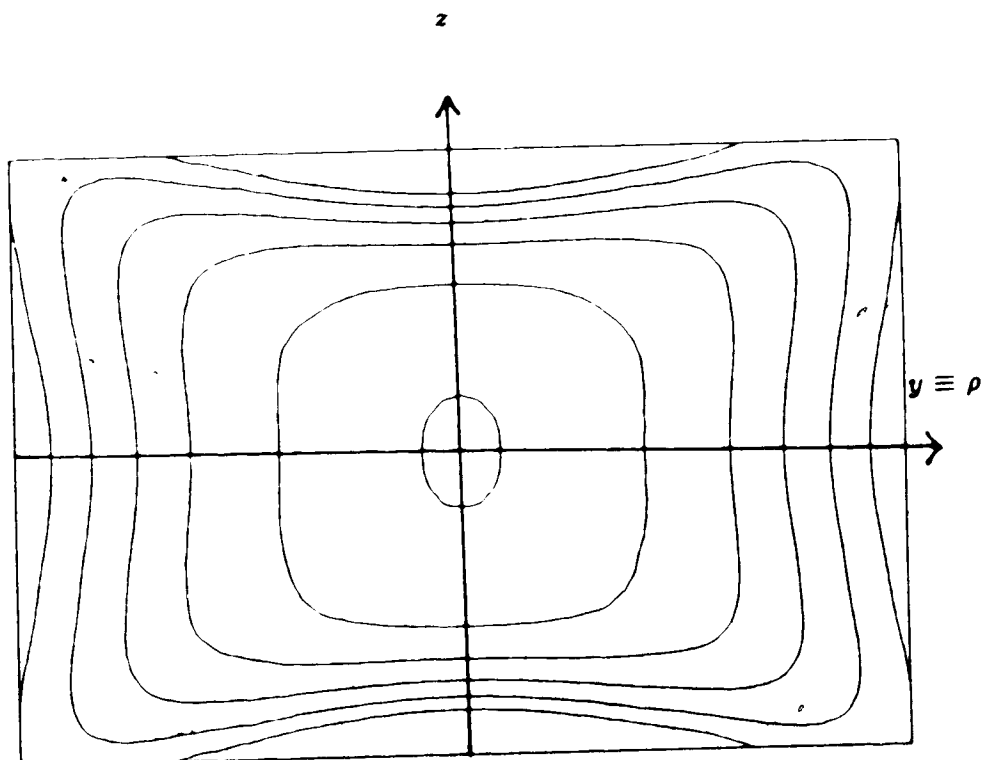


Figure 2.2 Contour diagram of the  $[\text{FHF}]^-$  *ab initio* Potential Energy Surface at  $R = 4.40$  a.u.

Innermost contour: -199.885 a.u.

Interval size: +0.010 a.u.

Figure 2.2 shows a contour diagram of  $V(z, \rho; R)$  for  $R=4.40$  a.u., slightly larger than the equilibrium value 4.29 a.u. The two fluorine nuclei are symmetrically placed at  $z=\pm 2.20$  a.u. (In this figure, maximum  $z$ -displacement is 0.4 a.u. while the maximum  $\rho$ -displacement is 0.6 a.u.) The change in potential (increasing outward) is 0.01 a.u. (Hartrees) for each contour from the minimum at  $(z, \rho)=(0,0)$ . This surface is closely similar to that used by Lohr and Sloboda [93] for their study of the proton motions at the equilibrium F...F distance. The potential is strongly anharmonic in the  $z$ -direction. The potential well is considerably steeper for the  $z$ -motion (fundamental  $\nu_3$ ) than it is for the  $\rho$ -motion (fundamental  $\nu_2$ ); this is to be expected since  $\nu_3$  has a larger magnitude than  $\nu_2$ .

Note also the 'square' contours, which imply a significant interaction of the two displacements; it is easier to bend the proton away from the F...F axis if we simultaneously displace it towards one of the F atoms than it is to move it in purely bending or stretching displacements. These sloping, narrow potential 'valleys' will become more pronounced as  $R$  increases.

We fitted the values of the potential function  $V(z, \rho; R=4.40)$  to a polynomial of the form

$$\bar{V}(z, \rho; R = 4.40) = \sum_{i,j} a_{ij} z^i \rho^j \quad , \quad (2.5)$$

using the same types and number of terms as Lohr and Sloboda did for their surface at  $R=4.3313$  a.u. Thirty *ab initio* data points from the SCF-CID calculation were used to fit the potential in (2.5) relative to the minimum at (0,0) by the least squares method, with a r.m.s. deviation of  $3.71 \times 10^{-4}$  a.u. ( $= 81.4 \text{ cm}^{-1}$ ). Table 2.2 lists these coefficients (TW) and for a rough comparison includes the values used by Lohr and Sloboda (LS) to fit their *ab initio* surface. The negative coupling term  $a_{22}z^2\rho^2$  obviously has a large effect and is mainly responsible for the lowering of the potential curvature in the 'corners' of the surface. The greater

Table 2.2

Fitting  $\bar{V}(z, \rho; R = 4.40)$  with a Polynomial in  $(z, \rho)$ 

i j	$a_{ij}(\text{TW})$	$a_{ij}(\text{LS})$
2 0	0.04413	0.07636
4 0	2.69665	2.86352
0 2	0.14894	0.13913
0 4	0.00031	0.01891
2 2	-1.23100	-1.33371
2 4	2.37450	2.22633
4 2	-10.50960	-10.28476

anharmonicity of the potential for stretching than for bending is also evident. These and other features of this surface are qualitatively like those of Lohr and Sloboda, although their surface is somewhat more anharmonic for  $\rho$  displacements and less anharmonic for  $z$  displacements than ours.

As  $R$  is further increased the potential minimum is further flattened in the  $z$ - direction until, in the range  $R=4.60-4.80$  a.u., two minima symmetrically placed about  $z=0.0$  and a potential maximum at  $z=0.0$  appear. This barrier increases in height as  $R$  increases and the minima move away from the origin, following the F atoms. At the same time the features evident at the 'corners' of the potential surface at  $R=4.40$  a.u. now develop into well-defined curved valleys surrounding each F atom. For example, Figure 2.3 shows the contour map for  $V(z,\rho;R=5.80)$ . The contour spacing and coordinate scale is the same as for Figure 2.2. (Maximum  $z$ - displacement is 0.9 a.u., while the maximum  $\rho$ - displacement is 0.75 a.u.) The proton now spends most of its time near one of the F atoms, and the bending motion is turning into a libration of HF about an equilibrium linear orientation towards  $F^-$ , which will eventually become a hindered rotation.

It follows that the cylindrical coordinates  $(z,\rho,\phi)$ , which might be appropriate to treat the proton dynamics at near-equilibrium values of  $R$  such as 4.40, are *not* suitable for a description at a larger value like 5.80 a.u. Instead we need a curvilinear coordinate system whose parametric lines more nearly follow the actual potential surface contours. Ideally we would like a global choice which can be used at all F...F distances.

For this purpose we have selected the *prolate spheroidal coordinate system*  $(\xi, \eta, \phi)$  (sometimes called the confocal elliptic system). The parametric surfaces of this system are ellipsoids whose foci are at the F atoms (surfaces of constant  $\xi$ ) and hyperboloids of the same foci (surfaces of constant  $\eta$ ). In Figure 2.4 the

grid lines of these curves are shown in a section for a fixed azimuthal angle  $\phi$ . The coordinates  $(\xi, \eta)$  are most conveniently defined in terms of the radii  $r_1$  and  $r_2$  measured from the two foci and the distance  $R$ :

$$\xi = \frac{(r_1 + r_2)}{R}, \quad 1 \leq \xi \leq \infty \quad (2.6a)$$

$$\eta = \frac{(r_1 - r_2)}{R}, \quad -1 \leq \eta \leq +1 \quad (2.6b)$$

The remaining proton coordinate is the (cyclic) azimuthal angle,  $0 \leq \phi \leq 2\pi$ .

Comparison of Figure 2.4 with Figures 2.2 and 2.3 shows that this system of coordinates is reasonably appropriate for both small and large  $F \dots F$  separations  $R$ , since the parametric curves do roughly follow the shape of the potential valleys in both types of situation. For smaller  $R$ , where the potential has a minimum at the origin, the curves of constant  $\xi$  and constant  $\eta$  do not deviate much from lines of constant  $\rho$  and constant  $z$ , respectively, of the cylindrical system. On the other hand, the increased curvature of ellipses and hyperbolas nearer to the foci more closely follows the surface at larger  $R$ -values where the double-minimum potential with valleys curving about the  $F$  atoms develops. An additional advantage of this coordinate system is its preservation of the central symmetry inherent in the problem.

The prolate spheroidal coordinates are probably best known as the system used to separate the equations of motion for the two-center, one-electron Coulomb problem (e.g. by Burrau [108] for  $H_2^+$ ). It may be helpful therefore to point out that while we normally think of the degrees of freedom associated with coordinates  $(\eta, \phi)$  in that problem as 'angular', and that associated with  $\xi$  as 'radial' motions, the physical situation here is somewhat different. The coordinates  $(\xi, \phi)$  are those associated with the two-dimensional 'bending' mode and its associated axial angular momentum, while the coordinate  $\eta$  corresponds to the proton

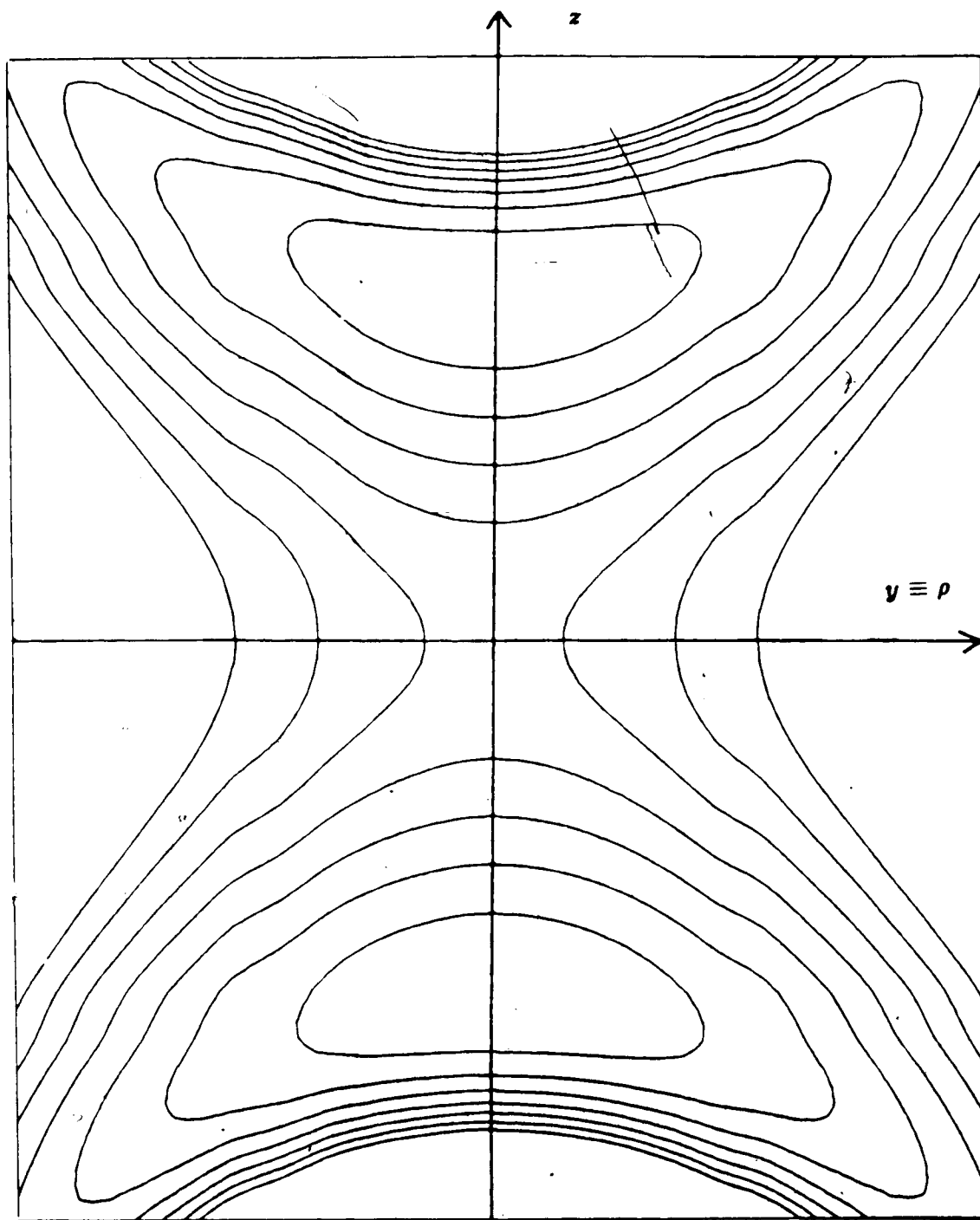


Figure 2.3 Contour diagram of the  $[\text{FHF}]^-$  *ab initio* Potential Energy Surface at  $R = 5.80$  a.u.

Innermost contour: -199.840 a.u.

Interval size: +0.010 a.u.



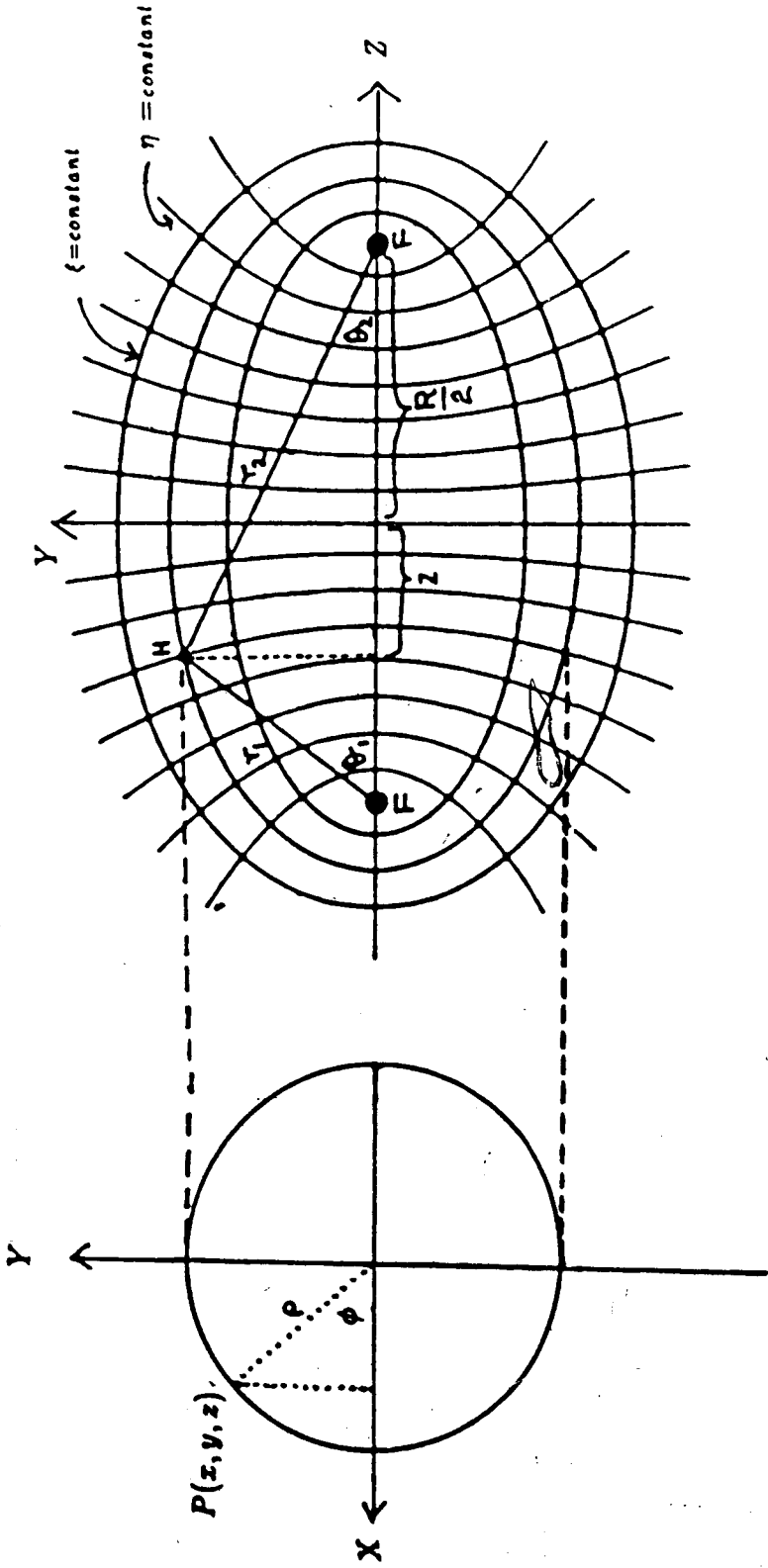


Figure 2.4 Prolate Spheroidal Coordinates ( $\xi, \eta, \phi$ )

$$\xi = \frac{r_2 + r_1}{R} \qquad \eta = \frac{r_2 - r_1}{R}$$



'stretching' mode. We are not aware of any previous instances of these coordinates being used for the vibrational analysis of any system or indeed even for a model representation of an *ab initio* potential function.

Of course the definitive test of the utility of this coordinate system will be the results of the SCF and SCF-CI calculations of proton vibrational energy levels. If a modal description as implied in the SCF separation of the problem proves to be a good approximation to exact behaviour, the choice will be vindicated. We shall see that this is very nearly the case, even though the model potential function we will use is not clearly separable in these coordinates.

A minor drawback of the prolate spheroidal system is the relatively greater complexity of the one-dimensional Schrödinger equations to be solved in these curvilinear coordinates. However, as we show in the chapters following this is not really much of an obstacle.

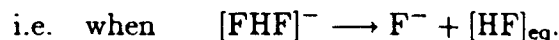
### C. Potential Surface Modelling

We now construct an analytical, global potential surface of the form  $V(\xi, \eta, R)$  for use in the dynamical calculations. This should provide a good fit to the 710 SCF-CID *ab initio* calculated points; in addition, we want this surface to meet the following criteria:

- (1). It should provide a smooth interpolation *between* calculated points.
- (2). It should give a physically realistic extrapolation of the surface beyond the range of the calculated points; this has an important effect on the upper vibrational levels.
- (3). The number of parameters in the fit should be reasonable with respect to the number of data points fitted.

(4). Ideally, the model should be conceptually simple, and offer some understanding of the relation of the H-bond system to its constituent species HF and  $F^-$ .

We will refer the *ab initio* potential values to the dissociation limit ( $HF + F^-$ ) as the zero of energy (see Figure 2.5); that is, if CIDR denote values of the *ab initio* potential, then  $CIDR \rightarrow 0$  when the H-bond is dissociated,



It seems reasonable to represent the main skeleton of our model, denoted by SK1, as the sum of two potential wells for the limiting HF molecules; these are functions respectively of the radii  $r_1$  and  $r_2$  from the F atom to the proton, (see Figure 2.1) and should asymptotically represent the behaviour of isolated HF. To construct these potentials we fitted a Morse potential function to the calculated *ab initio* points for the HF molecule (see Figure 2.6); a least squares fit with r.m.s. deviation of  $5.51 \times 10^{-3}$  a.u. was obtained. Although better fits could have been obtained—especially at H...F distances smaller than the equilibrium distance—by using more complicated forms, we selected the Morse function in the interests of computational simplicity. The forms we introduce can then be written

$$V_{HF1} = D\{1 - \exp[-a(r_1 - r_e)]\}^2, \quad (2.7a)$$

$$V_{HF2} = D\{1 - \exp[-a(r_2 - r_e)]\}^2, \quad (2.7b)$$

$$\text{with } SK1 = V_{HF1} + V_{HF2} - D. \quad (2.8)$$

The parameters appearing in equations (2.7 a,b) are

$$r_e = r_{\text{eq}}(\text{H} - \text{F}) = 1.756088 \text{ a.u.}$$

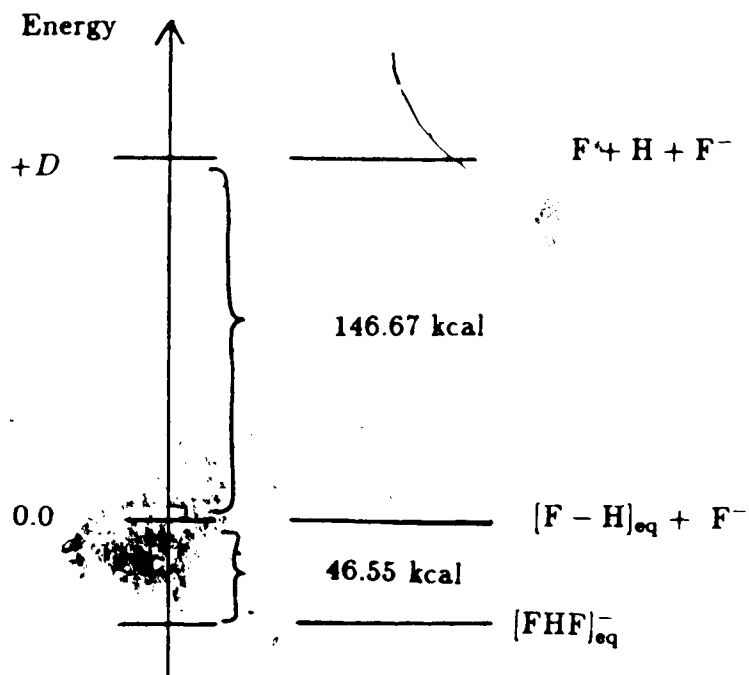


Figure 2.5 Reference Energy Levels for the  $[FHF]^-$  system.

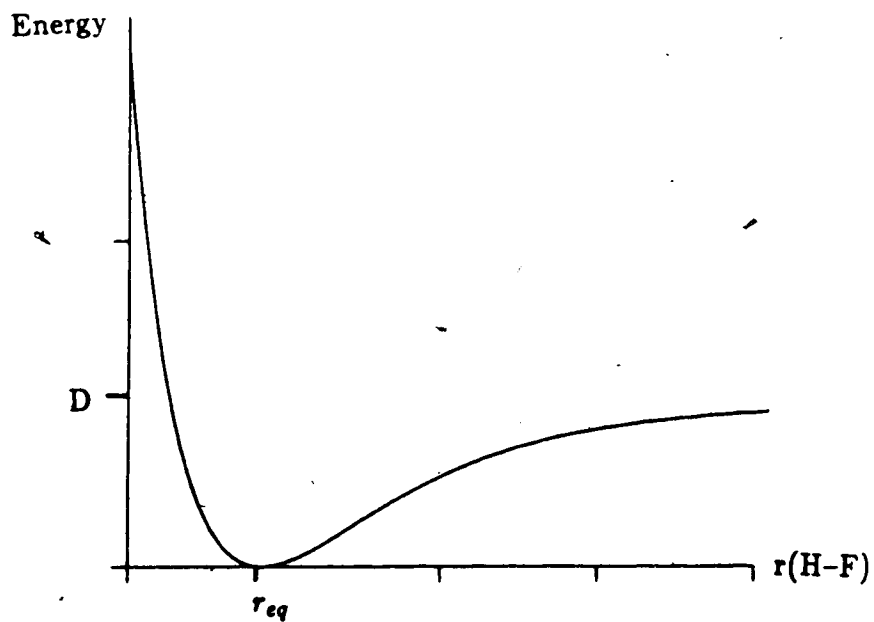


Figure 2.6 The Morse Potential Function

and the least-squares fitting parameters

$$D = 0.246419 \text{ a.u.} = 54083 \text{ cm}^{-1},$$

$$a = 1.197991.$$

In prolate spheroidal coordinates,

$$VHF1(2) = D \left[ 1 - \exp\left\{-a\left[\frac{R}{2}(\xi \pm \eta) - r_e\right]\right\} \right]^2. \quad (2.9)$$

SK1 has the limiting values of zero and  $+D$  in the dissociation limits  $HF_{\text{eq}} + F^-$  and  $F + H + F^-$ , respectively.

We found that the main skeleton function SK1 provides a fairly realistic mimic of the qualitative behaviour observed in CIDR; the difference, given by

$$VP \equiv CIDR - SK1, \quad (2.10)$$

proves to be a fairly slowly-varying function in comparison with either CIDR or SK1. We then used a least-squares procedure to fit all 710 *ab initio* data points for the function VP to the form

$$VP = \exp[-\beta(R - R_{\text{eq}})] \left\{ \sum_{i=0}^2 \sum_{j=0}^2 \sum_{k=0}^3 a_{ijk} (\xi - 1)^i \eta^{2j} (R - R_{\text{eq}})^k \right\}. \quad (2.11)$$

The decaying exponential factor ensures that  $VP \rightarrow 0$  at large  $R$  so that CIDR still tends correctly to zero in the dissociation limit  $[HF]_{\text{eq}} + F^-$  (and tends to  $+D$  in the dissociation limit  $F + H + F^-$ ). For a range of values of  $\beta$ , the 36 coefficients  $\{a_{ijk}\}$  were determined by least squares fitting, and the value  $\beta = 1.10$  was then chosen as optimal on the basis of minimum r.m.s. deviation. Table 2.3 gives the 36 coefficients obtained by this procedure.

Table 2.3

$$VP = \exp[-\beta(R - R_{eq})] \sum_{i=0}^2 \sum_{j=0}^2 \sum_{k=0}^3 a_{ijk} (\xi - 1)^i \eta^{2j} (R - R_{eq})^k$$

i	j	k	$a_{ijk}$	i	j	k	$a_{ijk}$
0	0	0	0.104098E+00	2	0	0	0.254922E+00
0	0	1	-0.230561E-01	2	0	1	0.467485E+00
0	0	2	-0.3999012E-01	2	0	2	0.506124E-01
0	1	0	-0.338661E+00	2	1	0	-0.376342E+01
0	1	1	0.197601E+00	2	1	1	-0.323951E+01
0	1	2	0.331007E+00	2	1	2	0.202667E+01
0	2	0	0.207155E+00	2	2	0	0.970764E+01
0	2	1	-0.118442E+01	2	2	1	-0.949928E+01
0	2	2	-0.448898E+00	2	2	2	-0.388667E+01
1	0	0	-0.257944E+00	0	0	3	-0.198637E-01
1	0	1	-0.205501E+00	0	1	3	0.460766E-01
1	0	2	0.610017E-01	0	2	3	0.140848E-01
1	1	0	0.229919E+01	1	0	3	0.822902E-01
1	1	1	0.102346E+01	1	1	3	-0.184929E-01
1	1	2	-0.130658E+01	1	2	3	-0.580361E-01
1	2	0	-0.387012E+01	2	0	3	-0.139133E+00
1	2	1	0.564683E+01	2	1	3	-0.901666E+00
1	2	2	0.233770E+01	2	2	3	0.161069E+01

The resulting analytical model surface  $V(\xi, \eta, R)$  fits the 710 *ab initio* points from the SCF-CID calculation with a r.m.s. deviation of  $65.6 \text{ cm}^{-1}$ . The fit is actually better than this in the most important regions because the largest deviations occur at points on the CIDR surface which have high potential energies. For the 650 points on the potential energy surface below  $20000 \text{ cm}^{-1}$ , the r.m.s. deviation is  $46.5 \text{ cm}^{-1}$  while for the 484 data points below  $15000 \text{ cm}^{-1}$  it is only  $26.3 \text{ cm}^{-1}$ . We therefore believe that the analytical function we have determined is an accurate representation of the *ab initio* calculated surface; that is, the fundamental uncertainties associated with the relevance or accuracy of the *ab initio* results themselves, and with correction effects not included in the vibrational dynamics, are more important as sources of error in the results than the discrepancies between CIDR and the function  $V(\xi, \eta, R)$  we have constructed to model it.

Figures 2.7-2.10 show perspective topographies using the fitted potential surfaces, denoted by  $\text{CIDR}_{\text{fit}}$  for  $R=4.20, 4.40, 4.80,$  and  $5.80 \text{ a.u.}$  (In Figures 2.7-2.9 the maximum  $z$ - and  $y$ -( $\rho$ -) displacements are  $1.0 \text{ a.u.}$ , while in Figure 2.10 they are  $1.5 \text{ a.u.}$ ). These again display the features described previously in Figures 2.2 and 2.3. Note that in Figure 2.7 ( $R=4.20 \text{ a.u.}$ ) the curvature of the surface for the stretching motion has increased relative to that near  $R_{\text{eq}} = 4.29 \text{ a.u.}$ , while the curvature for the bending motion has decreased. The features which produce the square contours in Figure 2.2 are visible in Figure 2.8 ( $R=4.40 \text{ a.u.}$ ) and their development into potential valleys in the double minimum regime is evident in Figure 2.9 ( $R=4.80 \text{ a.u.}$ ). (Note that the surfaces in Figures 2.9 and 2.10 have been rotated clock-wise by  $60^\circ$  for better viewing.) At  $R=5.80 \text{ a.u.}$  (Figure 2.10) the barrier between the minima is already about  $10000 \text{ cm}^{-1}$ ; at this and larger F...F separations the system is well on the way to dissociation into its constituent fragments.

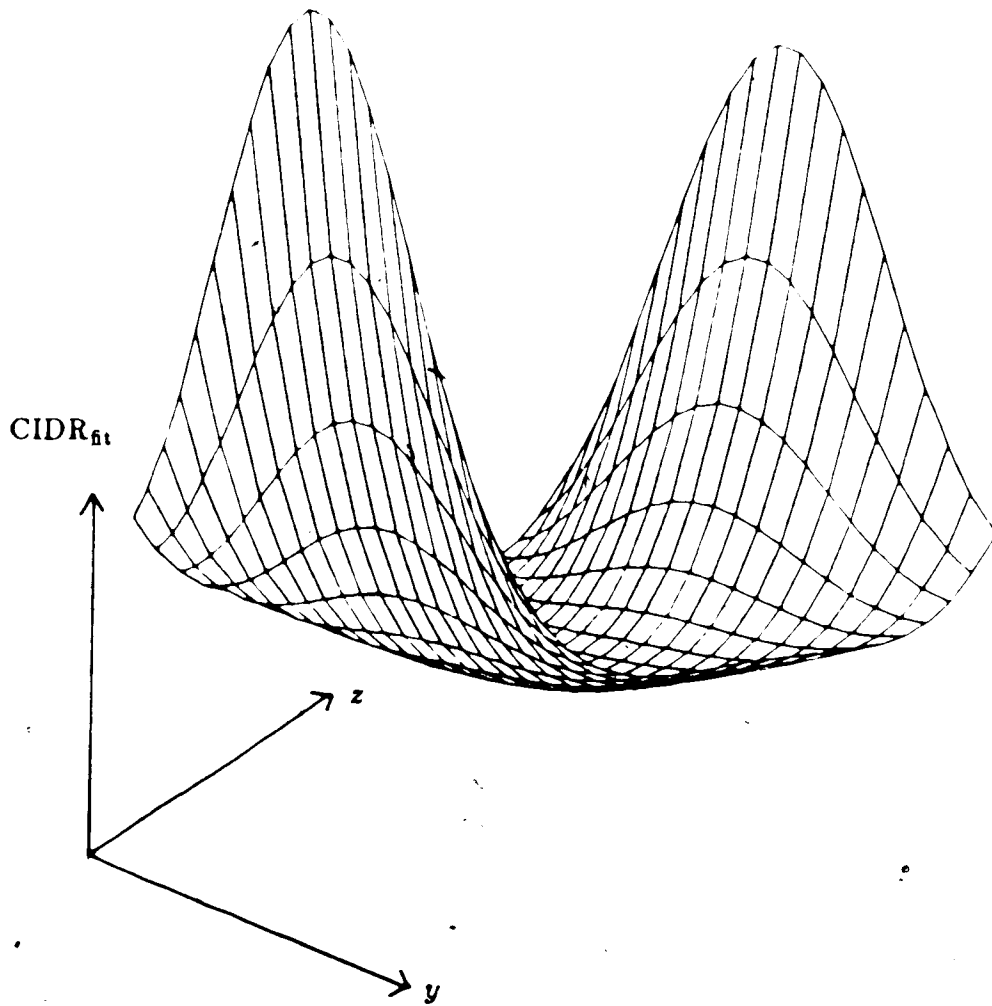


Figure 2.7

$$CIDR_{fit}(\xi, \eta; R = 4.20 \text{ a.u.})$$



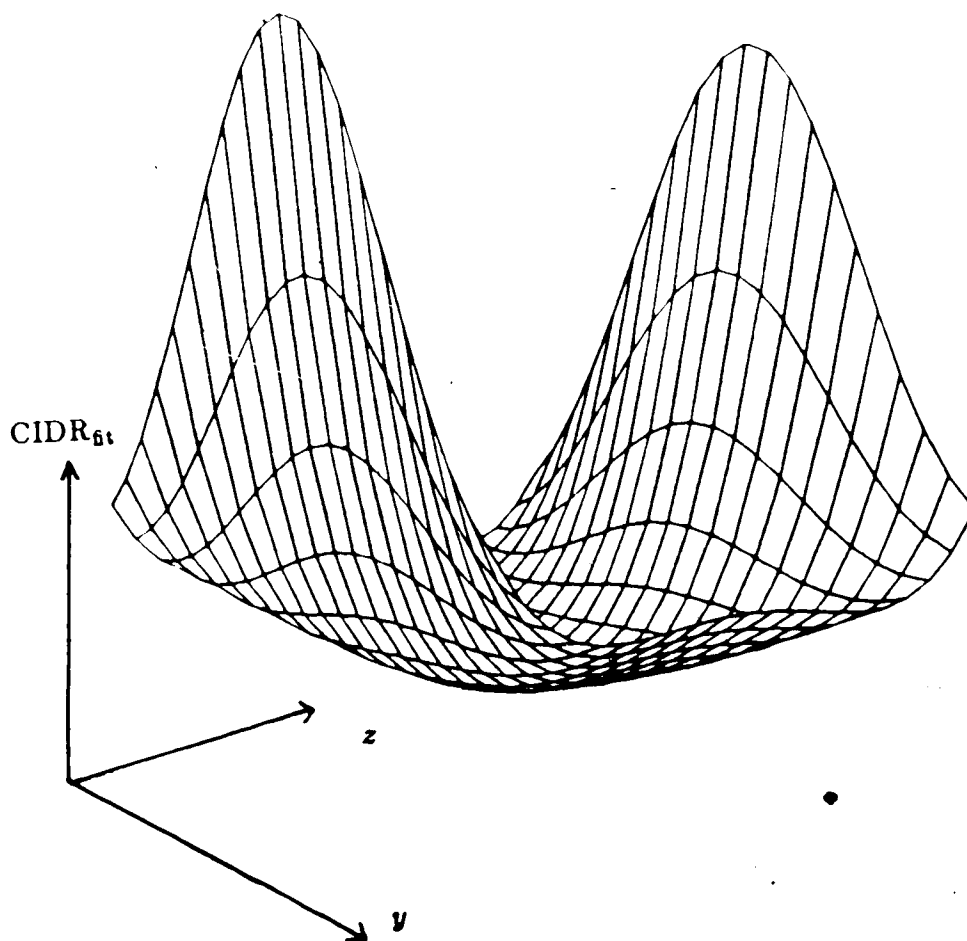


Figure 2.8

 $CIDR_{gt}(\xi, \eta; R = 4.40 \text{ a.u.})$

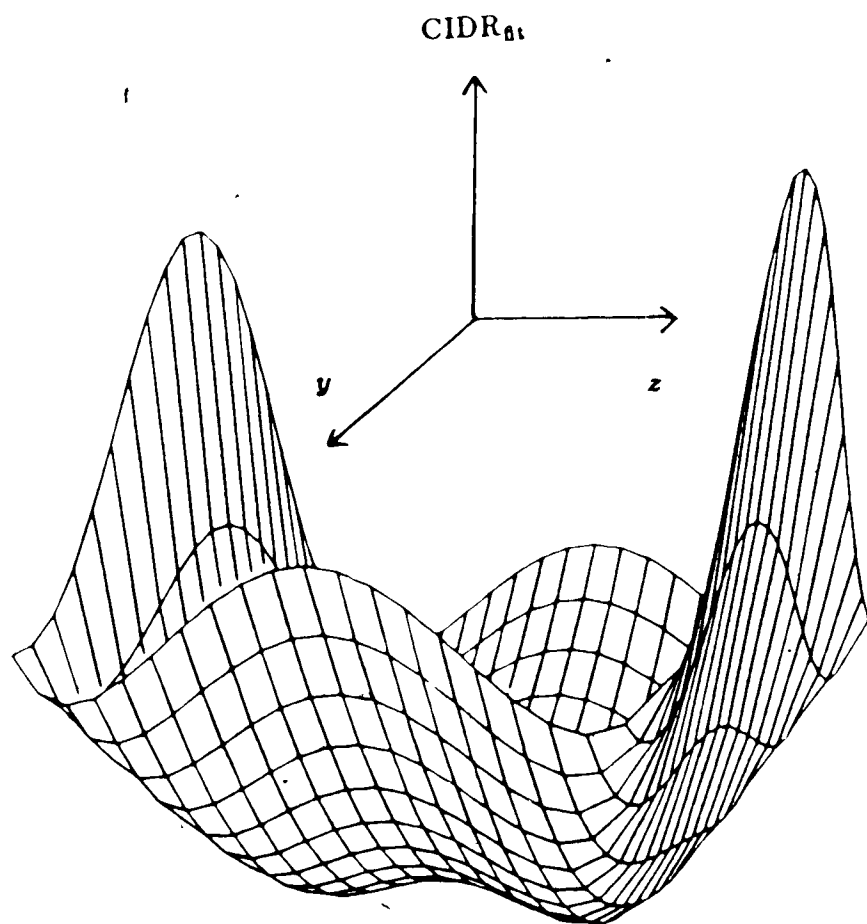


Figure 2.9

 $CIDR_{\eta t}(\xi, \eta; R = 4.80 \text{ a.u.})$

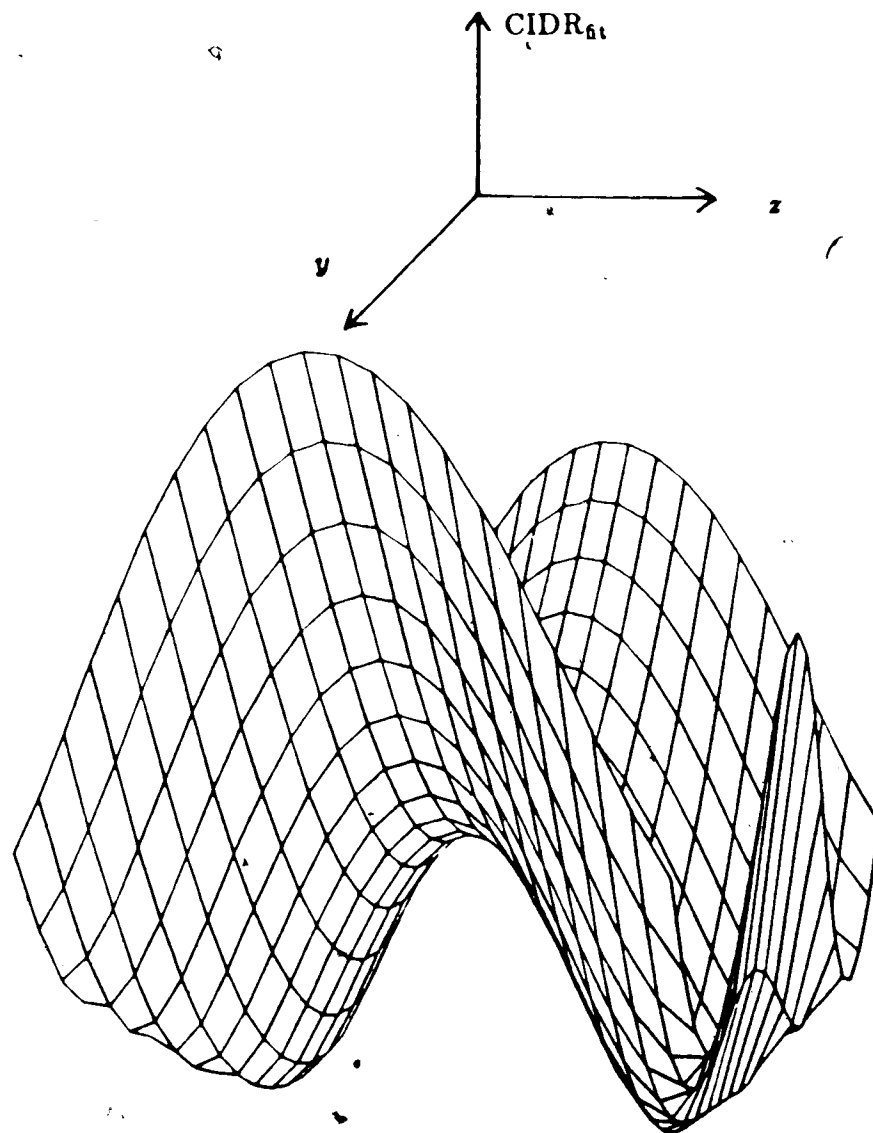


Figure 2.10

 $CIDR_{fit}(\xi, \eta; R = 5.80 \text{ a.u.})$

#### D. Summary

This chapter discussed construction of the model potential surface used for vibrational dynamics calculations. The Born-Oppenheimer separation of electronic and nuclear motions was assumed *a priori*, so that potential energy surface for the vibrational motion is the electronic energy,  $E^e(\vec{r}^N)$ . *Ab initio* calculations of the energy of the electronic ground state were carried out for a large number of points on a 3-dimensional surface (for vibrational coordinates corresponding to proton stretching and bending and F...F stretching motions). The properties of this surface, including behaviour in the dissociation region, suggest that prolate spheroidal coordinates offer an appropriate global choice for describing the vibrational dynamics. The model potential surface that we have constructed has the correct dissociation characteristics, and fits the calculated *ab initio* electronic energies with a r.m.s. deviation of  $65.6 \text{ cm}^{-1}$ .

### 3. VIBRATIONAL SCF THEORY

#### A. The Vibrational Schrödinger Equation

In the preceding chapter we discussed the electronic potential surface and constructed an analytical model to describe it. As vibrational coordinates for the problem, we used the F...F separation  $R$  and the vector coordinate  $\vec{r}$  of the proton, measured from the center of mass of the two F atoms. The explicit form of the potential  $V(\vec{r}, R)$  employs the prolate spheroidal coordinates,  $V=V(\xi, \eta, R)$ . Some further discussion of these vibrational coordinates and the form of the vibrational Hamiltonian seems appropriate.

Six coordinates are required to fix the relative configuration of the three atoms in  $[\text{FHF}]^-$ ; of these, two degrees of freedom describe the orientation of the system in space. Our model of the  $[\text{FHF}]^-$  system assumes that the electronic potential surface does *not* depend on the orientation of the system, but only on the four vibrational coordinates. (In the environment of a crystalline bifluoride, the orientational degrees of freedom correspond to lattice modes, and the assumption that the electronic potential surface does not depend on them really means we assume the vibrational dynamics can be understood with a local model.)

We can describe the  $[\text{FHF}]^-$  system with relative coordinates  $\vec{r}$  and  $\vec{R}$ , where  $\vec{R}$  is the vector from one of the F atoms to the other, and  $\vec{r}$  is the proton coordinate measured from the center of mass of the F atoms. Both coordinates are referred to a space-fixed frame. Then the kinematic Hamiltonian for the relative motion in these six degrees of freedom is rigorously given by

$$T_{rel} = \frac{\vec{p}^2}{2m_r} + \frac{\vec{P}^2}{2\mu} \quad (3.1)$$

where  $\vec{p}$  and  $\vec{P}$  are the momenta conjugate to  $\vec{r}$  and  $\vec{R}$ , respectively, and the reduced masses  $m_r, \mu$  are given in terms of the nuclear masses  $m_F, m_H$  by

$$m_r = \frac{m_H(2m_F)}{(m_H + 2m_F)} \quad \text{and} \quad \mu = \frac{m_F}{2} \quad (3.2)$$

We wish to extract the two rotational degrees of freedom associated with the orientation of the  $\vec{R}$  axis (angles  $\theta_R, \phi_R$ ). After suppressing the rotational motion associated with the coordinates  $\theta_R, \phi_R$  the effective Hamiltonian for the vibrational motion is given approximately by

$$H_{vib} = -\left(\frac{1}{2m_r}\right)\vec{\nabla}_r^2 - \left(\frac{1}{2\mu}\right)\left(\frac{\partial^2}{\partial R^2}\right) + V(\vec{r}, R) \quad (3.3)$$

and we need to solve the Schrödinger equation

$$H_{vib}\Psi_n(\vec{r}, R) = E_n^{total}\Psi_n(\vec{r}, R) \quad (3.4)$$

for the total vibrational eigenvalues  $E_n^{total}$  and eigenfunctions  $\Psi_n(\vec{r}, R)$ .

## B. Adiabatic Description of the Proton Motion

Our analysis of the vibrational dynamics in the  $[\text{FHF}]^-$  ion follows the approach taken by Barton and Thorson [29], who showed in their two-dimensional study that in most cases the proton stretching motion (associated with a reduced mass  $m_r$ ) can be separated very accurately from the F...F motion (associated with a reduced mass  $\mu$ ) by an *adiabatic* approximation. We define adiabatic ‘protonic’ states  $\chi_{n_p}(\xi, \eta, \phi; R)$  as the eigenfunctions of the *protonic Schrödinger equation*

$$\left\{ \frac{-1}{2m_r} \vec{\nabla}_r^2 + V(\xi, \eta; R) \right\} \chi_{n_p}(\xi, \eta, \phi; R) = E_{n_p}(R) \chi_{n_p}(\xi, \eta, \phi; R) \quad (3.5)$$

at each fixed F...F separation  $R$ . The protonic eigenvalues  $E_{n_p}(R)$  and the eigenfunctions  $\chi_{n_p}(\xi, \eta, \phi; R)$  depend parametrically on  $R$ . ( $n_p$  designates the set of quantum numbers specifying a protonic state.) At each  $R$  we may assume that they form a complete orthonormal set of basis states spanning the protonic Hilbert space, and that they can be continued analytically in an unique manner as functions of  $R$ . Hence  $\{\chi_{n_p}(\xi, \eta, \phi; R)\}$  may be used as an expansion basis for solutions to equation (3.4) of the form

$$\Psi_n(\vec{r}, R) = \sum_{n_p} \Phi_{n, n_p}(R) \chi_{n_p}(\xi, \eta, \phi; R) \quad (3.6)$$

Such an expansion is an *adiabatic representation* of the solutions to equation (3.4).

In general, the substitution of (3.6) into the Schrödinger equation (3.4) leads to a system of coupled second-order differential equations for the amplitude coefficient functions  $\{\Phi_{n_p}(R)\}$ . (See for example Chapter 6.) However, Barton and Thorson showed in their study of the two-dimensional problem involving only the stretching modes that in essentially every case solutions to equation (3.4) can be accurately approximated by a single term in the sum, i.e.

$$\Psi_n(\vec{r}, R) \simeq \Psi_{n_{\nu_1}, n_p}^{AD}(\xi, \eta, \phi, R) = \Phi_{n_{\nu_1}, n_p}(R) \chi_{n_p}(\xi, \eta, \phi; R) \quad (3.7)$$

This is called the *adiabatic approximation*. ( $n_{\nu_1}$  denotes the quantum number for motion in the coordinate  $R$ .)

If the adiabatic approximation (3.7) is valid a simple interpretation of the vibrational dynamics follows from it, because to good approximation it may then be shown that the function  $\Phi_{n_{\nu_1}, n_p}(R)$  is simply a solution to the one-dimensional Schrödinger equation

$$\left\{ \frac{-1}{2\mu} \frac{d^2}{dR^2} + E_{n_p}(R) \right\} \Phi_{n_{\nu_1}, n_p}(R) = E_{n_{\nu_1}, n_p}^{total} \Phi_{n_{\nu_1}, n_p}(R) \quad (3.8)$$

That is, the protonic eigenvalue curve  $E_{n_p}(R)$  plays the part of an effective potential function for the F...F vibration, in complete analogy to the role played by the electronic eigenvalue surface as an effective potential for molecular vibrations (section A of Chapter 2). (Thus the F...F stretching mode frequency depends on the protonic eigenstate, and this mode is described by the function  $\Phi_{n\nu_1, n_p}(R)$ .) It follows that the frequencies and intensities of combination bands of the type  $\nu_3 + n\nu_1$  or  $\nu_2 + n\nu_1$ ;  $n = 0, 1, 2, \dots$  etc. which appear strongly in many H-bond IR spectra can be understood very simply by analogy with the Franck-Condon interpretation of progressions of vibrational bands in the electronic spectra of a diatomic molecule, as was noted by Sheppard [8] for H-bonds in general.

The rationalization usually offered for an adiabatic separation of protonic motion in these systems is the significant disparity in the 'proton' and 'heavy particle' masses  $m_r, \mu$ ; in the case of  $[\text{FHF}]^-$  the ratio  $(m_r/\mu) = 0.1033$ . That is, because of this difference in masses, the proton goes through many cycles of motion during the time in which the heavy particle configuration changes appreciably. In other words, the proton eigenfunction adjusts itself instantaneously to any change in the heavy mass configuration. Therefore it should be valid to quantize the proton dynamics for a fixed heavy particle geometry (i.e. a fixed value of  $R$ ). However, there may be criteria other than the mass in determining the success of the adiabatic approximation. It is noteworthy that studies by Ezra [110] and by Caswell and Danos [111] showed that for model coupled oscillator systems the adiabatic approximation is able to give accurate eigenvalues for a very wide range of characteristic frequency ratios of the coupled modes.

It is evident that the protonic eigenvalue curves  $E_{n_p}(R)$  have physical significance and offer fundamental insight into the vibrational dynamics of  $[\text{FHF}]^-$ . In the rest of this Chapter, as well as in the further discussion of Chapter 4, we



restrict our attention entirely to the solution of the protonic Schrödinger equation (3.5).

### C. SCF Mode Separation of Proton Dynamics

Since the azimuthal angle  $\phi$  is a cyclic coordinate, the corresponding angular momentum (associated with the bending mode) is a constant of the motion with values  $m=0, \pm 1, \pm 2, \dots$ ; the solutions  $\chi_{n_p}(\xi, \eta, \phi; R)$  have the form

$$\chi_{n_p}(\xi, \eta, \phi; R) = \bar{\chi}_{n_p}(\xi, \eta; R)[(2\pi)^{-1/2} \exp(im\phi)] \quad (3.9)$$

Substituting (3.9) in equation (3.5) we have, since

$$\bar{\nabla}_r^2 = \frac{4}{R^2(\xi^2 - \eta^2)} \left\{ \frac{\partial}{\partial \xi} \left[ (\xi^2 - 1) \frac{\partial}{\partial \xi} \right] + \frac{\partial}{\partial \eta} \left[ (1 - \eta^2) \frac{\partial}{\partial \eta} \right] + \frac{\xi^2 - \eta^2}{(\xi^2 - 1)(1 - \eta^2)} \frac{\partial^2}{\partial \phi^2} \right\} \quad (3.10)$$

$$\left\{ \frac{a}{(\xi^2 - \eta^2)} \left[ \frac{\partial}{\partial \xi} \left[ (\xi^2 - 1) \frac{\partial}{\partial \xi} \right] + \frac{\partial}{\partial \eta} \left[ (1 - \eta^2) \frac{\partial}{\partial \eta} \right] - \frac{m^2}{(\xi^2 - 1)} - \frac{m^2}{(1 - \eta^2)} \right] + V(\xi, \eta; R) \right\} \bar{\chi}_{n_p} = E_{n_p}(R) \bar{\chi}_{n_p} \quad (3.11)$$

where  $a = \frac{-2}{R^2 m_r}$

Then, we have to solve equation (3.11) for  $E_{n_p}(R)$  and  $\bar{\chi}_{n_p}(\xi, \eta; R)$ . To solve equation (3.11) we again seek methods which offer conceptual understanding and simple physical interpretation of the dynamics. In principle, an expansion in any complete basis (e.g. products of harmonic oscillator functions) would provide a solution; however, such methods offer little insight and in addition may converge on the correct solution only slowly unless the basis is selected in a way reflecting the physical solution.

As a basis for solving the proton dynamics we have selected the Self-Consistent Field (SCF) method, which again permits a mode separation of the bending (along the  $\xi$ - coordinate) and stretching (along the  $\eta$ - coordinate) motions. In the SCF method the eigenfunctions of (3.11) are approximated by a simple product of two single-coordinate functions,  $\alpha_{n_\xi, m}(\xi; R)$  and  $\beta_{n_\eta, m}(\eta; R)$ :

$$\text{i.e. } \chi_{n_p}(\xi, \eta, \phi; R) \simeq \chi_{n_\xi, n_\eta, m}^{(SCF)}(\xi, \eta, \phi; R) = \alpha_{n_\xi, m}(\xi; R)\beta_{n_\eta, m}(\eta; R)[(2\pi)^{-1/2}e^{im\phi}] \quad (3.12)$$

and the equations for the two 'modal' wave functions  $\alpha$  and  $\beta$  are determined by the requirement that the expectation value of the protonic Hamiltonian is stationary with respect to variations in  $\alpha$  and  $\beta$ . This leads to one-dimensional Schrödinger equations for the modal wave functions in (3.12) which are coupled, in that the effective potential determining one modal function is an average of the potential over a distribution determined by the other and the two equations are solved self-consistently. Explicit derivation of the SCF equations for this case is given below.

The SCF approximate solutions given by equation (3.12) are characterized by three quantum numbers  $(n_\xi, n_\eta, m)$ ; for given  $m$ ,  $n_\xi$  and  $n_\eta$  specify the number of nodes in the functions  $\alpha$  and  $\beta$ , and may be directly related to assignments of excitation levels for the  $\nu_2$  and  $\nu_3$  vibrational modes, respectively (see Chapter 5). If the SCF approximation were *exact*, it would then be possible to identify each protonic level uniquely in terms of the corresponding mode excitation quantum numbers  $n_{\nu_2}, n_{\nu_3}, (m)$ , and, even though the system is far from harmonic and the quantitative level spacings predicted by harmonic models would not occur, such an approach would obviously offer the best conceptual grasp of the problem.

Although we have chosen the prolate spheroidal coordinate system because it is more nearly able to provide such a quantitative mode separation, the

potential  $V(\xi, \eta; R)$  is not in fact exactly separable in these coordinates and the SCF wave functions given by (3.12) are only approximate solutions to equation (3.11). However, it is reasonable to assume they can still provide a useful and computationally efficient representation as an expansion basis for the correct solutions (see Chapter 6).

Although the SCF method in vibrational dynamics is a fairly recent development, considerable attention has been given to it [71-92] since the first formulations by Carney et al. [69] and Bowman [70]. Some studies considered abstract model systems of coupled oscillators [74,75,79,82] while other work has been concerned with applications to specific molecular systems such as  $H_2O$  [73, 77],  $SO_2$ , HCN [91], HCHO [73,78], HNO, HOF, HOCl [90], and  $[FHF]^-$  [71]. Work by Ratner et al. and Farrelly et al. [83-87] has focused on semi-classical formulations of the SCF method. In vibrational problems the SCF method is simpler than it is for a many-electron system because the permutation symmetry requirements of Hartree-Fock theory are not present [73].

The general experience resulting from these studies has been that the SCF method usually gives rather good results, especially for levels which are low-lying and non-degenerate. For example in  $H_2O$ , Bowman et al. showed that the average error of the SCF energy for levels up to  $13000\text{ cm}^{-1}$  above the ground state was  $117\text{ cm}^{-1}$ ; in the six-mode system HCHO, Bowman [73] found an average error as low as  $33\text{ cm}^{-1}$ . As a rule, errors in the SCF energies increase as vibrational energies and amplitudes of motion increase, but serious failures of the SCF approximation occur only in cases of Fermi resonance (degeneracies or near-degeneracies of SCF levels of the same symmetry). Even in such cases, Thompson and Truhlar [82] showed that by mixing in just the degenerate SCF states they could recover 99% of the exact result. Thompson and Choi [139] reached similar con-

clusions in their application of the SCF approximation in *Cartesian* coordinates to the two-dimensional quartic oscillator, i.e. the potential  $V = ar^4$ .

#### D. Self-Consistent Field Equations

In order to find the best functions  $\alpha$  and  $\beta$  satisfying the form (3.12) we apply the variation principle. i.e. we require that the energy  $E$  be stationary w.r.t. a small variation in the wave function,  $\delta\chi$ , (with  $\chi$  expressed as a product of the two modal functions as in (3.12)) leading to the condition

$$\langle \delta\chi | \hat{H} - E | \chi \rangle = 0 \quad (3.13)$$

where the usual Dirac bra-ket notation has been adopted and the integration is over the coordinates  $\xi, \eta, \phi$ ; the volume element is

$$d\tau = \left(\frac{R}{2}\right)^3 (\xi^2 - \eta^2) d\xi d\eta d\phi. \quad (3.14)$$

We normalize the individual modal wave functions,

$$\int_{+1}^{+\infty} d\xi [\alpha_{n\xi, m}(\xi; R)]^2 = 1, \quad (3.15a)$$

$$\int_{-1}^{+1} d\eta [\beta_{n\eta, m}(\eta; R)]^2 = 1. \quad (3.15b)$$

Consider a small arbitrary variation  $\delta\alpha$  of the function  $\alpha$ ; the corresponding variation in  $\chi$  is:

$$\delta\chi = (\delta\alpha)\beta$$

Then from equation (3.13) we obtain (assuming  $\alpha, \beta$  to be real),

$$\int_{+1}^{+\infty} d\xi \delta\alpha \left\{ \int_{-1}^{+1} d\eta (\xi^2 - \eta^2) \beta [\hat{H} - E] \alpha \beta \right\} = 0, \quad (3.16)$$

(dropping the labels for the purpose of this derivation).

$$\text{Now, from (3.12),} \quad (\xi^2 - \eta^2)\hat{H} = \hat{h}_\xi + \hat{h}_\eta + U(\xi, \eta, R) \quad (3.17a)$$

$$\text{where} \quad \hat{h}_\xi = a \frac{\partial}{\partial \xi} (\xi^2 - 1) \frac{\partial}{\partial \xi} \quad (3.17b)$$

$$\hat{h}_\eta = a \frac{\partial}{\partial \eta} (1 - \eta^2) \frac{\partial}{\partial \eta} \quad (3.17c)$$

$$\text{and} \quad U(\xi, \eta, R) = (\xi^2 - \eta^2)V \quad (3.17d)$$

For relationship (3.16) to be true for arbitrary  $\delta\alpha$ ,

$$\int_{-1}^{+1} d\eta (\xi^2 - \eta^2) \beta [\hat{H} - E] \alpha \beta = 0$$

Thus equation (3.16) reads

$$\left[ \hat{h}_\xi + \int_{-1}^{+1} d\eta U \beta^2 \right] \alpha = \left[ \xi^2 E - E \int_{-1}^{+1} d\eta \eta^2 \beta^2 - \int_{-1}^{+1} d\eta \beta \hat{h}_\beta \beta \right] \alpha \quad (3.18)$$

Next, we make the substitutions

$$\alpha(\xi; R) = (\xi^2 - 1)^{-1/2} f(\xi; R) \quad (3.19)$$

$$\text{and} \quad \beta(\eta; R) = (1 - \eta^2)^{-1/2} g(\eta; R) \quad (3.20)$$

$$\text{Then,} \quad \hat{h}_\xi \alpha = a(\xi^2 - 1)^{1/2} \frac{d^2}{d\xi^2} f + \frac{a(1 - m^2)}{(\xi^2 - 1)^{3/2}} f$$

$$\text{and} \quad \beta \hat{h}_\beta \beta = a g \frac{d^2}{d\eta^2} g + \frac{a(1 - m^2)}{(1 - \eta^2)^2} g^2$$

Therefore equation (3.18) becomes,

$$\left\{ \frac{d^2}{d\xi^2} + \frac{(1 - m^2)}{(\xi^2 - 1)^2} + \frac{1}{a(\xi^2 - 1)} \int_{-1}^{+1} d\eta \frac{(\xi^2 - \eta^2)}{(1 - \eta^2)} V g^2 \right\} f(\xi; R) = \left\{ \frac{\xi^2 E}{a(\xi^2 - 1)} - \frac{E}{a(\xi^2 - 1)} \int_{-1}^{+1} d\eta \frac{\eta^2 g^2}{(1 - \eta^2)} - \frac{1}{(\xi^2 - 1)} \int_{-1}^{+1} d\eta g \left[ \frac{d^2}{d\eta^2} + \frac{(1 - m^2)}{(1 - \eta^2)^2} \right] g \right\} f(\xi; R)$$

or,

$$\left\{ \frac{d^2}{d\xi^2} + \frac{(1-m^2)}{(\xi^2-1)^2} - \frac{A}{(\xi^2-1)} \int_{-1}^{+1} d\eta \frac{(\xi^2-\eta^2)}{(1-\eta^2)} [V-E]g^2 + \frac{\epsilon_g}{(\xi^2-1)} \right\} f(\xi; R) = 0 \quad (3.21)$$

where  $f(\xi; R) \equiv f_{n_\xi, m}(\xi; R)$ ,  $g(\eta; R) \equiv g_{n_\eta, m}(\eta; R)$ ,

$$A = \frac{-1}{a} = \frac{R^2 m_r}{2}$$

$$\text{and } \epsilon_g = \int_{-1}^{+1} d\eta g \left[ \frac{d^2}{d\eta^2} + \frac{(1-m^2)}{(1-\eta^2)^2} \right] g \quad (3.22)$$

Likewise, considering a small arbitrary change in  $\beta$ ,  $\beta \rightarrow \beta + \delta\beta$ , we obtain,

$$\left[ \hat{h}_\eta + \int_{+1}^{+\infty} d\xi U \alpha^2 \right] \beta = \left[ \eta^2 E - E \int_{+1}^{+\infty} d\xi \xi^2 \alpha^2 - \int_{+1}^{+\infty} d\xi \alpha \hat{h}_\xi \alpha \right] \beta \quad (3.23)$$

And after making the substitutions (3.19), (3.20),

$$\left\{ \frac{d^2}{d\eta^2} + \frac{(1-m^2)}{(1-\eta^2)^2} - \frac{A}{(1-\eta^2)} \int_{+1}^{+\infty} d\xi \frac{(\xi^2-\eta^2)}{(\xi^2-1)} [V-E]f^2 + \frac{\epsilon_f}{(1-\eta^2)} \right\} g(\eta; R) = 0 \quad (3.24)$$

$$\text{where, } \epsilon_f = \int_{+1}^{+\infty} d\xi f \left[ \frac{d^2}{d\xi^2} + \frac{(1-m^2)}{(\xi^2-1)^2} \right] f \quad (3.25)$$

The one-dimensional equations (3.21) and (3.24) are the SCF equations of motion in the  $\xi$ - and  $\eta$ - coordinates, respectively. The new functions  $f(\xi; R)$  and  $g(\eta; R)$  were introduced in order to obtain the differential equations in the 'normal' form (which are more convenient from the computational point of view). These two equations are coupled through the 'SCF interaction potential' terms  $A \int_{-1}^{+1} d\eta \frac{(\xi^2-\eta^2)}{(1-\eta^2)} [V-E]g^2$  and  $A \int_{+1}^{+\infty} d\xi \frac{(\xi^2-\eta^2)}{(\xi^2-1)} [V-E]f^2$ , and the 'coupling constants'  $\epsilon_g$  and  $\epsilon_f$ . Thus they are solved iteratively until convergence is reached.

This iterative procedure is initiated by forming a suitable estimate of the coupling constant and the SCF interaction potential in one of the two SCF equations. The solution of this equation is used to compute the coupling constant and SCF interaction potential in the other equation. Then the solution of this second equation is in turn used to calculate the coupling constant and potential necessary to solve the first equation in a *new* iterative cycle. The iteration is continued until consistency in the eigenvalue  $E^{(SCF)}$  from both equations is achieved. A detailed description of this process can be found in Section E of Chapter 4.

The SCF energies  $E_{n_\xi, n_\eta, m}^{(SCF)}$  and modal eigenfunctions  $\alpha_{n_\xi, m}(\xi; R)$ , and  $\beta_{n_\eta, m}(\eta; R)$  which result, as well as the SCF potentials and coupling constants  $\epsilon_g$ ,  $\epsilon_f$ , are characterized by the quantum numbers  $(n_\xi, n_\eta, m)$ . Since the SCF potentials and parameters of equations (3.21) and (3.24) each depend on both quantum numbers, modal eigenfunctions for different nodal quantum numbers are *not orthogonal*:

$$\int_{-1}^{+1} d\eta \beta_{n', m}(\eta; R) \beta_{n, m}(\eta; R) \neq 0, \quad n' \neq n$$

$$\int_{+1}^{+\infty} d\xi \alpha_{n', m}(\xi; R) \alpha_{n, m}(\xi; R) \neq 0, \quad n' \neq n$$

although these overlap integrals are usually fairly small compared to 1.

The expectation value of the kinetic energy of a protonic SCF state  $\chi_{n_\xi, n_\eta, m}^{(SCF)}$  is given by,

$$\langle T \rangle = \frac{\langle \chi_{n_\xi, n_\eta, m}^{(SCF)} | \hat{T} | \chi_{n_\xi, n_\eta, m}^{(SCF)} \rangle}{\langle \chi_{n_\xi, n_\eta, m}^{(SCF)} | \chi_{n_\xi, n_\eta, m}^{(SCF)} \rangle} \quad (3.26)$$

where

$$\hat{T} = \frac{-1}{2m_r} \frac{4}{R^2(\xi^2 - \eta^2)} \left\{ \frac{\partial}{\partial \xi} \left[ (\xi^2 - 1) \frac{\partial}{\partial \xi} \right] + \frac{\partial}{\partial \eta} \left[ (1 - \eta^2) \frac{\partial}{\partial \eta} \right] + \frac{\xi^2 - \eta^2}{(\xi^2 - 1)(1 - \eta^2)} \frac{\partial^2}{\partial \phi^2} \right\} \quad (3.27)$$

$$\text{and } \left\langle \chi_{n_\xi, n_\eta, m}^{(SCF)} \mid \chi_{n_\xi, n_\eta, m}^{(SCF)} \right\rangle = \text{constant} = s, \quad \text{say.} \quad (3.28)$$

Using equations (3.22), (3.25), (3.27), and (3.28) in (3.26),

$$\langle T \rangle = -\left(\frac{R}{4m_r s}\right)(\epsilon_f + \epsilon_g) \quad (3.29)$$

i.e. The sum of the coupling constants gives, apart from a negative multiplicative constant, the expectation value of the kinetic energy of the protonic state. So we should expect the variation in  $-(\epsilon_f + \epsilon_g)$  to parallel that of the total SCF energy among protonic states calculated at a particular  $R$  value.

Multiplying equation (3.24) by  $g(\eta; R)$  and integrating over  $\eta$  (using (3.17), (3.28) and (3.22)) yields the explicit expression for energy,

$$-E = \left(\frac{R}{4m_r s}\right)(\epsilon_f + \epsilon_g) - \left(\frac{1}{s}\right) \int_{+1}^{+\infty} \int_{-1}^{+1} d\xi d\eta \left(\frac{R}{2}\right)^3 \frac{(\xi^2 - \eta^2) V f^2(\xi; R) g^2(\eta; R)}{(\xi^2 - 1)(1 - \eta^2)} \quad (3.30)$$

A rough interpretation of the individual parameters  $\epsilon_g$  and  $\epsilon_f$  as scaled kinetic energies associated with the other degree of freedom in equations (3.21) and (3.24) respectively is qualitatively useful, and these quantities are found to vary with the various quantum numbers in a fashion which renders this interpretation plausible. No rigorous interpretation of these parameters as 'modal energies' as possible, however; this is in contrast to the situation in the Hartree-Fock SCF equations for a many-electron system, where Koopmans' theorem [112] also gives a physical significance to the one-electron eigenvalues or 'orbital energies'.

Finally, note that the SCF equations (3.21) and (3.24) contain the 'azimuthal angular momentum' term  $(1 - m^2)/(\xi^2 - 1)^2$ , and  $(1 - m^2)/(1 - \eta^2)^2$ , respectively. However, since these terms become significant only when  $\xi \rightarrow 1$  and  $\eta \rightarrow \pm 1$ , they play a much more important role in the  $\xi$ - equation (3.21),



than in the  $\eta$ - equation (3.24). This is because while the region  $\eta = \pm 1$  (corresponding to the straight lines obtained by extending  $F_1 \dots F_2$  to the left of  $F_1$  and to the right of  $F_2$ ) is physically inaccessible to the proton, the region  $\xi = +1$  (i.e. the straight line joining  $F_1$  and  $F_2$ ) is very much accessible. Thus the kinetic energy associated with angular momentum  $m$  appears primarily in the 'bending' mode dynamics, rather than in the 'stretching' mode.

### E. Summary

The solutions to the vibrational Schrödinger equation can, in general, be expanded in a basis set of adiabatic 'protonic' states. Earlier work has shown that the *adiabatic* approximation is valid in the case of  $[FHF]^-$ . i.e. the total vibrational wave function may be written as a simple product of the protonic eigenfunction  $\chi_{n_p}(\xi, \eta, \phi; R)$  and the  $\nu_1$ - mode function,  $\Phi_{n_{\nu_1}, n_p}(R)$ . Then the *self-consistent field* approximation is used to separate the motion in the  $\xi$ - coordinate (bending mode) from that in the  $\eta$ - coordinate (anti-symmetric stretching mode). Application of the SCF approximation to the protonic vibrational dynamics results in two one-dimensional Schrödinger equations in the modal functions  $\alpha_{n_\xi, m}(\xi; R)$  and  $\beta_{n_\eta, m}(\eta; R)$ . Since these equations are coupled through the SCF interaction potentials, they have to be solved iteratively until convergence in the SCF energy eigenvalue is reached. The numerical technology used to solve the SCF equations will be described in Chapter 4.

## 4. NUMERICAL SOLUTION OF THE SCF EQUATIONS

### A. General Discussion of Milne's (Quantal Momentum) Method

The SCF equations (3.21) and (3.24) have the form of the one-dimensional Schrödinger equation

$$\frac{d^2}{dy^2} h(y; R) + k^2(y; R)h(y; R) = 0 \quad (4.1)$$

where the function  $k^2(y; R)$ , which we may interpret roughly as the square of a classical momentum function, has positive values in some domain of the independent variable  $y$ . In general,  $k^2(y; R)$  depends upon some effective potential function as well as on an energy  $E$ ; for the cases we consider, the effective potential and the energy  $E$  are such that the 'classically allowed' domain(s) for which  $k^2(y; R) \geq 0$  is bounded, and acceptable solutions exist only for discrete eigenvalues  $E_n$  with corresponding bound-state eigenfunctions  $h_n(y; R)$ . In the applications made here, the nodal quantum number  $n$  is specified and we seek only the solution for that  $n$ . Several cases have to be considered, as follows:

(1). In equation (3.21), the domain of the variable  $y \equiv x = \xi - 1$  is  $0 \leq x \leq +\infty$  and *either*

(a).  $k^2(x; R)$  is positive in a domain bounded by two zeroes  $x_i, x_o$  (classical turning points), *or*

(b).  $k^2(x; R)$  has only a single (outer) zero  $x_o$  and is positive in the domain  $0 \leq x \leq x_o$ .

In case (1b) certain computational complexities arise which we discuss in Section B.

(2). In equation (3.24), the domain of the variable  $y \equiv \eta$  is  $-1 \leq \eta \leq +1$ ,  $k^2(\eta; R)$  is an even function of  $\eta$ , and *either*

- (a).  $k^2(\eta; R)$  is positive in a domain  $-\eta_0 \leq \eta \leq +\eta_0$  ('no barrier'), or
- (b).  $k^2(\eta; R)$  is positive in two symmetrically placed wells bounded by  $\eta_i \leq \eta \leq \eta_0$  and  $-\eta_0 \leq \eta \leq -\eta_i$ , separated by a 'barrier' region where  $k^2(\eta; R) < 0$ .
- In either case the outer turning points are well inside the limits  $\eta = \pm 1$ . Case (2b) poses some additional computational complexity which we discuss in Section C.

For clarity, the discussion of this Section considers the simplest case where  $k^2(y; R) \geq 0$  in a single region  $y_i \leq y \leq y_0$  within the domain of  $y$  ( $a \leq y \leq b$ ). The method discussed is readily extended to the more complicated cases (1b) and (2b).

Milne [102] showed in 1930 that bound-state eigenfunctions of (4.1) can be expressed

$$h(y; R) = Cw(y; R) \sin \theta(y; R) \quad (4.2a)$$

$$\text{where } \theta(y; R) = \int_a^y dy' [w(y'; R)]^{-2}, \quad (4.2b)$$

and  $C$  is the normalization constant, when the energy  $E$  in (4.1) satisfies the quantization condition,

$$\int_a^b dy [w(y; R)]^{-2} = (n + 1)\pi; n = 0, 1, 2, \dots, \quad (4.3)$$

with  $w(y; R)$  any particular solution of the second-order non-linear differential equation (the so-called 'Milne's equation'),

$$\frac{d^2}{dy^2} w(y; R) + k^2(y; R)w(y; R) = [w(y; R)]^{-3}. \quad (4.4)$$

Since Milne's formulation, this approach to the one-dimensional Schrödinger equation has been modified and applied to specific problems by various workers [113-132].

Sometimes it is convenient to express these equations and solve them in their complex forms. We write,

$$h(y; R) = \exp\left[i \int^y q(y'; R) dy'\right] \quad (4.5)$$

where  $q(y; R)$  is the so-called 'quantal momentum' (in general, a complex quantity) in the  $y$  coordinate (and  $i^2 = -1$ ).

Substituting (4.5) in the equation (4.1), we have the Riccati equation

$$i \frac{d}{dy} q(y; R) - q^2(y; R) + k^2(y; R) = 0 \quad (4.6)$$

$$\text{Let } q(y; R) = q_{Re}(y; R) + i q_{Im}(y; R) \quad (4.7)$$

Substituting (4.7) in equation (4.6),

$$q_{Im}(y; R) = \frac{[q_{Re}(y; R)]'}{2q_{Re}(y; R)} \quad (4.8a)$$

$$\text{and } -q_{Re}^2 + q_{Im}^2 - q_{Im}'' + k^2 = 0 \quad (4.8b)$$

(The ' and '' denotes first and second differentiation w.r.t.  $y$ ). From relationships (4.8a) and (4.8b) we obtain,

$$\left[ q_{Re}(y; R)^{-1/2} \right]'' + k^2(y; R) \left[ q_{Re}(y; R)^{-1/2} \right] = \left[ q_{Re}(y; R)^{-1/2} \right]^{-3} \quad (4.9)$$

Comparing equation (4.9) with (4.4) we see that there is an one-to-one correspondence between the solutions  $w(y; R)$  of equation (4.4) and solutions  $q_{Re}(y; R)$  of equation (4.6):

$$w(y; R) \longleftrightarrow \left[ q_{Re}(y; R)^{-1/2} \right], \text{ for all } y. \quad (4.10)$$

Thus the eigenfunction  $h(y; R)$  may be written as,

$$h(y; R) = C \left[ q_{Re}(y; R) \right]^{-1/2} \sin[\theta(y; R)] \quad (4.11a)$$

and the Milne quantization condition is,

$$\int_a^b dy q_{Re}(y; R) = (n + 1)\pi ; n = 0, 1, 2, \dots \quad (4.12)$$

The relations stated still do not define either the Milne's function  $w(y; R)$  or the quantal momentum  $q(y; R)$  uniquely; to do so it is necessary to impose an initial condition defining  $q_{Re}(y; R)$  and  $q_{Im}(y; R)$  (or  $w(y; R)$  and its first derivative) at some suitable point  $y = y_1$ . Milne proved that the above results hold for any solution  $w(y; R)$ ; in general however, an arbitrary choice for the initial conditions on  $q(y; R)$  leads to a solution  $q_{Re}(y; R)$  which exhibits oscillatory behaviour in regions where  $k^2(y; R) > 0$ .

A major concern of much of the later literature on this method has been the establishment of an unique choice of initial conditions which render the function  $q_{Re}(y; R)$  computationally convenient (i.e. smooth and non-oscillatory). Newman and Thorson [119] devised an algorithm for generating initial values  $q_{Re}(y_1; R)$  and  $q_{Im}(y_1; R)$  leading to a  $q_{Re}(y; R)$  with the desired properties by iterative solution of equation (4.6), with  $q_{Re}(y_1; R) \simeq k(y_1; R)$  as the zero-order approximation.

Studies by Korsch and Laurent [130-132] show that the zero-order approximation is already quite satisfactory for most purposes (i.e. gives a very smooth and non-oscillatory solution over the entire domain of interest), *provided that the point  $y_1$  is taken to be at a minimum of the function  $-k^2(y; R)$* . i.e. They propose the 'classical' initial conditions

$$q_{Re}(y = y_1; R) = k(y = y_1; R) \quad (4.13a)$$

$$\text{and } q_{Im}(y = y_1; R) = 0 \quad (4.13b)$$

with the integration initiated at  $y = y_1$ , the minimum of  $-k^2(y; R)$ , i.e.

$$[-k^2(y; R)]'_{y=y_1} = 0 \quad (4.13c)$$

In terms of the Milne's function  $w(y; R)$  the classical conditions are,

$$w(y_1; R) = [k(y_1; R)]^{-1/2}, \quad (4.14a)$$

$$\text{and} \quad [w(y_1; R)]' = 0 \quad (4.14b)$$

where  $y = y_1$  is the minimum of  $-k^2(y; R)$ .

It should be noted that these classical initial conditions guarantee (from (4.4))

$$[w(y = y_1; R)]'' = 0, \quad (4.15a)$$

and also (from differentiating (4.4))

$$[w(y = y_1; R)]^{(3)} = 0. \quad (4.15b)$$

Thus the Milne's function (and the real part of the quantal momentum function) is quite smooth and flat at the minimum of  $-k^2(y; R)$ . The non-oscillatory behaviour of  $w(y; R)$  (and  $q_{Re}(y; R)$ ) enables us to obtain greater numerical accuracy with a much larger step size (compared with the numerical integration of the Schrödinger equation (4.1) itself). This increased efficiency in the computation as well as in storage and retrieval of the computed function and the easy generation of the initial conditions makes this method attractive.

This behaviour is illustrated by Figures (4.1) and (4.2), which show the quantal momentum (real part) function  $q_{Re}(\tilde{z}; R)$ , and the corresponding eigenfunction,  $u(\tilde{z}; R)$  (in a coordinate  $\tilde{z} = \ln(\xi - 1)$  which will be explained later) for the protonic state  $(3, 0, 1)_{R=4.40}$ .

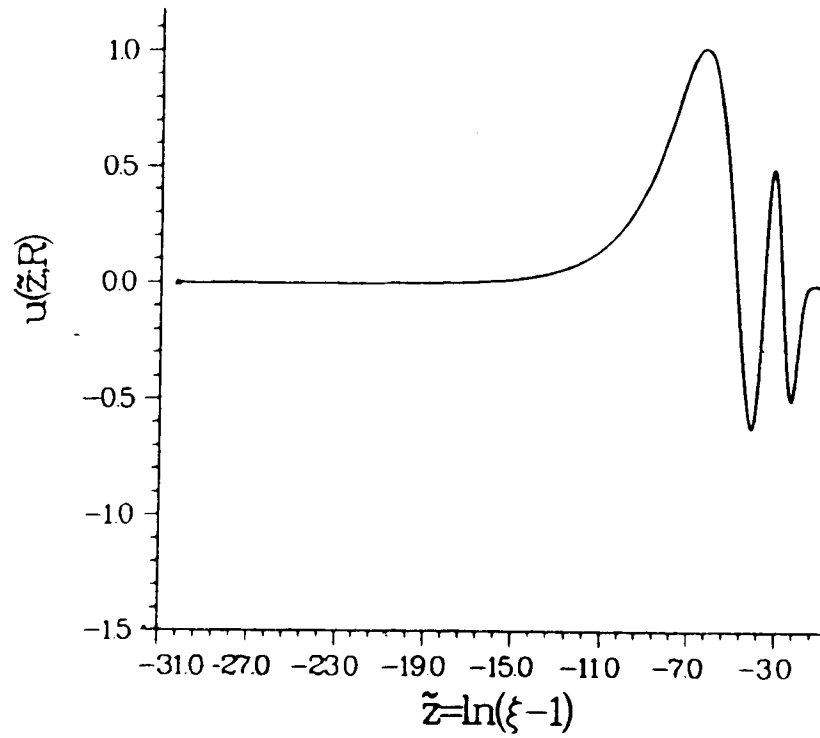


Figure 4.1  $u(\bar{z}; R)$  vs.  $\bar{z}$  for  $(3, 0, 1)_{R=4.40}$

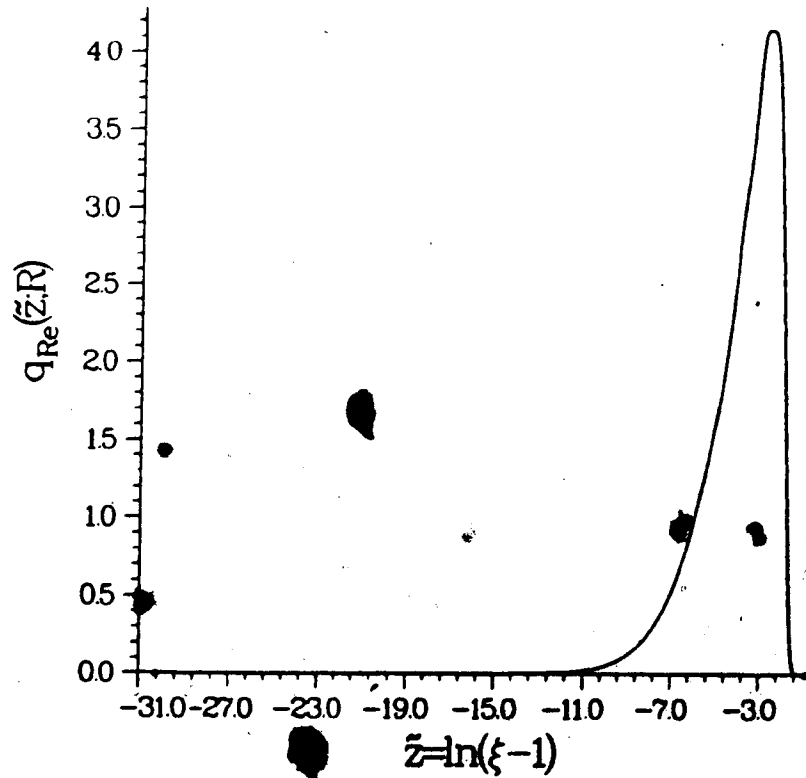


Figure 4.2  $q_{Re}(\bar{z}; R)$  vs.  $\bar{z}$  for  $(3, 0, 1)_{R=4.40}$

In principle, numerical integration of the Riccati equation (4.6) (or equivalently integration of Milne's equation (4.4)), with specified initial conditions  $q_{Re}(y_1; R)$  and  $q_{Im}(y_1; R)$  at some suitable point  $y = y_1$ , leads to generation of a global function  $q_{Re}(y; R)$  over the entire domain  $a \leq y \leq b$ . In situations where  $k^2(y; R)$  has a single classically allowed region with two bounding zeroes  $y_i$  and  $y_o$ , this is in fact the case. The problem is more complicated for the case (1b) cited above for equation (3.21), because in such cases the function  $k^2(x; R)$  is unbounded at the origin ( $x \rightarrow 0$ ), the quantal momentum  $q_{Re}(x; R)$  increases rapidly and may also exhibit an integrable singularity at  $x = 0$ ; as a result direct numerical integration cannot give sufficiently accurate values for  $q_{Re}(x; R)$  and the phase function  $\theta(x; R)$  in the neighbourhood of the origin. We discuss the technical solutions to these problems in detail in Section B. Another problem arises in the double well situation encountered in case (2b) for equation (3.24), and we discuss the required modifications of the method for that case in Section C.



## B. Numerical Solution of the Differential Equation for $\xi$ - Motion

Using the transformation  $x = \xi - 1$ ;  $0 \leq x \leq +\infty$  equation (3.21) reads,

$$\left\{ \frac{d^2}{dx^2} + k^2(x; R) \right\} f(x; R) = 0 \quad (4.16)$$

where

$$-k^2(x; R) = \frac{(m^2 - 1)}{(x(x+2))^2} + \frac{A}{x(x+2)} \int_{-1}^{+1} d\eta \frac{((x+1)^2 - \eta^2)}{(1 - \eta^2)} [V - E] g^2 - \frac{\epsilon_g}{x(x+2)} \quad (4.17)$$

The limiting behaviour of  $k^2(x; R)$  as  $x \rightarrow +\infty$  is governed by the SCF interaction potential term

$$\frac{A}{x(x+2)} \int_{-1}^{+1} d\eta \frac{((x+1)^2 - \eta^2)[V - E]}{(1 - \eta^2)} g^2 \quad (\text{i.e. } V \xrightarrow{x \rightarrow +\infty} +\infty).$$

This term guarantees that for sufficiently large  $x$  and all energies of interest to us here  $-k^2(x; R) \gg 0$ . Hence there is always an outer turning point  $x_o$ .

The behaviour of  $-k^2(x; R)$  at  $x \rightarrow 0$  is controlled (except when  $m = 1$ ) by the angular momentum term,

$$\frac{m^2 - 1}{(x(x+2))^2} \quad (x \rightarrow 0 \rightarrow +\infty \text{ for } m > 1).$$

Thus for  $m > 1$ , this ensures the existence of an inner turning point  $x_i$  as well. Hence  $k^2(x; R) \geq 0$  in a simple domain bounded by these two zeroes, and Milne's method as described in Section A can be applied directly.

The numerical integration of equation (4.6) is initiated (initial conditions (4.13)) at the minimum of  $-k^2(x; R)$ ,  $x = x_1$ , and carried out in both directions: to the left towards  $x = 0$ , and to the right until  $q_{Re}(x; R)$  becomes smaller than a certain threshold criterion (usually,  $1.0 \times 10^{-10}$ ). The quantization condition (4.12)

(with  $a \equiv 0$ ,  $b \equiv +\infty$ ,  $n \equiv n_\xi$ ) is applied to obtain the eigenvalue  $E$ . For example, Figures 4.3, 4.4, and 4.5 show the functions  $-k^2(x; R)$ ,  $\theta(x; R)$ , and  $q_{Re}(x; R)$ , respectively in the  $x$  coordinate for the protonic SCF state  $(n_\xi = 0, n_\eta = 0, m = 2)_{R=4.40}$ . (In this example,  $V = SK1$  only; but the general behaviour is just the same for the complete potential.) Note that in these simple cases ( $m > 1$ ),

$$q_{Re}(x; R) \longrightarrow 0 \text{ as } x \rightarrow 0 \text{ and as } x \rightarrow +\infty.$$

Note also that (see Figures 4.2 and 4.5) the qualitative characteristics of the function  $q_{Re}(x; R)$  for the states  $(3, 0, 1)_{R=4.40}$  and  $(0, 0, 2)_{R=4.40}$  are the same, despite the difference of three nodes in their corresponding wave functions. Likewise, the phase function  $\theta(x; R)$  shows the same smooth behaviour for both states.

However, the numerical computation becomes more complicated when states with  $m = 0$  and  $m = 1$  are considered. In these cases,  $-k^2(x; R)$  has a singularity at the origin  $x = 0$ : For the  $m = 0$  cases the denominator of the angular momentum term, and for the  $m = 1$  cases the denominator of the SCF interaction potential term (the numerator tends to a finite value at  $x = 0$  or  $\xi = 1$ ) ensures that

$$-k^2(x; R) \xrightarrow{x \rightarrow 0} -\infty.$$

For example, Figure 4.6 depicts  $-k^2(x; R)$  vs.  $x$  for the state  $(0, 0, 0)_{R=4.40}$  ( $V = SK1$  only). The nature of the resultant  $q_{Re}(x; R)$  function (for the state  $(0, 0, 0)_{R=4.40}$ ) is shown in Figure 4.7.

i.e. for  $m = 0$ ,

$$w(x; R) \xrightarrow{x \rightarrow 0} 0, \quad (4.18a)$$

$$\text{and } q_{Re}(x; R) \xrightarrow{x \rightarrow 0} +\infty; \quad (4.18b)$$

for  $m = 1$ ,

$$w(x; R) \xrightarrow{x \rightarrow 0} \text{non-zero constant}, \quad (4.19a)$$

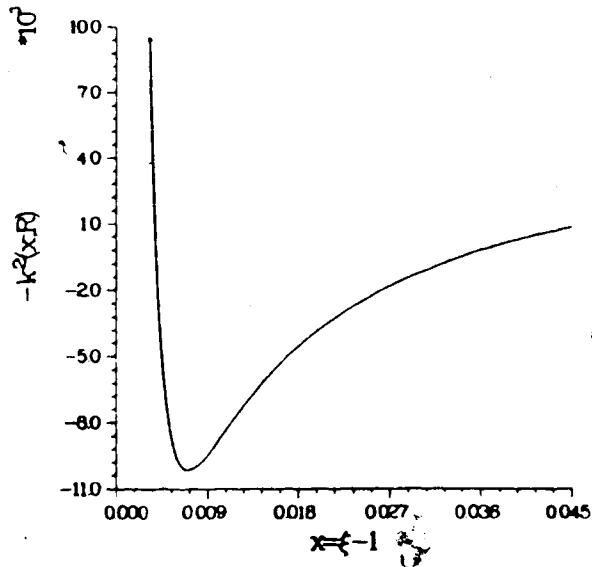


Figure 4.3  $-k^2(x; R)$  vs.  $x$  for  $(0, 0, 2)_{R=4.40}$

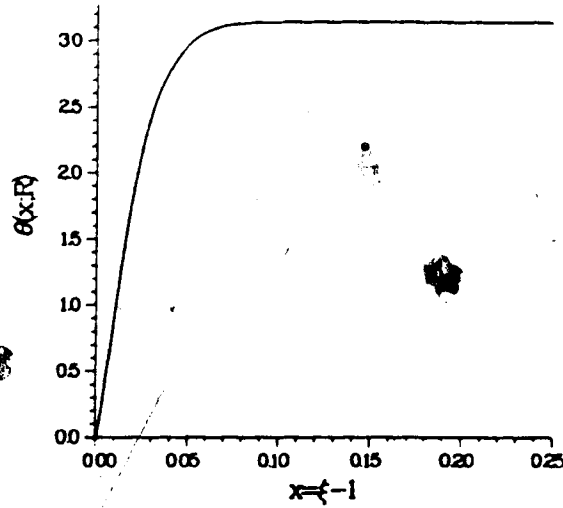


Figure 4.4  $\theta(x; R)$  vs.  $x$  for  $(0, 0, 2)_{R=4.40}$

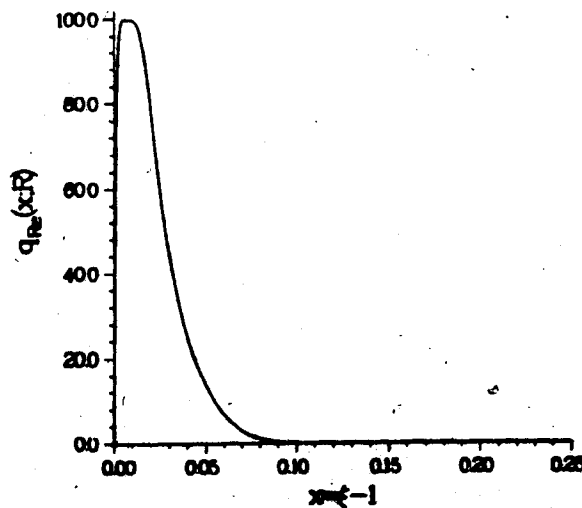


Figure 4.5  $q_{R_2}(x; R)$  vs.  $x$  for  $(0, 0, 2)_{R=4.40}$

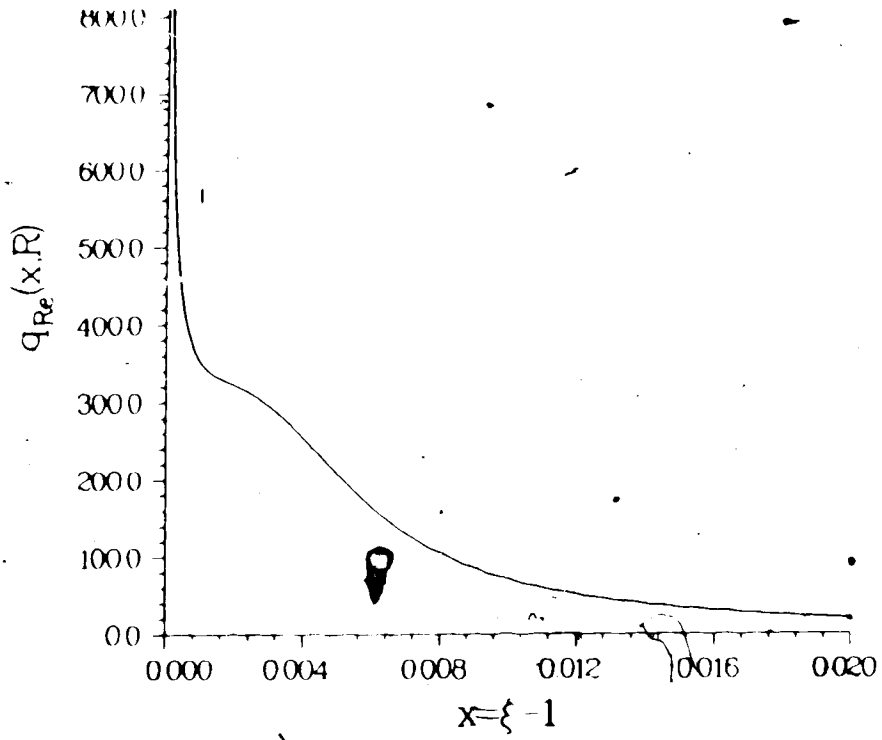


Figure 4.6  $-k^2(x; R)$  vs.  $x$  for  $(0, 0, 0)_{R=4.40}$

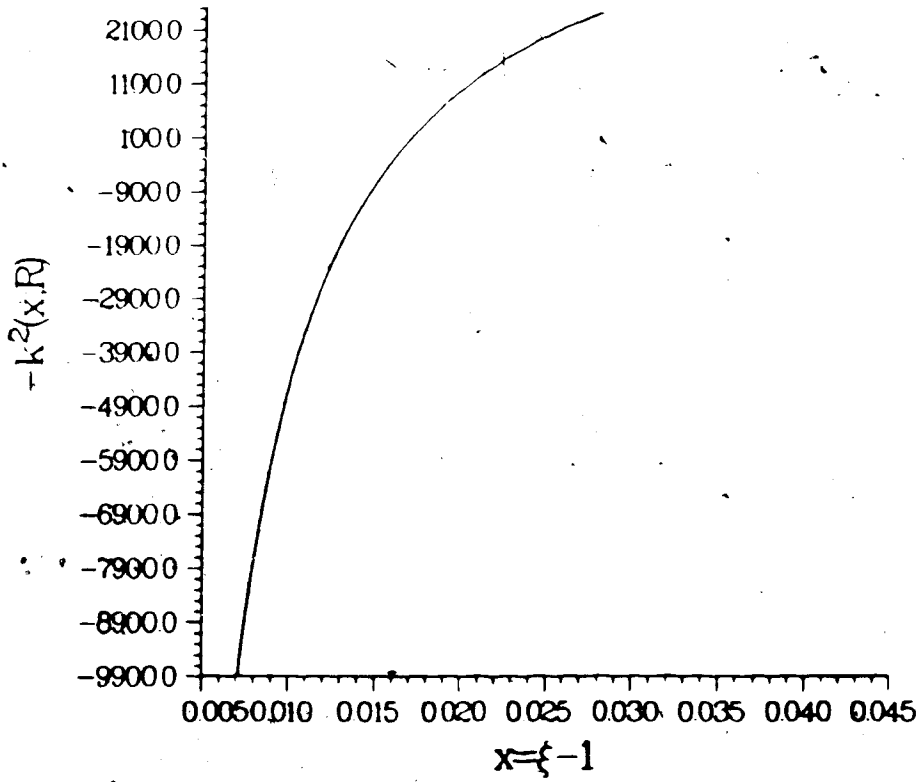


Figure 4.7  $q_{Re}(x; R)$  vs.  $x$  for  $(0, 0, 0)_{R=4.40}$

$$\text{and } q_{Re}(x; R) \xrightarrow{x \rightarrow 0} \text{large constant} \quad (4.19b)$$

In both cases, the real part of the quantal momentum increases very sharply in the vicinity of the origin. This makes stable, accurate numerical integration of the quantity  $q_{Re}(x; R)$  near the origin difficult. At the same time, high numerical accuracy in the integration of  $q_{Re}(x; R)$  in this region is extremely important in the  $m = 1$ , and particularly the  $m = 0$  cases because relatively large amounts of the quantum number function  $\frac{1}{\pi} \int_0^{+\infty} dx q_{Re}(x; R)$ , come from the neighbourhood of the singularity.

For example, for a model calculation with  $V = SK1$  (which approximation makes no significant change in the qualitative nature of the problem) the values of the integral  $I = \frac{1}{\pi} \int_0^{0.0002} dx q_{Re}(x; R)$  for the states  $(0, 0, m)_{R=4.40}$  were as follows:

$$\text{For } m = 2, \quad I = 0.0006$$

$$\text{For } m = 1, \quad I = 0.0177$$

For  $m = 0$ ,  $I = 0.1493$  (i.e. almost 15% of the total value of the quantum number function.)

Clearly, we need some more accurate technique for computing the quantal momentum and phase functions for  $m = 0, 1$ . In this work, we have investigated two different schemes for this purpose:

- (i) Method of series solutions.
- (ii) Langer transformation method.

### 1. Method of series solutions

If it is assumed that the SCF interaction potential in (4.17) can be expanded in a convergent Taylor series about  $x = 0$ , then the differential equation (4.16) may be solved in terms of power series expansions about the regular singular point  $x = 0$ . The characteristic behaviour of these solutions near  $x = 0$  is

controlled by the value of  $m$ ; the solution regular at the origin is given by

$$f_1(x; R) = \sum_{r=0}^{\infty} a_r x^{1/2+m/2+r}, \quad (4.20)$$

while the irregular solution has the form

$$f_2(x; R) = K \ln x \sum_{r=0}^{\infty} a_r x^{1/2+m/2+r} + \sum_{s=0}^{\infty} b_s x^{1/2-m/2+s}, \quad (4.21)$$

where the series coefficients  $\{a_i; i = 1, 2, \dots, \infty\}$ ,  $\{b_j; j = 1, 2, \dots, \infty\}$ , and the constant  $K$  are determined by certain recursion relations derivable from the differential equation and the known series expansion for the SCF interaction potential (see the Appendix). The series are constructed such that the Wronskian of  $f_1(x; R)$  and  $f_2(x; R)$  is given by,

$$W(f_1, f_2) = 1 \quad (4.22)$$

The general solution of Milne's equation

$$[w(x; R)]'' + k^2(x; R)w(x; R) = [w(x; R)]^{-3}$$

can be written in terms of the linearly independent series solutions  $f_1$  and  $f_2$  (and constants  $A, B, C$ ) by,

$$w(x; R) = \left[ (C^2 + A^2)f_1^2 + B^2f_2^2 + 2ABf_1f_2 \right]^{1/2} \quad (4.23)$$

$$\text{with } BC = \left[ W(f_1, f_2) \right]^{-2} = 1 \quad (4.24)$$

Therefore, given the constants  $A, B$ , and  $C$ , the quantal momentum and the phase function near the origin may be calculated from the formulae

$$q_{Re}(x; R) = \left[ (C^2 + A^2)f_1^2 + B^2f_2^2 + 2ABf_1f_2 \right]^{-1}, \quad (4.25a)$$

$$\text{and } \theta(x; R) = \int_0^x dx' q_{Re}(x'; R) = \tan^{-1} \left[ \frac{C f_1(x; R)}{A f_1(x; R) + B f_2(x; R)} \right] \quad (4.25b)$$

Solution of the  $\xi$ -motion equation for  $m = 0$  and  $m = 1$  can then be carried out as follows:

(a). At some suitable point  $x = x_1$  in the classically allowed region  $0 \leq x \leq x_0$ , initial values are determined for  $q_{Re}(x; R)$  and  $q_{Im}(x; R)$ . Since the function  $-k^2(x; R)$  has *no* minimum in these cases, instead of the classical initial conditions (4.13) we use the algorithm of Newman and Thorson [119] to generate an iterative solution to the Riccati equation (4.6) at  $x = x_1$ .

(b). With these initial values, equation (4.6) is integrated numerically outward to generate  $q_{Re}(x; R)$  in the domain  $x_1 \leq x \leq \infty$ , until, as usual,  $q_{Re}(x; R) \rightarrow 0$ .

(c). Equation (4.6) is integrated inward from  $x = x_1$  to some (pre-determined) point  $x = x_{match}$ . At that point, the constants  $B, A$ , and  $C$  can be found from the formulae obtained by matching the Milne function (and its derivative) from the integrated solution with that constructed from the series solutions (generated at  $x = x_{match}$ ) as in (4.23):

$$B = \left[ f_1^2 q_{Re} + f_1^2 \frac{q_{Im}^2}{q_{Re}} + \frac{f_1'^2}{q_{Re}} + \frac{2q_{Im} f_1' f_1}{q_{Re}} \right]^{1/2}, \quad (4.26a)$$

$$A = \frac{1}{B} \left[ \frac{q_{Im}}{q_{Re}} + \frac{f_1'}{f_1 q_{Re}} \right] - B \left[ \frac{f_2}{f_1} \right], \quad (4.26b)$$

$$\text{and } C = \frac{1}{B}, \quad (4.26c)$$

With the constants  $A, B$ , and  $C$  determined from the equations (4.26) (evaluated at  $x = x_{match}$ ), we now know the Milne's function  $w(x; R)$  (or the quantal momentum  $q(x; R)$ ) to the left of  $x_{match}$  (up to the origin) in terms of the series solutions, and of course to the right of  $x_{match}$  in terms of the integrated

numerical solution. We can now accurately evaluate the quantum number function and the eigenfunctions over the entire domain of  $x$  without any difficulty.

However, we found here that to minimize numerical errors in the integration of equation (4.6) it is necessary to choose values  $x_{match}$  which are not too close to the origin; however, when this is done, the number of terms required in the power series solutions to obtain accurate convergence increases sharply. Since the recursion relations needed to generate higher coefficients in these series increase rapidly in complexity as the index increases, this technique was found to be not sufficiently efficient, and instead the second method, described below, was used. However, it must be noted that even though it is not the most efficient way of solving the differential equation, the series solution method is significant for the information it gives on the limiting behaviour of the solutions at the origin.

## 2. Langer transformation method

Apply the transformation

$$\bar{z} = \log_e x = \log_e(\xi - 1) \quad (4.28)$$

with a new eigenfunction defined,

$$u(\bar{z}; R) = \frac{f(x; R)}{x^{1/2}} \quad (4.29)$$

to the differential equation (4.1). The result is,

$$\left\{ \frac{d^2}{d\bar{z}^2} + k^2(\bar{z}; R) \right\} u(\bar{z}; R) = 0, \quad (4.30)$$

with

$$-k^2(\bar{z}; R) = \frac{(m^2 - 1)}{(e^{\bar{z}} + 2)^2} + \frac{1}{4} + \frac{Ae^{\bar{z}}}{(e^{\bar{z}} + 2)} \int_{-1}^{+1} d\eta \frac{((e^{\bar{z}} + 1)^2 - \eta^2)[V - E]g^2}{(1 - \eta^2)} - \frac{\epsilon_g e^{\bar{z}}}{(e^{\bar{z}} + 2)} \quad (4.31)$$



This coordinate transformation was first proposed by R. E. Langer [133] in 1937 when it was applied in a Coulomb potential case. More recently, it has been applied by Lee and Light [134] in a Thomas-Fermi type calculation of the electron density in the Kr atom.

The result is a transformation from a semi-infinite coordinate space ( $0 \leq x \leq +\infty$ ) to an infinite coordinate space ( $-\infty \leq \tilde{z} \leq +\infty$ ). And there are no singularities in the new differential equation (4.30).

The function  $-k^2(x; R)$  has the boundary properties,

$$-k^2(\tilde{z}; R) \xrightarrow{\tilde{z} \rightarrow -\infty (x \rightarrow 0)} + \frac{(m^2 - 1)}{4} + \frac{1}{4}, \quad (4.32a)$$

$$\text{and } -k^2(\tilde{z}; R) \xrightarrow{\tilde{z} \rightarrow +\infty (x \rightarrow +\infty)} +\infty, \text{ for all } m \quad (4.32b)$$

This means that  $-k^2(\tilde{z}; R)$  will have a minimum for all  $m$  values, and while there are two 'classical turning points' for all  $m > 0$  states, for  $m = 0$  there will only be an outer turning point. ( $-k^2(\tilde{z}; R) \rightarrow 0$  as  $\tilde{z} \rightarrow -\infty$  for  $m = 0$ ).

Furthermore, the eigenfunction has the boundary properties,

$$u(\tilde{z}; R) \xrightarrow{\tilde{z} \rightarrow -\infty} \text{non-zero constant; for } m = 0 \quad (4.33a)$$

$$\text{while } u(\tilde{z}; R) \xrightarrow{\tilde{z} \rightarrow -\infty} 0; \text{ for } m > 0 \quad (4.33b)$$

$$\text{Also } u(\tilde{z}; R) \xrightarrow{\tilde{z} \rightarrow +\infty} 0; \text{ for all } m \quad (4.33c)$$

The Milne's equation corresponding to (4.30) is

$$\frac{d^2}{d\tilde{z}^2} w(\tilde{z}; R) + k^2(\tilde{z}; R) w(\tilde{z}; R) = [w(\tilde{z}; R)]^{-3} \quad (4.35)$$

And the eigenfunction  $u(\tilde{z}; R)$  is expressed in terms of the Milne's function by,

$$u(\tilde{z}; R) = C w(\tilde{z}; R) \sinh[\theta(\tilde{z}; R)] \quad (4.36)$$

where  $C$  is the normalization constant, and

$$\theta(\bar{z}; R) = \int_{-\infty}^{\bar{z}} d\bar{z} [w(\bar{z}; R)]^{-2} = \int_{-\infty}^{\bar{z}} d\bar{z} q_{Re}(\bar{z}; R) \quad (4.37)$$

The eigenvalue condition is,

$$\int_{-\infty}^{+\infty} d\bar{z} [w(\bar{z}; R)]^{-2} = \int_{-\infty}^{+\infty} d\bar{z} q_{Re}(\bar{z}; R) = (n_\xi + 1)\pi \quad (4.38)$$

where  $n_\xi = 0, 1, 2, 3, \dots$

$$\text{Since } \left[ \theta(\bar{z}; R) \right]' = [w(\bar{z}; R)]^{-2}, \quad (4.39)$$

and  $w(\bar{z}; R)$  is a real quantity, the phase function  $\theta(\bar{z}; R)$  is a monotonically increasing function. As the bound-state eigenfunction  $u(\bar{z}; R)$  cannot have infinitely many nodes, this means that  $\theta(\bar{z}; R)$  must approach some finite constant values in the limits  $\bar{z} \rightarrow \pm\infty$ .

$$\text{i.e. } \lim_{\bar{z} \rightarrow \pm\infty} \left[ \theta(\bar{z}; R) \right]' = 0 \quad (4.40)$$

Therefore from (4.39),

$$\lim_{\bar{z} \rightarrow \pm\infty} w(\bar{z}; R) = +\infty, \text{ for all } m \quad (4.41)$$

$$\lim_{\bar{z} \rightarrow \pm\infty} q_{Re}(\bar{z}; R) = 0, \text{ for all } m \quad (4.42)$$

The procedure to be followed in solving our differential equation (4.35) (or the corresponding Riccati equation for  $q(\bar{z}; R)$ ) is now clear: First, locate the minimum of the function  $-k^2(\bar{z}; R)$ ,  $\bar{z} = \bar{z}_1$ , and apply the classical initial conditions

$$q(\bar{z} = \bar{z}_1; R) = k(\bar{z} = \bar{z}_1; R). \quad (4.43)$$

Then carry out the numerical integration to the left of  $\bar{z}_1$  towards  $-\infty$ , and to the right of  $\bar{z}_1$  towards  $+\infty$ , until  $q_{Re}(\bar{z}; R)$  vanishes (in practice, becomes less than  $1.0 \times 10^{-10}$ ). For computational convenience we found it easiest to compute solutions for all  $m$  values using the Langer transformation method, although it is necessary to do so only for  $m \leq 1$ .

While for states with  $m > 0$ ,  $w(\bar{z}; R)$  grows very fast in the limit  $\bar{z} \rightarrow -\infty$ , it may be shown that for  $m = 0$  cases,  $w(\bar{z}; R)$  grows only as  $|\bar{z}|$  (as  $\bar{z} \rightarrow -\infty$ ). Therefore in the  $m = 0$  cases one has to integrate leftwards to very large distances before  $q_{Re}(\bar{z}; R)$  decays below an acceptable threshold value. For this reason, in the numerical integration of the  $\bar{z}$ - differential equation for  $m = 0$  states, a variable step-size integrator based on the rational extrapolation method of Bulirsch and Stoer [135] was used. (A somewhat more sophisticated version of this algorithm can be found in the IMSL routine 'DREBS' [136]).

Figures 4.8 and 4.9 show the behaviour of the functions  $-k^2(\bar{z}; R)$  and  $q_{Re}(\bar{z}; R)$  in the Langer coordinate  $\bar{z}$  for the protonic state  $(0, 0, 0)_{R=4.40}$ . It is evident that the transformed representation of the problem offers a much more conventional-looking depiction of the solutions than the original one (compare with Figures 4.6 and 4.7).

The method of Langer transformation has the following advantages over the first method:

- (1). The Langer transformation always produces a minimum in  $-k^2(\bar{z}; R)$  for bound states of all  $m$  values. Therefore, the classical initial conditions (which are known to result in a very well-behaved Milne's function) can always be non-arbitrarily applied at this well-defined point.
- (2). The absence of any singularities in the differential equation in the  $\bar{z}$ - coordinate means that the eigenvalues and the eigenfunctions can be calculated efficiently

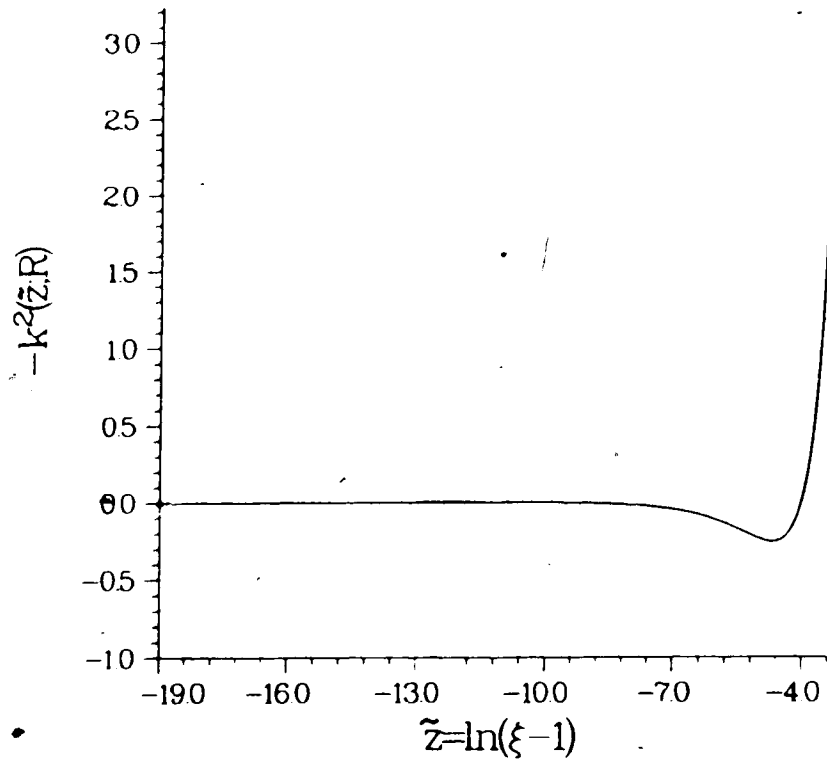


Figure 4.8  $-k^2(\tilde{z}; R)$  vs.  $\tilde{z}$  for  $(0, 0, 0)_{R=4.40}$

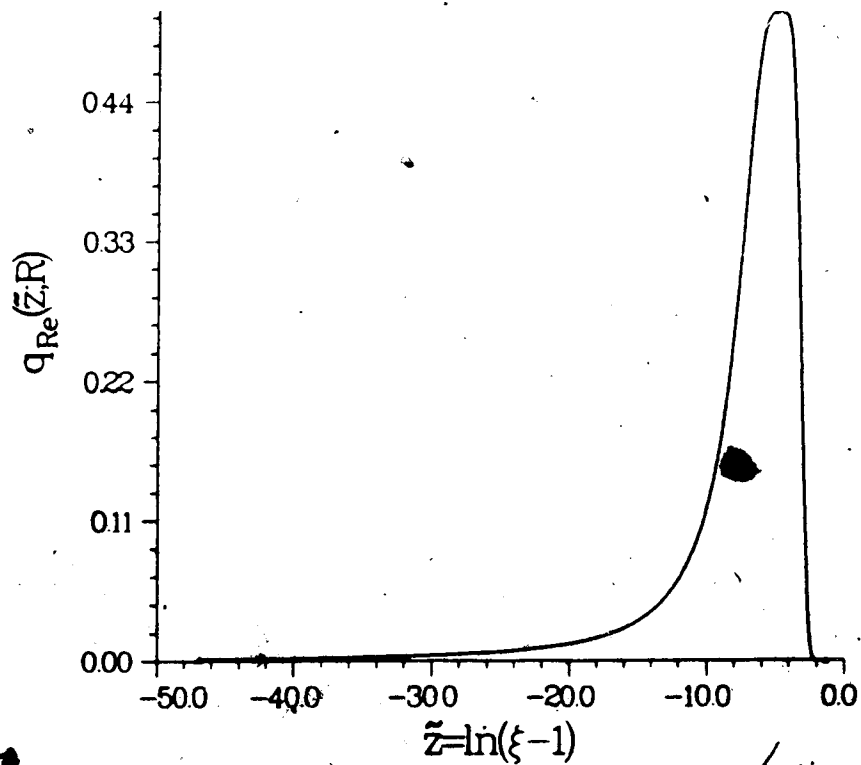


Figure 4.9  $q_{Re}(\tilde{z}; R)$  vs.  $\tilde{z}$  for  $(0, 0, 0)_{R=4.40}$

and accurately by numerical integration alone, without any need for techniques such as generation of series solutions, etc.

(3). Application of the Langer transformation has the effect of 'expanding' (in the new  $\bar{z}$ - coordinate) the physically significant region very close to the origin  $x = 0$ . As a result, numerical calculations can be done much more accurately, particularly for the  $m \rightarrow 0$  and  $m = 1$  cases, where this region is quite important. (Despite this 'expansion', because one can use a step-size that is considerably larger (by 1-2 magnitudes) than was the case during integration in the old  $x$ - (or  $\xi$ -) coordinate, there is no significant increase in the number of steps with a fixed step-size integrator.)

$$\text{Now, } A = \frac{R^2 m_r}{2}$$

$$\text{for } [\text{FHF}]^-, \quad \frac{1}{m_r} = \frac{1}{m_H} + \frac{1}{m_F + m_F}$$

$$\text{for the isotope } ^{19}\text{F}, \quad m_F = \frac{18.993466 m_H}{1.007276}$$

$$\text{Therefore, } m_r = \frac{37.986932 m_H}{38.986932}$$

$$\text{Also, } m_H = 1836.152375 m_e \quad (m_e = \text{electronic mass})$$

$$\text{Thus, } m_r = 1788.733927 \text{ a.u.} \quad \text{or,}$$

$$A = (894.527882)R^2; (R \text{ in Bohrs.})$$

For the isotopic system  $[\text{FDF}]^-$ ,

$$m_D = \frac{2.013553 m_H}{1.007276}$$

$$m_r = 3485.717482 \text{ a.u.}, \quad \text{or,}$$

$$A = (1742.858741)R^2$$

For the 'isotopic' system  $[F\mu F]^-$ , (where the H atom has been replaced by the Muonium  $\mu^+e^-$ ),

$$m_{\mu^+} = 0.112610m_H,$$

$$m_r = 206.152937 \text{ a.u.}, \quad \text{or,}$$

$$A = (103.076468)R^2$$

### C. Numerical Solution of the Differential Equation for $\eta$ - motion

The differential equation is,

$$\frac{d^2}{d\eta^2}g(\eta; R) + k^2(\eta; R)g(\eta; R) = 0 \quad (4.44a)$$

with

$$-k^2(\eta; R) = \frac{(m^2 - 1)}{(1 - \eta^2)^2} + \frac{A}{(1 - \eta^2)} \int_{+1}^{+\infty} d\xi \frac{(\xi^2 - \eta^2)(V - E)}{(\xi^2 - 1)} f^2(\xi; R) - \frac{\epsilon_f}{(1 - \eta^2)} \quad (4.44b)$$

Once again we use Milne's method to solve this equation. The relevant Milne's equation is

$$\frac{d^2}{d\eta^2}w(\eta; R) + k^2(\eta; R)w(\eta; R) = [w(\eta; R)]^{-3} \quad (4.45a)$$

and the corresponding equation for the quantal momentum is

$$i \frac{d}{d\eta}q(\eta; R) - q^2(\eta; R) + k^2(\eta; R) = 0 \quad (4.45b)$$

Using the fact that  $-k^2(\eta; R)$  (like the *ab initio* potential function  $V$  itself) is symmetric w.r.t.  $\eta$ , the quantization condition is given by,

$$2 \int_{-1}^0 d\eta q_{Re}(\eta; R) = (n_\eta + 1)\pi; \quad n_\eta = 0, 1, 2, \dots \quad (4.46)$$

The procedure for states at  $R < 4.60$  a.u. is quite straightforward: i.e. simply apply the classical initial conditions

$$q(\eta = 0; R) = k(\eta = 0; R) \quad (4.47)$$

at the minimum of  $-k^2(\eta; R)$ ,  $\eta = 0.0$ , and integrate leftwards until  $q_{Re}(\eta; R)$  vanishes. (This holds regardless of the value of  $m$ ). The SCF interaction potential is such that the singularities in  $-k^2(\eta; R)$  at  $\eta = \pm 1$  play no real part in the physical behaviour of the system (these regions are not physically accessible to the proton); effectively they are at ' $\pm\infty$ ', and the eigenfunctions  $g(\eta; R)$  always decay to zero well before the regions where the singular terms affect the equation are reached. Figures 4.10, 4.12, and 4.14 show the functions  $-k^2(\eta; R)$ ,  $q_{Re}(\eta; R)$ , and  $\theta(\eta; R)$ , respectively for the protonic SCF state  $(0, 0, 2)_{R=4.40}$ .

However, at larger F...F distances the situation is more complicated. (This generally applies to most states at  $R \geq 4.60$  a.u.) In such instances,  $-k^2(\eta; R)$  (like  $V$ ) consists of two minima symmetrically placed about  $\eta = 0.0$ . In each well there are outer and inner turning points, at  $\pm\eta_o$  and  $\pm\eta_i$ , respectively. Then we are unable to find a single  $q_{Re}(\eta; R)$  function that is slowly varying (i.e. non-oscillatory) in the entire domain,  $-1 \leq \eta \leq +1$ . For example, applying the classical initial conditions at one minimum would result in a quantal momentum that is well-behaved in that potential well, but would oscillate in the other well. On the other hand, initiation of integration with the classical conditions at the central barrier maximum ( $\eta = 0.0$ ) would give  $q_{Re}(\eta; R)$  that is oscillatory in both wells [130].

This difficulty has been overcome by a modification of Milne's method by Lee and Light [124]. Integration of the differential equation is initiated with the classical conditions at both minima separately, and the resultant wave functions

(and their derivatives) are matched at the central barrier maximum,  $\eta = 0.0$ . This leads to the following eigenvalue conditions:

For protonic states symmetric w.r.t.  $\eta = 0.0$  (from the vanishing of the derivative of the wave function at  $\eta = 0.0$ ),

$$\int_{-1}^0 d\eta q_{Re}(\eta; R) - \cot^{-1} \left[ \frac{[q_{Re}(\eta; R)]'}{2[q_{Re}(\eta; R)]^2} \right]_{\eta=0} = n\pi, \quad (4.48a)$$

where  $n = 1, 2, 3, \dots$ , and  $n_\eta = 2n - 2$ .

For protonic states anti-symmetric w.r.t.  $\eta = 0.0$  (from the vanishing of the wave function at  $\eta = 0.0$ ),

$$\int_{-1}^0 d\eta q_{Re}(\eta; R) = n\pi, \quad (4.48b)$$

where  $n = 1, 2, 3, \dots$ , and  $n_\eta = 2n - 1$ .

This procedure is valid regardless of the value of  $m$ . Figures 4.11, 4.13, and 4.15, for example, illustrate  $-k^2(\eta; R)$ ,  $q_{Re}(\eta; R)$ , and  $\theta(\eta; R)$ , respectively for the SCF state  $(0, 0, 2)_{R=4.60}$ .

#### D. Calculation of the Protonic States

The iterative solution of the two SCF equations for motion in the  $\xi$ - and  $\eta$ - coordinates may be broken down into the following consecutive steps:

(1). Start the procedure with a guess function for  $g(\eta; R)$ , the corresponding value of  $\epsilon_g$ , and the energy. (We prefer to start the iteration by solving the  $\xi$ - equation first since guessing  $g(\eta; R)$  with its inherent symmetry is easier than it would be for  $f(\xi; R)$ ). For the very first SCF state calculated, i.e.  $(0, 0, 1)_{R=4.40}$ , the guess function  $g(\eta; R) = C_{NG}(1 - \eta^2)^2$  was chosen. The normalization constant  $C_{NG} = 1.045825$ . This gives  $\epsilon_g = -2.666667$ .



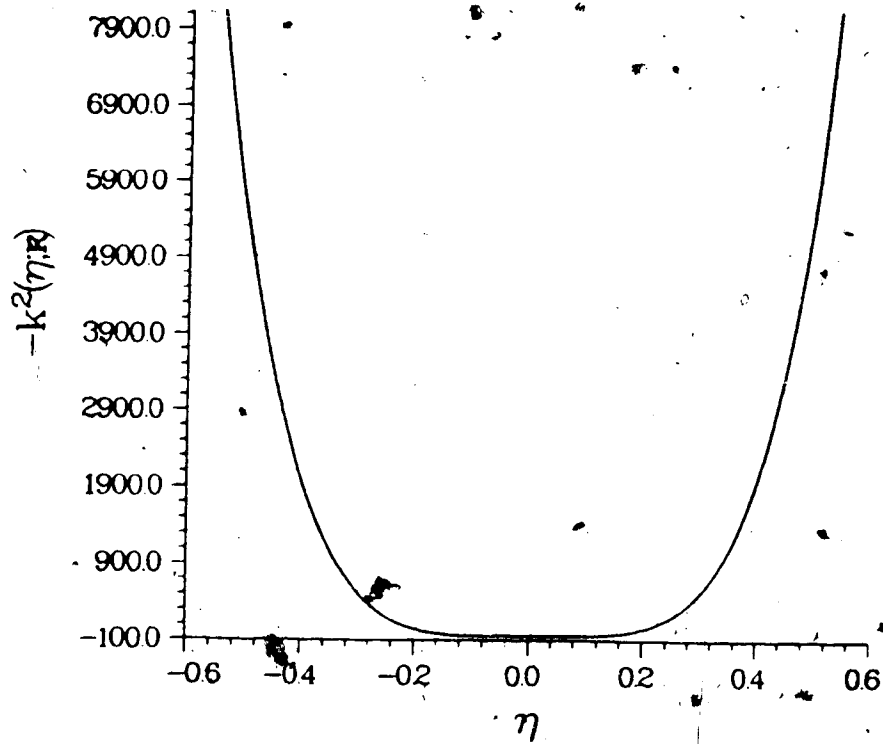


Figure 4.10  $-k^2(\eta; R)$  vs.  $\eta$  for  $(0, 0, 2)_{R=4.40}$

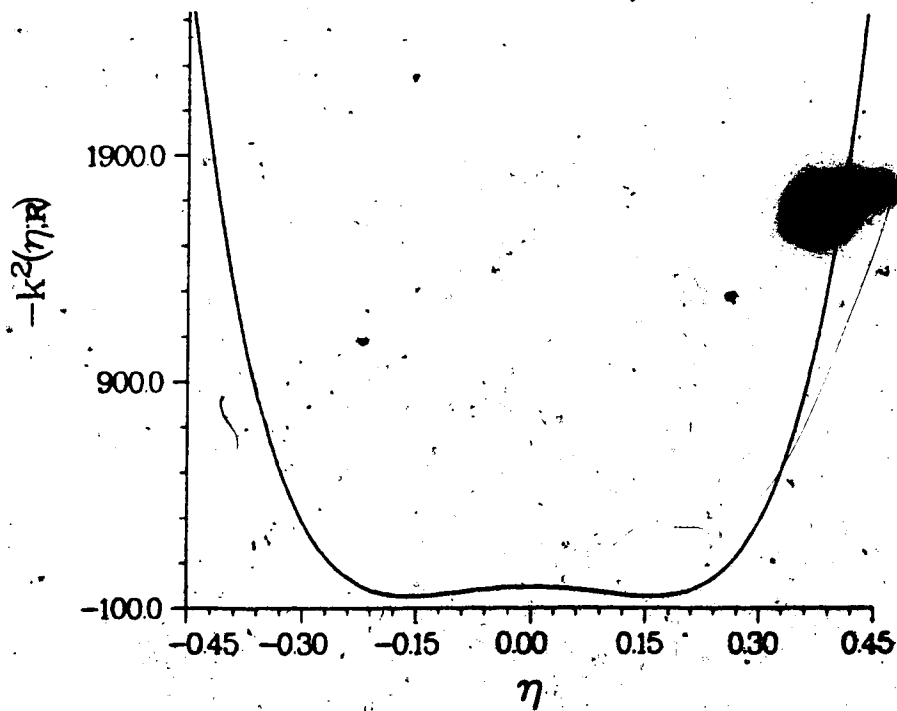


Figure 4.11  $-k^2(\eta; R)$  vs.  $\eta$  for  $(0, 0, 2)_{R=4.60}$

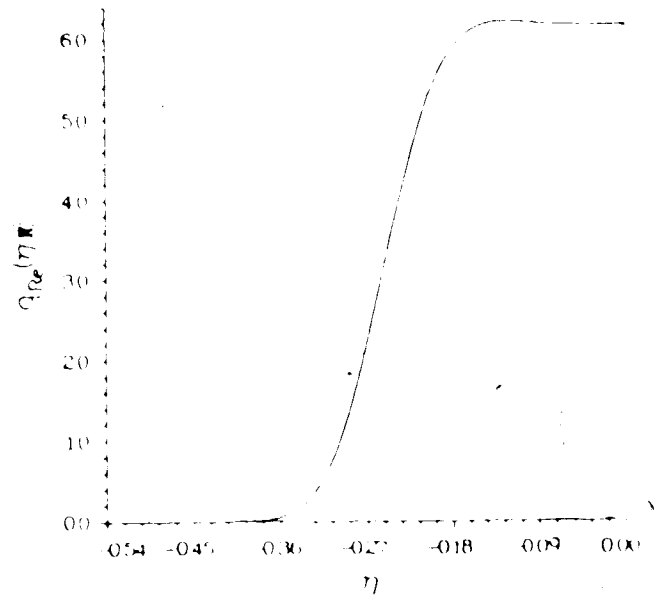


Figure 4.12  $q_{Re}(\eta; R)$  vs.  $\eta$  for  $(0, 0, 2)_{R=4.40}$

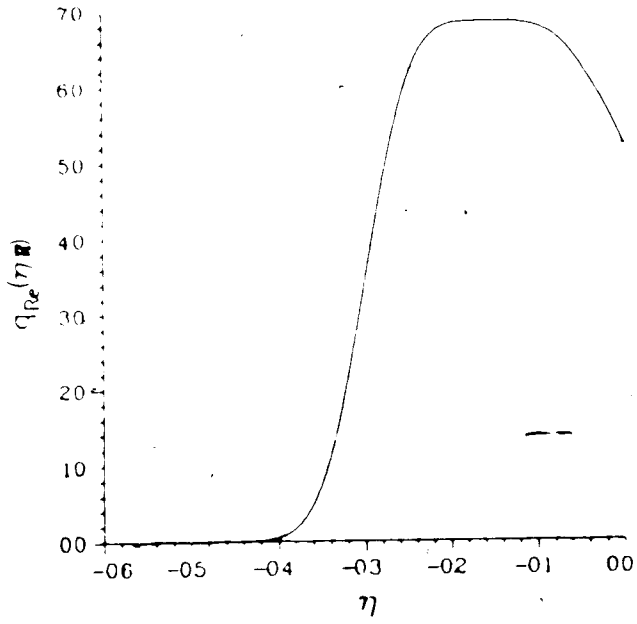


Figure 4.13  $q_{Re}(\eta; R)$  vs.  $\eta$  for  $(0, 0, 2)_{R=4.60}$

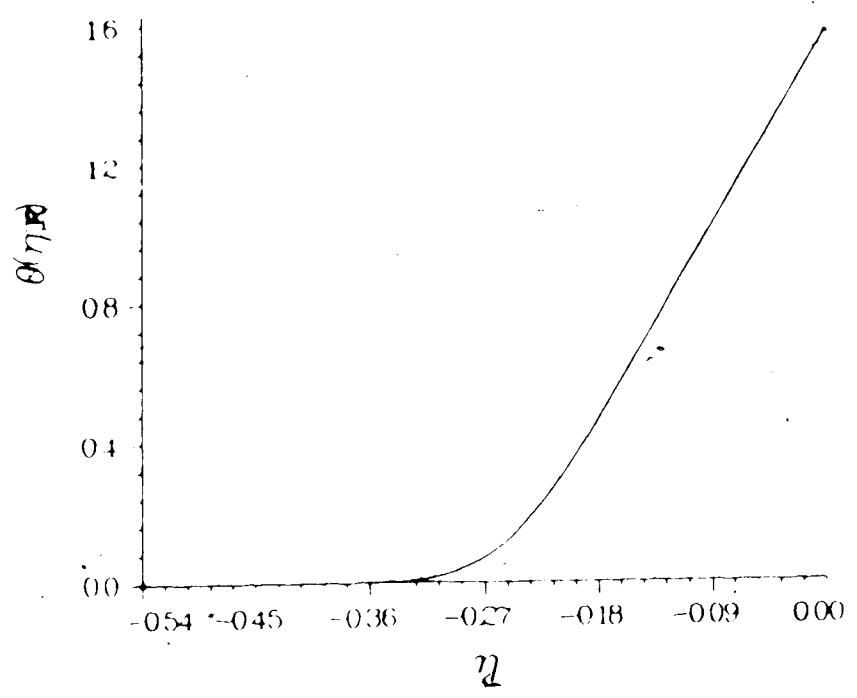


Figure 4.14  $\theta(\eta, R)$  vs.  $\eta$  for  $(0, 0, 2)_{R=4.40}$

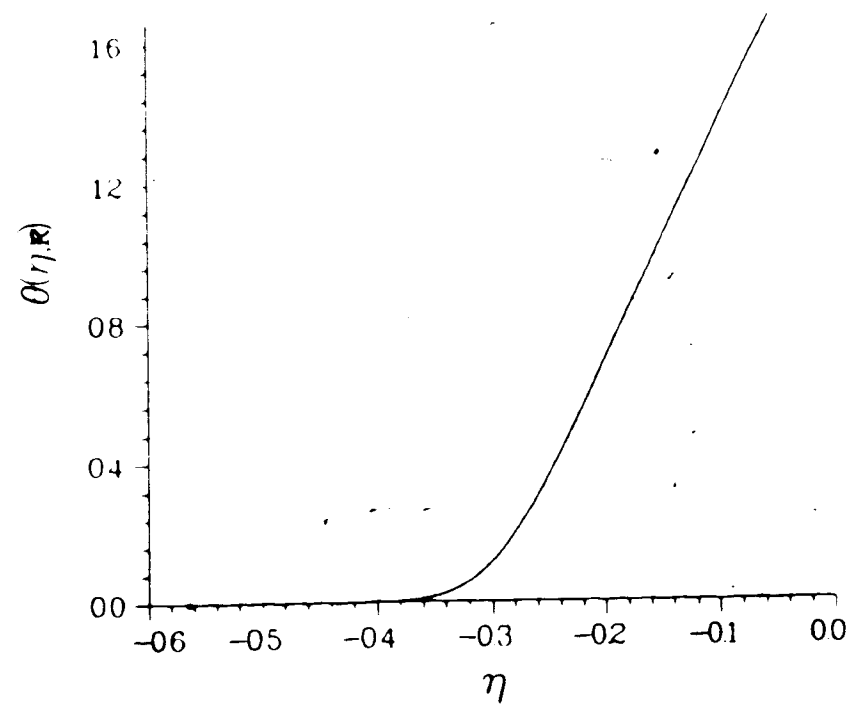


Figure 4.15  $\theta(\eta, R)$  vs.  $\eta$  for  $(0, 0, 2)_{R=4.60}$

(2). Solve the Milne equation (or the corresponding equation for the complex quantal momentum) for  $\xi$ - motion. (As mentioned earlier, this is done after first transforming into the Langer coordinate  $\tilde{z}$ ). For states  $m \geq 1$ , the numerical integration is done by the familiar fourth order Runge-Kutta algorithm with a step-size of 0.01. States with  $m = 0$  are integrated with the variable step-size integrator due to Bulirsch and Stoer [135].

Convergence to the desired quantum number  $n_\xi$  is done by means of a Newton-Raphson iterative algorithm. If  $E^{(i-1)}$  and  $E^{(i)}$  are the eigenvalues on the  $(i-1)$ th and  $i$ th *Newton-Raphson iterations*, then the eigenvalue on the  $(i+1)$ th iteration is given by,

$$E^{(i+1)} = E^{(i)} - \frac{N^{(i)}}{(N^{(i)} - N^{(i-1)})/(E^{(i)} - E^{(i-1)})} \quad (4.49a)$$

$$\text{where } N(E) = \frac{1}{\pi} \int_{-\infty}^{+\infty} d\tilde{z} q_{Re}(\tilde{z}; R) - (n_\xi + 1) \quad (4.49b)$$

This iteration is started by choosing two values for  $E^{(i)}$  and  $E^{(i-1)}$  (generally  $1.0 \times 10^{-5}$  Hartrees apart) and converges to better than  $1.0 \times 10^{-13}$  Hartrees.

(3). The  $\xi$ - Milne equation is solved with  $E$  now equal to the eigenvalue found in step (2), followed by calculation of the eigenfunction  $f(\xi; R)$ , normalization, and finally evaluation of  $\epsilon_f$ . This coupling constant  $\epsilon_f$  is easily calculated from

$$\begin{aligned} \epsilon_f &= \int_{+1}^{+\infty} d\xi f(\xi; R) \left[ \frac{d^2}{d\xi^2} + \frac{(1-m^2)}{(\xi^2-1)^2} \right] f(\xi; R) \quad (4.23) \\ &= \int_{+1}^{+\infty} d\xi f(\xi; R) \left[ \frac{A}{(\xi^2-1)} \int_{-1}^{+1} d\eta \frac{(\xi^2-\eta^2)[V-E]}{(1-\eta^2)} g^2 - \frac{\epsilon_g}{(\xi^2-1)} \right] f(\xi; R) \quad (4.50) \end{aligned}$$

i.e. evaluate the integral in (4.50) instead of the one in (4.23). All quadratures were computed using Simpson's rule or the trapezoidal rule.

(4). Next, with these values of  $E$ ,  $f(\xi; R)$ , and  $\epsilon_f$ , solve the  $\eta$ -Milne equation. The numerical integration of the differential equation (for all  $m$ ) was performed by the fourth order Runge-Kutta algorithm with a step-size of 0.001. Once more, the Newton-Raphson iterative procedure is used to converge on the required quantum number,  $n_\eta$ .

(5). Solve the  $\eta$ -Milne equation again with substitution of the eigenvalue calculated in step (4) for  $E$ . Calculate the wavefunction  $g(\eta; R)$ , normalize, and calculate  $\epsilon_g$  by,

$$\epsilon_g = \int_{-1}^{+1} d\eta g(\eta; R) \left[ \frac{A}{(1-\eta^2)} \int_{+1}^{+\infty} d\xi \frac{(\xi^2 - \eta^2)[V - E]}{(\xi^2 - 1)} f^2 - \frac{\epsilon_f}{(1-\eta^2)} \right] g(\eta; R) \quad (4.51)$$

With this new value of  $E$ ,  $g(\eta; R)$ , and  $\epsilon_g$ , go back to step (2).

The SCF equations are solved in this iterative manner until convergence is achieved. This occurs when the value of  $E$  in two consecutive SCF cycles agrees to better than  $1.0 \times 10^{-8}$  Hartrees ( $\simeq 0.002 \text{ cm}^{-1}$ ). At this point the solution ( $E$ ) from the  $\xi$ -equation has converged to within  $1.0 \times 10^{-9}$  Hartrees of that from the  $\eta$ -equation. For most of the protonic states calculated so far, SCF convergence occurs in 2-6 iteration cycles. (In general, the higher energy states need more cycles to converge than the low energy ones.)

Once a SCF state is evaluated, this can be used as the initial guess for subsequent calculation of SCF states. For example, suppose that the state  $(n_\xi, n_\eta, m)_R$  has been calculated. Then the  $g(\eta; R)$  from this state may be used to initiate the calculation of  $(n_\xi + 1, n_\eta, m)_R$  (or the state  $(n_\xi - 1, n_\eta, m)_R$ , for that matter), while the  $f(\xi; R)$  from this state can be used to compute  $(n_\xi, n_\eta + 1, m)_R$  (or  $(n_\xi, n_\eta - 1, m)_R$ ). On the other hand, either the  $g(\eta; R)$  or the  $f(\xi; R)$  may be used to evaluate  $(n_\xi, n_\eta, m')_R$  as well as  $(n_\xi, n_\eta, m)_R$ . All the necessary protonic states of  $[\text{FHF}]^-$  were calculated in this manner. Of course, two different initial

guesses should lead to the same final converged solution. This was used to confirm the precision of the states evaluated (precise to better than  $0.001 \text{ cm}^{-1}$ ). SCF states were also calculated in this thesis for the isotopic systems  $[\text{FDF}]^-$  and  $[\text{F}\mu\text{F}]^-$ .

### E. Summary

In this Chapter, the numerical solution of the SCF equations for motion in the  $\xi$  and  $\eta$  coordinates is discussed. Each equation is solved using Milne's method, which involves converting them into the corresponding Milne's equations. The success of this method is based upon the fact that the Milne's function, unlike the wave function, exhibits smooth, non-oscillatory behaviour, *when* the classical initial conditions are used for the numerical integration. Two methods are proposed to overcome the problems posed by the singularity in the  $\xi$ - equation for  $m = 0$  and  $m = 1$  cases. The first method is the generation of series solutions near the origin and matching them with the numerically integrated solutions. The second method (the one that was actually used) is transforming to the Langer coordinate,  $\tilde{z} = \ln(\xi - 1)$ . The SCF iteration cycle converges to better than  $10^{-8}$  Hartrees. The SCF converged wave functions from one SCF state are used as the guesses to initiate the iteration for another state.

## 5. DISCUSSION OF SELF-CONSISTENT FIELD RESULTS

### A. SCF Energy vs. R Curves

As was stated in the preceding Chapter, the protonic SCF states are designated by the nodal quantum numbers  $(n_\xi, n_\eta, m)$  at each given  $R$  value. Using the technology described in Chapter 4, 27 SCF states with nodal indices  $n_\xi = 0 - 3$ ,  $n_\eta = 0 - 6$ , and  $m = 0 - 2$  were calculated. They were computed at values of  $R$  ranging from 3.80 a.u. up to 6.40 a.u., usually at 0.20 a.u. intervals (approximately 300 SCF calculations in total).

Since the system has  $D_{\infty h}$  symmetry, both the exact protonic states and the approximate SCF states described here can be labelled by the irreducible representations of  $D_{\infty h}$  to which they belong. These are denoted by  $\sigma_g$ ,  $\sigma_u$  ( $m = 0$ ),  $\pi_g$ ,  $\pi_u$  ( $m = \pm 1$ ),  $\delta_g$ ,  $\delta_u$  ( $m = \pm 2$ ), etc. For the SCF states the inversion symmetry ( $g$  or  $u$ ) is given by the joint parity of  $m$  and the  $\eta$ -motion nodal quantum number  $n_\eta$ , i.e. a state is *gerade* or *ungerade* according as  $(n_\eta + m)$  is even or odd.

The SCF protonic energy levels  $(n_\xi, n_\eta, m)$  can also be labelled according to the 'spectroscopic' designation,  $(n_{\nu_2}, n_{\nu_3})$ . The 'quantum numbers'  $n_{\nu_2}$  and  $n_{\nu_3}$  refer to the degree of excitation in the bending, and the anti-symmetric stretching modes, respectively. Conversion from the nodal quantum numbers to the spectroscopic quantum numbers is defined by,

$$2n_\xi + |m| = n_{\nu_2}, \quad (5.1a)$$

$$\text{and,} \quad n_\eta = n_{\nu_3}, \quad (5.1b)$$

This definition comes from the analogy between the mode description given by the SCF description here and that offered by the harmonic oscillator

model in cylindrical coordinates which is used to describe vibrations in a normal linear triatomic molecule like  $\text{CO}_2$ . The coordinate  $\eta$  corresponds to the asymmetric stretching coordinate  $z$ , and the coordinate  $\xi$  corresponds to the bending coordinate  $\rho$ . (For the cylindrically symmetric harmonic oscillator, the energy of the motion corresponding to the doubly degenerate bending modes is  $(2n_\rho + |m| + 1)\hbar\omega$  while the energy of the motion corresponding to the anti-symmetric stretching mode is  $(n_z + 1/2)\hbar\omega'$  [109]).

Figure 5.1 shows the SCF energy level curves for  $(1,0,0)$ ,  $(1,1,0)$ ,  $(0,0,2)$ , and  $(0,1,2)$ . The components of the pairs  $\{(1,0,0), (0,0,2)\}$  and  $\{(1,1,0), (0,1,2)\}$  are nearly degenerate throughout the entire range of  $R$  values. (At  $R \sim 4.60$  a.u., the levels  $(1,0,0)$  and  $(0,0,2)$  are only  $9 \text{ cm}^{-1}$  apart.) Note that in each case both components of the nearly-degenerate pair have the same spectroscopic notation: i.e.  $(n_{\nu_2} = 2, n_{\nu_3} = 0)$  for the first pair and  $(n_{\nu_2} = 2, n_{\nu_3} = 1)$  for the second. This confirms the validity of the relationship between the nodal quantum numbers and the spectroscopic quantum numbers given in equations (5.1). Likewise, the SCF energy levels  $(2,0,0)$  and  $(1,0,2)$ , and also  $(2,1,0)$  and  $(1,1,2)$  are nearly degenerate at all  $R$ .

Table 5.1 lists representative SCF energies at  $R$  values of 3.80, 4.40, and 5.80 a.u.

It is important to understand that the protonic energy eigenvalues (for exact protonic eigenstates, as well as the SCF states computed here) can be *positive* with respect to the reference zero for the system corresponding to the dissociation limit  $\text{F}^- + [\text{HF}]_{\text{eq}}$  (see the definition of the potential surface model in Chapter 2). The situation is completely analogous to that of excited electronic state potential curves for a diatomic molecule which lie above the dissociation limit for the ground electronic state; such states remain bound *electronically* even though they lie formally in the dissociation continuum. In the same way, SCF (or exact) protonic



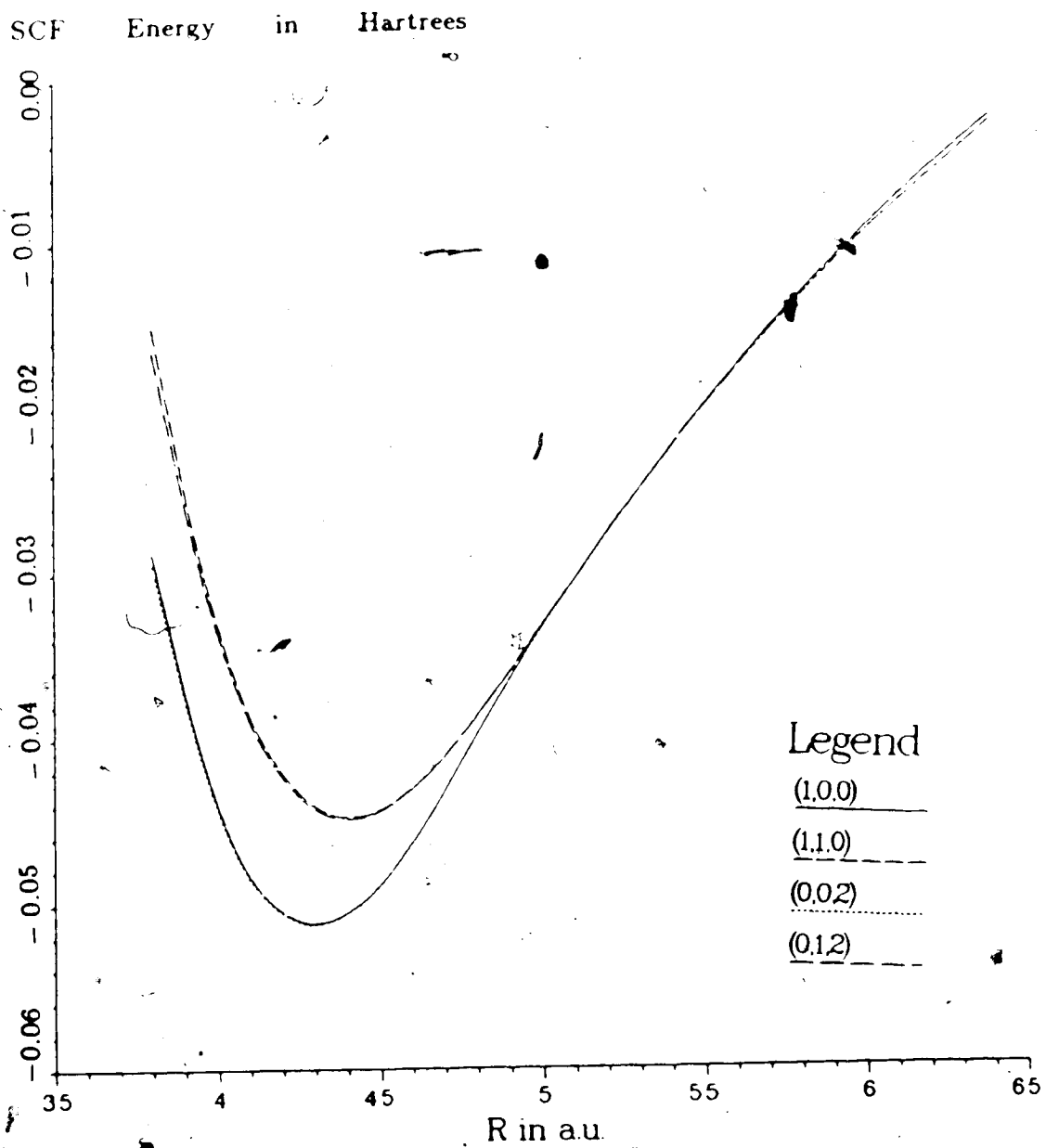


Figure 5.1 Near - degeneracy of SCF pairs  $\{(1,0,0), (0,0,2)\}$  and  $\{(1,1,0), (0,1,2)\}$

Table 5.1

## Some SCF Energies of Protonic States

State ( $n_\xi, n_\eta, m$ )	Energy in Hartrees		
	R=3.80 a.u.	R=4.40 a.u.	R=5.80 a.u.
0,0,0	-0.037272	-0.063431	-0.022999
1,0,0	-0.028723	-0.050539	-0.013592
0,2,0	-0.006468	-0.047387	-0.008849
1,2,0	-0.000172	-0.036809	+0.000554
2,0,0	-0.018313	-0.037435	-0.003970
0,1,0	-0.021842	-0.056427	-0.022999
1,1,0	-0.015001	-0.044754	-0.013592
0,3,0	+0.007653	-0.037105	-0.008848
2,1,0	-0.006006	-0.032638	-0.003970
1,3,0	+0.015178	-0.027715	+0.000554
0,1,1	-0.019560	-0.050705	-0.018382
1,1,1	-0.010997	-0.038770	-0.008865
0,3,1	+0.008189	-0.032704	-0.004206
2,1,1	-0.001179	-0.026507	+0.000860
1,3,1	+0.016555	-0.022674	+0.005246
0,0,1	-0.033624	-0.057045	-0.018382
1,0,1	-0.023814	-0.044022	-0.008866
0,2,1	-0.005363	-0.042288	-0.004206

(Table 5.1 continued)

State	Energy in Hartrees		
$(n_\xi, n_\eta, m)$	R=3.80 a.u.	R=4.40 a.u.	R=5.80 a.u.
1,2,1	+0.002641	-0.031276	+0.005246
2,0,1	-0.012818	-0.030855	+0.000860
0,4,1	+0.020665	-0.022256	+0.008448
2,2,1	+0.011475	-0.019721	+0.014823
3,0,1	-0.001135	-0.017649	+0.010757
0,0,2	-0.029433	-0.050612	-0.013829
1,0,2	-0.018755	-0.037492	-0.004199
0,1,2	-0.016465	-0.044904	-0.013829
1,1,2	-0.006809	-0.032762	-0.004199

states whose energies lie above the reference zero corresponding to *ground state* dissociation remain bound *protonically*.

At a more elementary level of discussion, we note that each protonic state is computed in a particular electronic potential well  $\text{CIDR}_{\text{fit}}(\xi, \eta; R)$  in which there is no freedom to vary  $R$ , and thus the reference level of  $\text{F}^- + [\text{HF}]_{\text{eq}}$  (corresponding to  $R \rightarrow \infty$ ) has no direct relevance as far as this particular configuration at finite  $R$  is concerned. At each  $R$  value the surface  $\text{CIDR}_{\text{fit}}(\xi, \eta; R)$  does have a dissociation limit— i.e. energy plateau — corresponding to the hypothetical configuration  $[\text{F}\dots\text{F}]^- + \text{H}$ , but this lies at a positive energy far above the zero reference level of our potential model or any positive energy level computed here.

As can be seen from Table 5.1, protonic SCF states with positive energies are found at high values of the quantum numbers, and also at very low and very large values of  $R$ . As far as the interpretation of the IR spectrum is concerned, such states have no direct importance. However, they may be useful as basis functions in obtaining more exact energies for the lower protonic states (see Chapter 6).

Figures 5.2-5.6 illustrate the variation of the SCF energy level curves with  $R$  for  $\sigma_g$ ,  $\sigma_u$ ,  $\pi_u$ ,  $\pi_g$ , and  $\delta$  states, respectively.

The many crossings among the SCF energy level curves seen in Figures 5.2-5.6 all obey the *non-crossing rule* given by J. D. Power [137], who derived it in the context of the separable two-center Coulomb problem. Since the SCF approximation artificially makes our problem separable, this non-crossing rule will apply. That is, 'for a crossing to occur between two energy level curves  $(n_\xi, n_\eta, m)$  and  $(n'_\xi, n'_\eta, m')$ , at least two of the three nodal quantum numbers between the two levels must be different'. It should be noted, however, that not all of these crossings *remain* crossings when the *exact* states corresponding to these SCF approximations are calculated. For the non-separable potential the only symmetry is that of  $D_{\infty h}$ ,

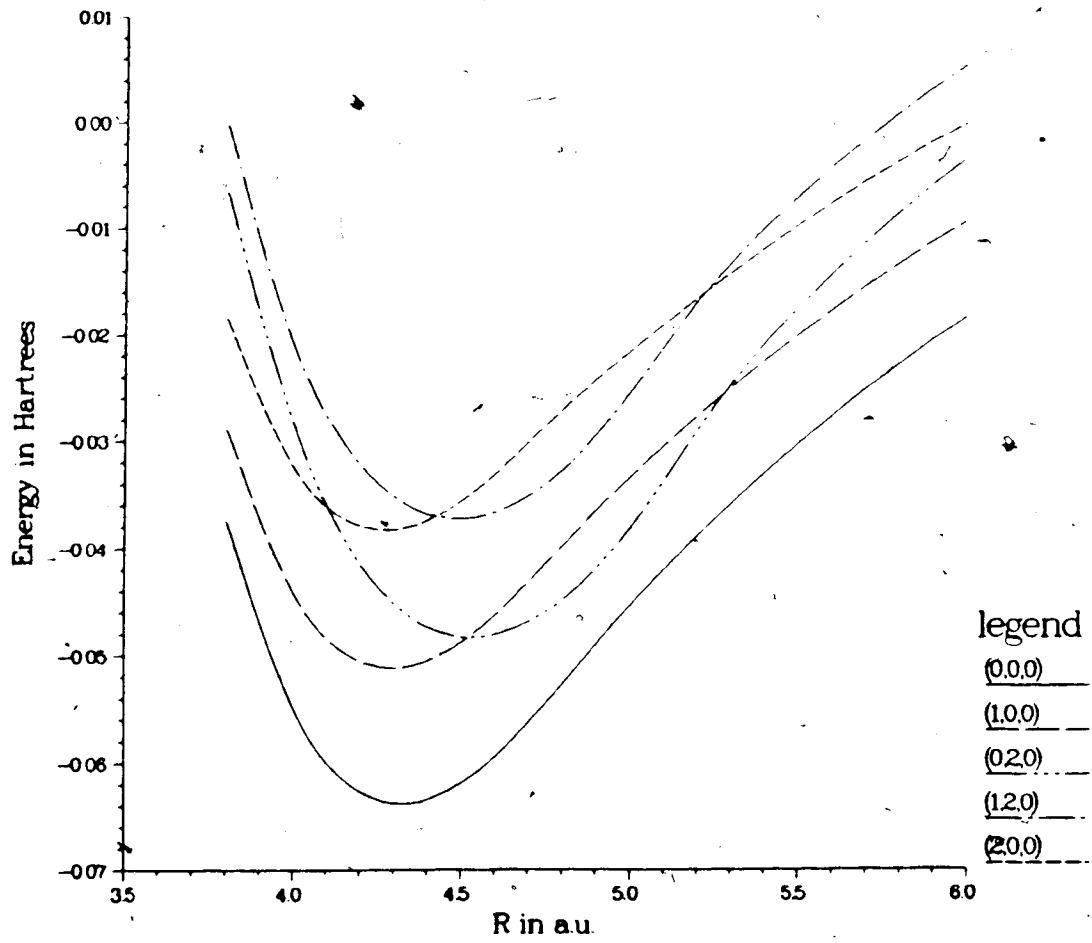


Figure 5.2 SCF Energy vs. R for  $\sigma_g$  states

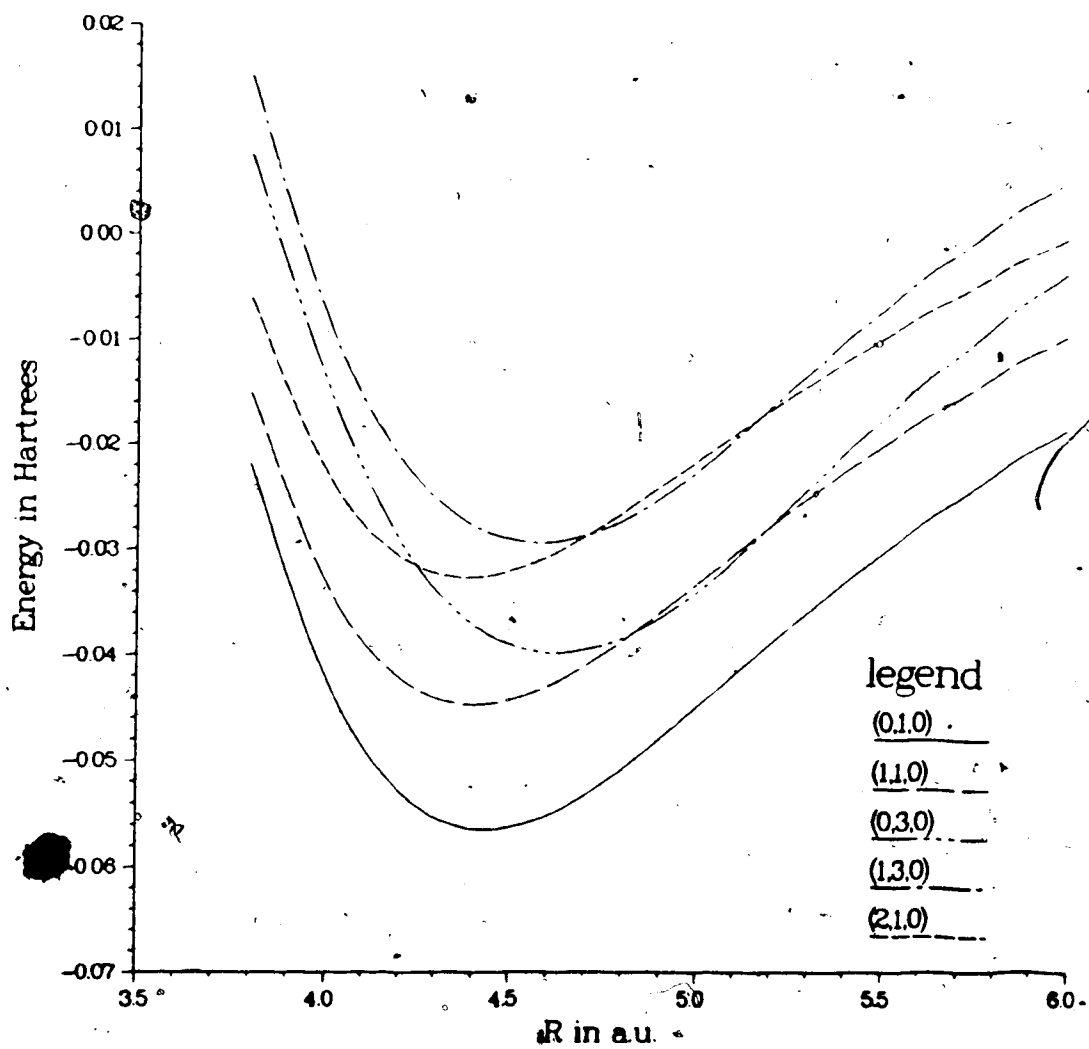


Figure 5.3 SCF Energy vs. R for  $\sigma_g$  states

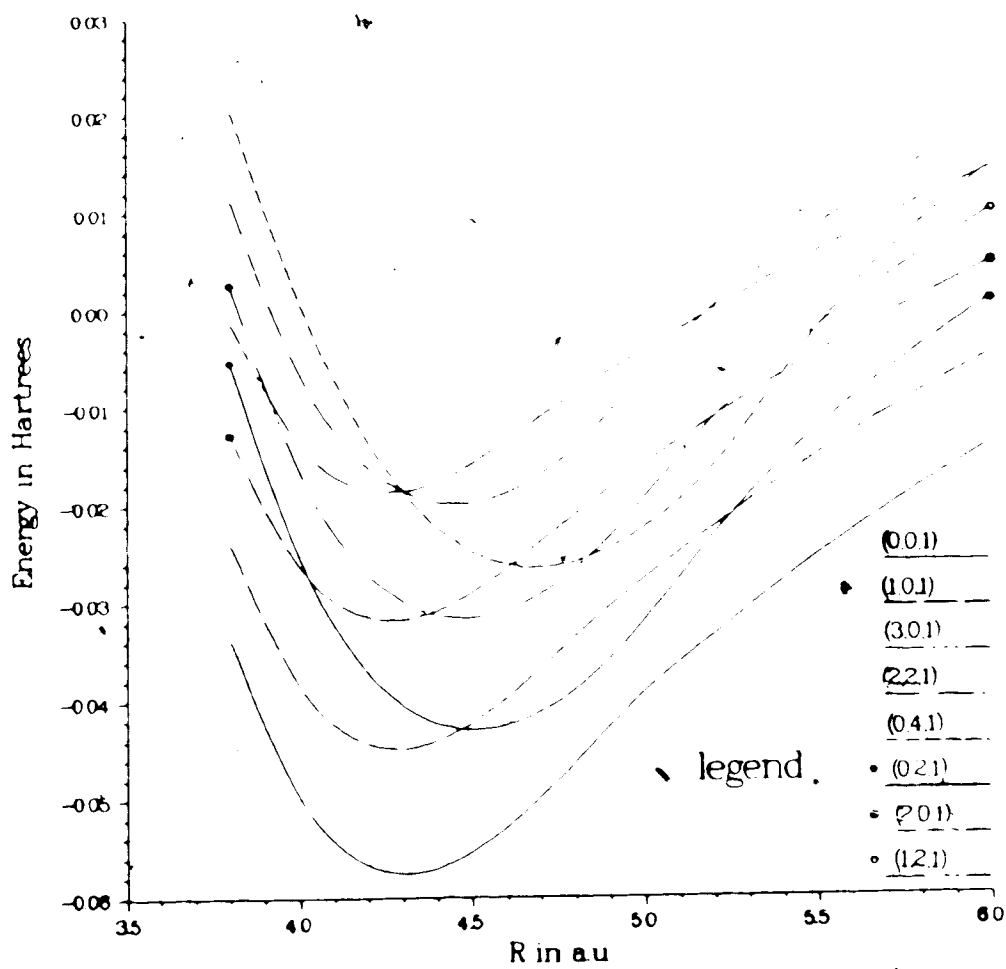


Figure 5.4 SCF Energy vs. R for  $\pi_n$  states

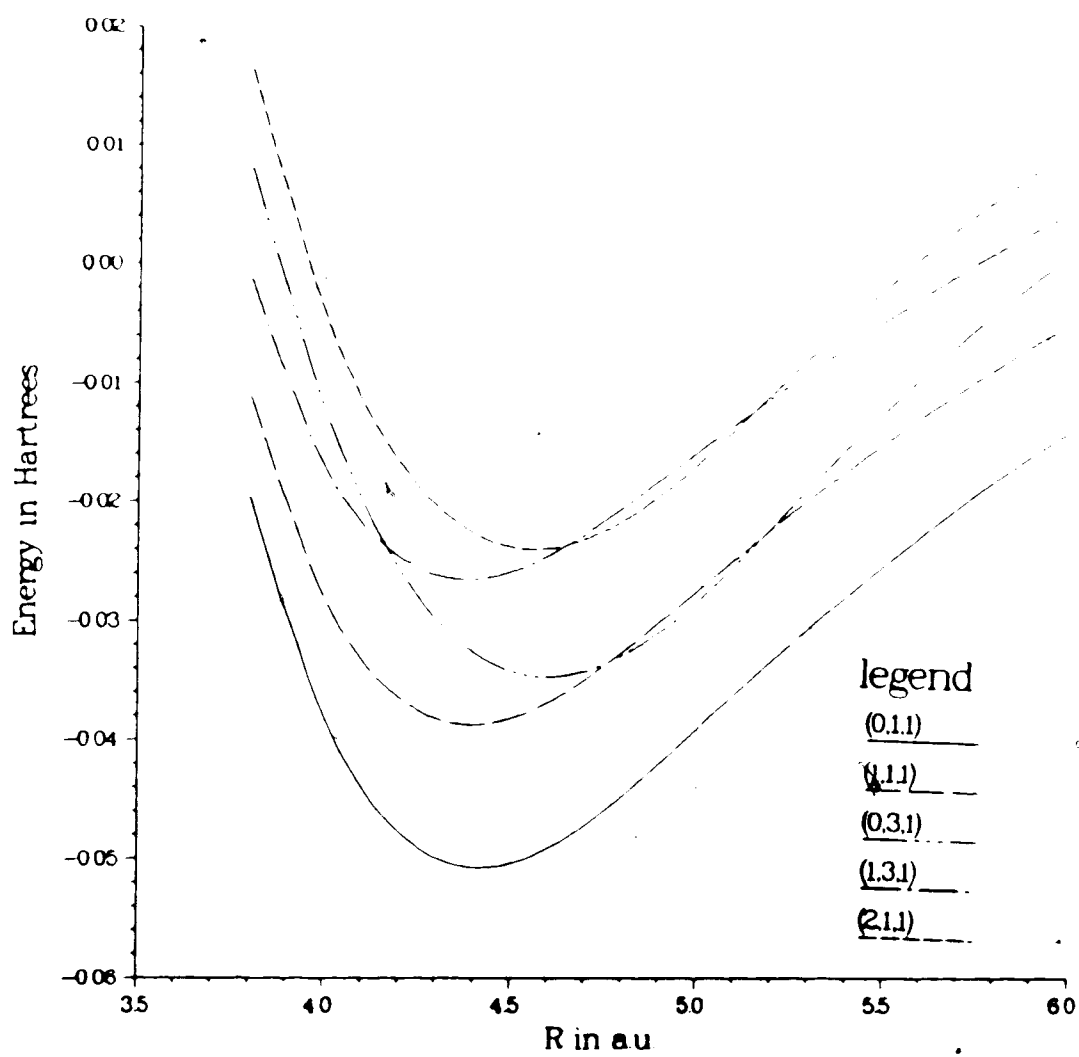


Figure 5.5 SCF Energy vs. R for  $\pi_g$  states



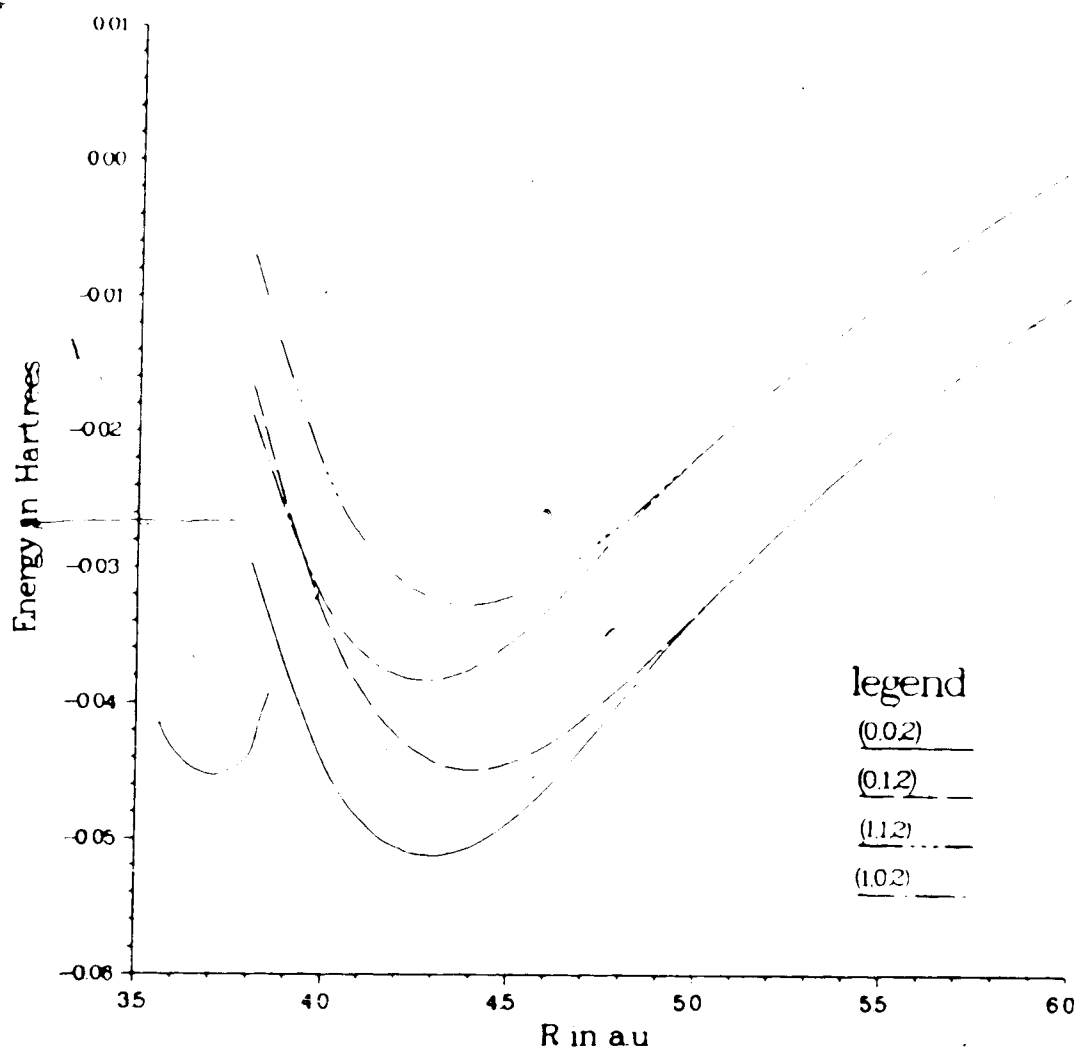


Figure 5.6 SCF Energy vs. R for  $\delta$  states

hence no pair of exact states with the same symmetry under  $D_{\infty h}$  will cross. (This will be discussed in more detail in Chapter 6.)

We noted in Chapter 2 that near the equilibrium configuration at  $R_{\text{eq}} = 4.290513$  a.u. the potential surface  $\text{CIDR}_{\text{fit}}$  behaves differently for the stretching and bending motions. The curvature of the surface for stretching displacements (coordinate  $z$  or  $\eta$ ) decreases as  $R$  increases from the equilibrium value, while the curvature for bending displacements (coordinate  $\rho$  or  $\xi$ ) decreases as  $R$  decreases. The magnitude of this variation with  $R$  is markedly greater for stretching than for bending. These characteristics of the surface have interesting consequences for the SCF potential curves: In general, the zero-point energy and the size of the vibrational quanta for the stretching mode decrease as  $R$  increases, while those for the bending mode decrease as  $R$  decreases (the decrease of the curvature of the potential well has the effect of pulling down the energy levels of the bound states), and the effects for stretching are larger than those for bending.

This results in the minimum of the SCF potential curve for the ground state  $(0,0,0)$  being shifted by  $+0.035$  a.u. (or  $0.018 \text{ \AA}$ ) from the true minimum of the potential itself at  $R_{\text{eq}} = 4.290513$  a.u. Furthermore, the SCF energy level curves  $\{(n_{\nu_2} = n', n_{\nu_3} = 0); n' = 1, 2, 3, \dots\}$  have their minima displaced to the left of  $R_e^0$  (see Figure 5.7) while the SCF energy curves  $\{(n_{\nu_2} = 0, n_{\nu_3} = n''); n'' = 1, 2, 3, \dots\}$  have their minima displaced to the right of  $R_e^0$  (see Figure 5.8). As the degree of excitation in one mode becomes greater in a SCF state it is affected to a greater degree by the nature of the potential surface in the direction of that particular vibrational motion. Therefore the curves  $\{(n', 0)\}$  and  $\{0, n''\}$  would have their minima shifted progressively further away from  $R_e^0$  (to the left and right, respectively) as  $n'$  and  $n''$  are increased.

From the figures we also note that (as expected) the displacements in the minima for the  $\{(0, n'')\}$  curves are much larger than they are for the  $\{(n', 0)\}$

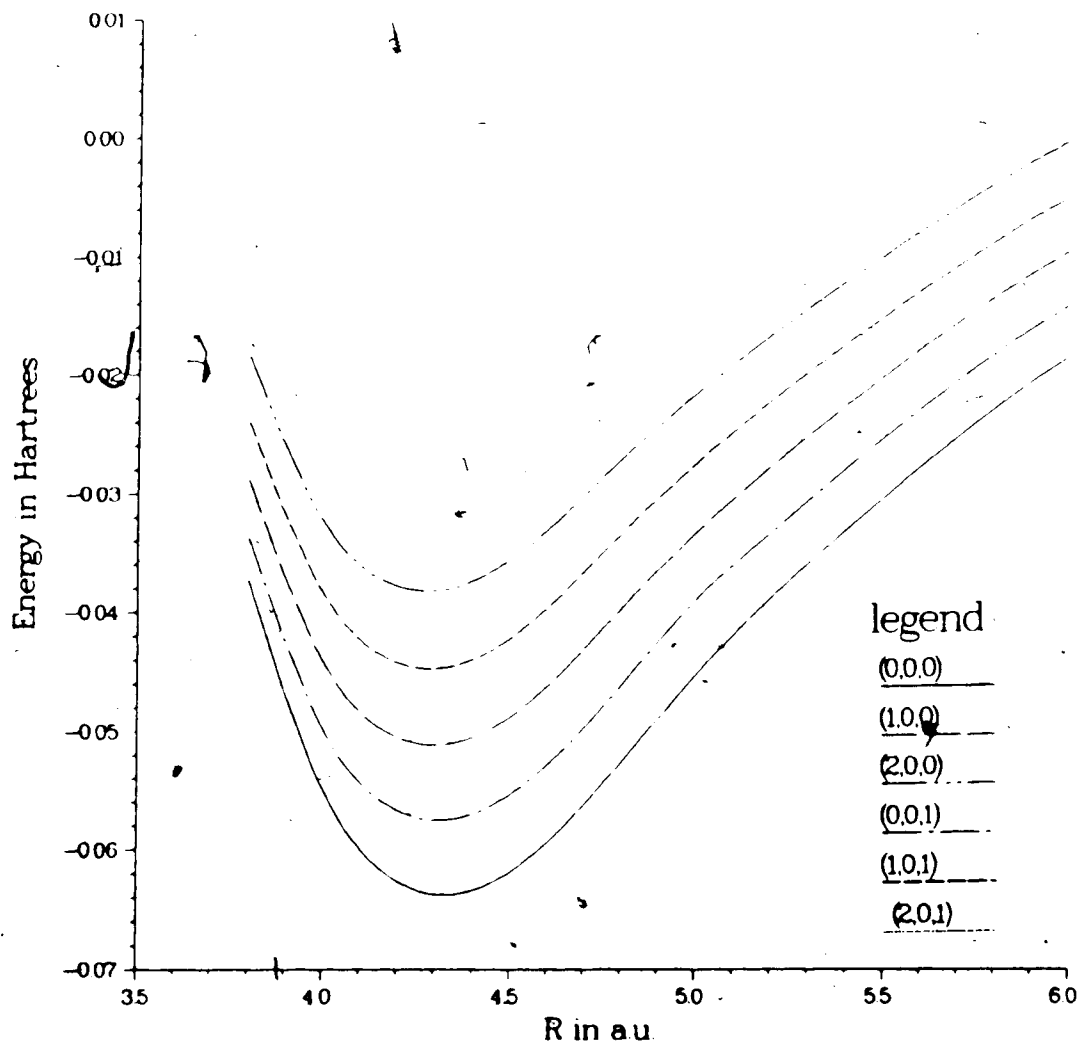


Figure 5.7 SCF Energy vs. R for  $(n', 0)$  states

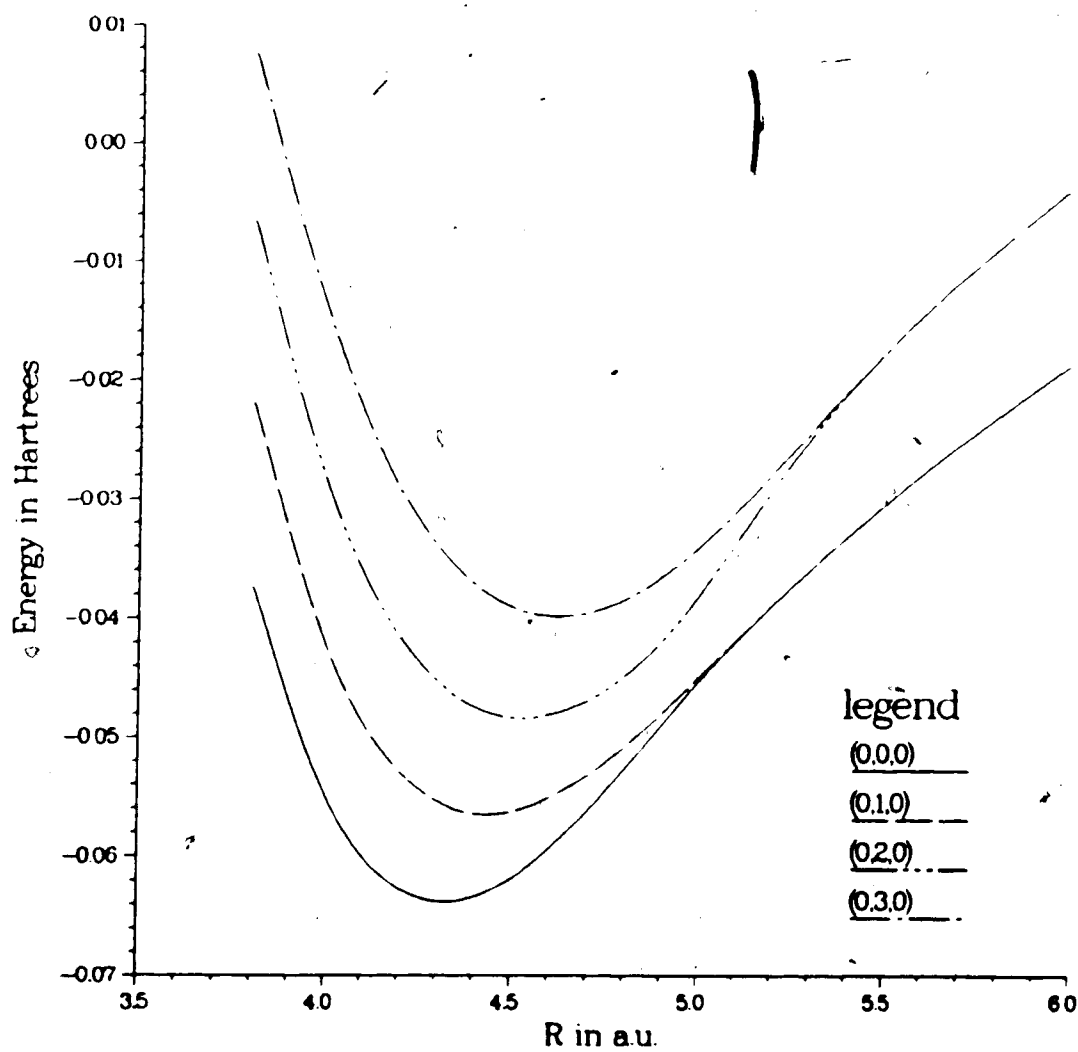


Figure 5.8 SCF Energy vs. R for  $(0, n^l)$  states

curves. For example, vibrational excitation in the anti-symmetric stretching mode to the (0,3) state leads to  $\Delta R_{min}$  of +0.297 a.u. while it is -0.038 a.u. when excited in the bending mode to the (3,0) state.

The plots of SCF energy vs.  $R$  also show that SCF levels ( $n_\xi, n_\eta = n_1, m$ ) and ( $n_\xi, n_\eta = n_1 + 1, m$ ), where  $n_1$  is even, become asymptotically degenerate at large  $R$ . For example (0,0,2) and (0,1,2) become degenerate at  $R \sim 5.00$  a.u. (see Figure 5.6) while (0,0,0) and (0,1,0) become degenerate at  $R \sim 5.35$  a.u. (see Figure 5.8). This (g,u) pair-wise degeneracy is caused by the potential surface  $CIDR_{fit}$  progressing from a single minimum to double minimum well as  $R$  increases. As the two minima move apart and the 'interaction' between them decreases, the (g,u) pair become more closely degenerate.

Figures 5.9 and 5.10 illustrate the effect change in  $R$  has on the  $\eta$ - motion wave functions  $g(\eta; R)$  for the *gerade* state (0,2,0), and *ungerade* state (0,3,0), respectively. In each case, as the potential energy surface  $CIDR_{fit}(\xi, \eta; R)$  changes from a single minimum (at  $R=4.00$  a.u.) to a fairly well-separated double minimum (at  $R=6.00$  and  $6.20$  a.u.),  $g(\eta; R)$  changes from a wave function localised around  $\eta = 0$ , to one that is almost completely localised within the two potential wells.

Figure 5.11 shows the SCF wave function for  $\xi$ - motion,  $f(\xi; R)$ , for the states (0, 0,  $m$ ),  $m=0,1,2$ , at  $R=4.40$  a.u. (Shape of the SCF potential for this motion shows no drastic change vs.  $R$ .) As  $m$  increases, the effect of the centrifugal potential term  $(m^2 - 1)/(\xi^2 - 1)^2$  on this bending mode wave function is clearly seen. The concentration of the amplitude close to the origin, especially for  $m = 0$ , makes the advantages of the Langer transformation that we used to solve the  $\xi$ - equation quite clear (see Chapter 4) since the region at the origin is then greatly expanded.

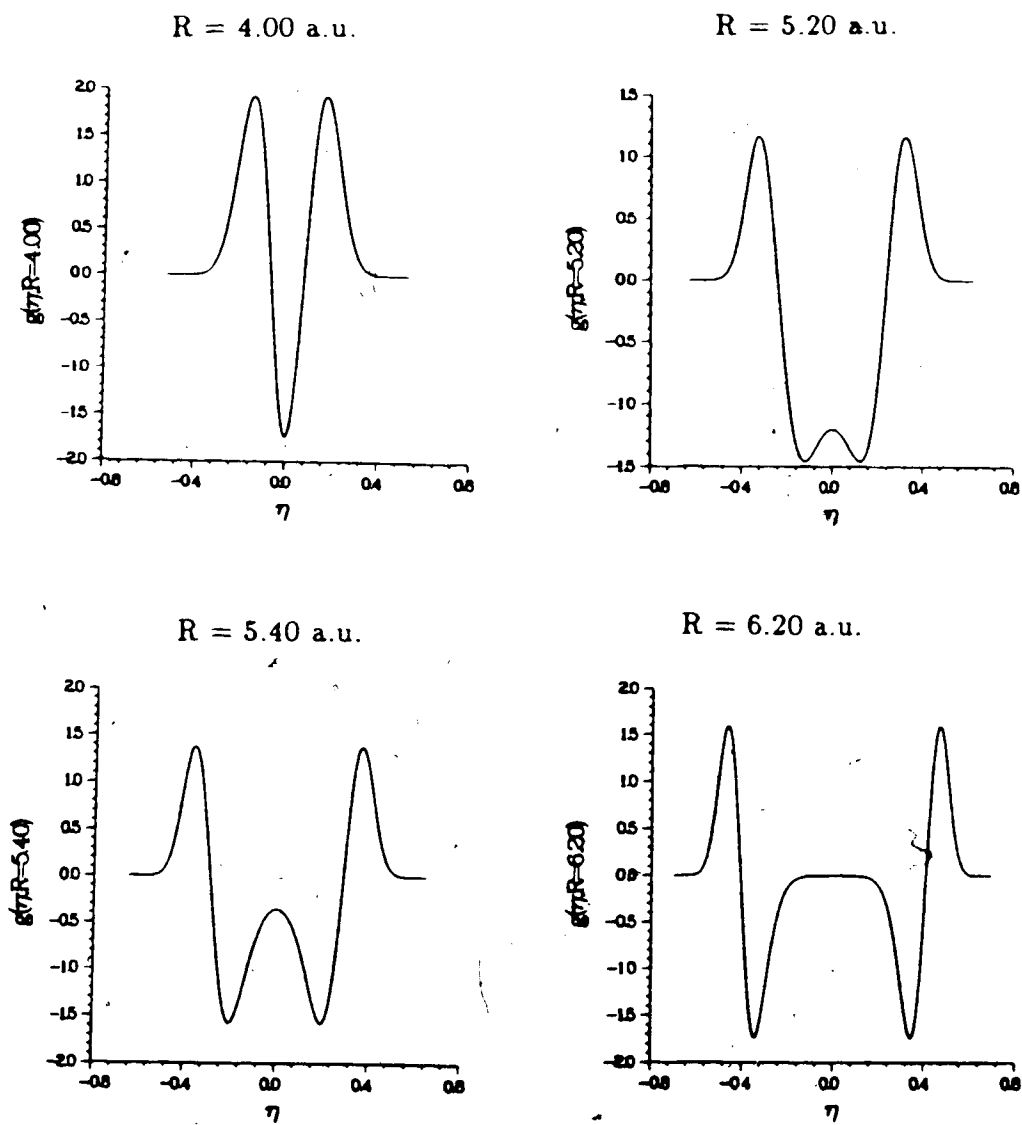


Figure 5.9

 $g(\eta; R)$  in  $(0, 2, 0)_R$

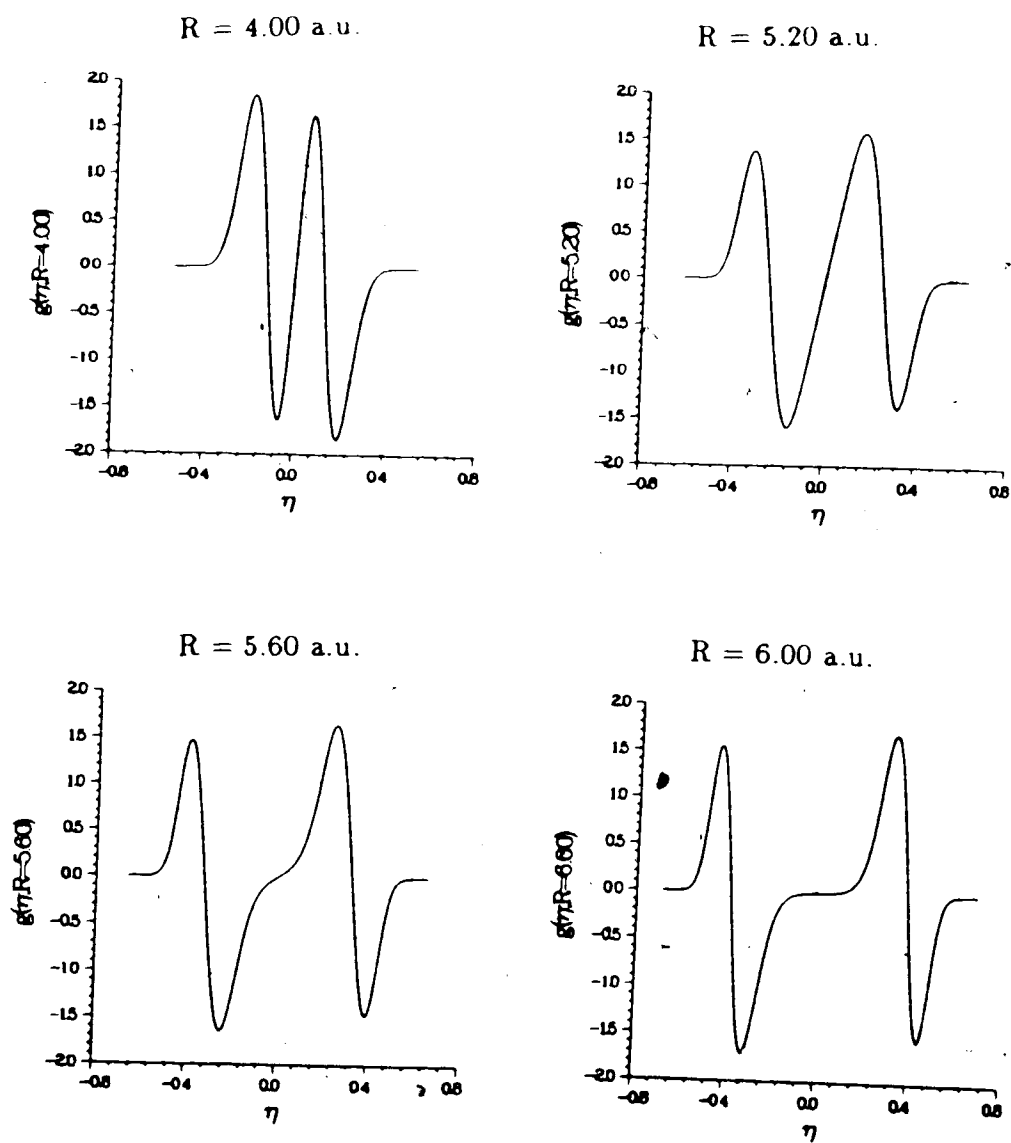


Figure 5.10  $g(\eta; R)$  in  $(0, 3, 0)_R$

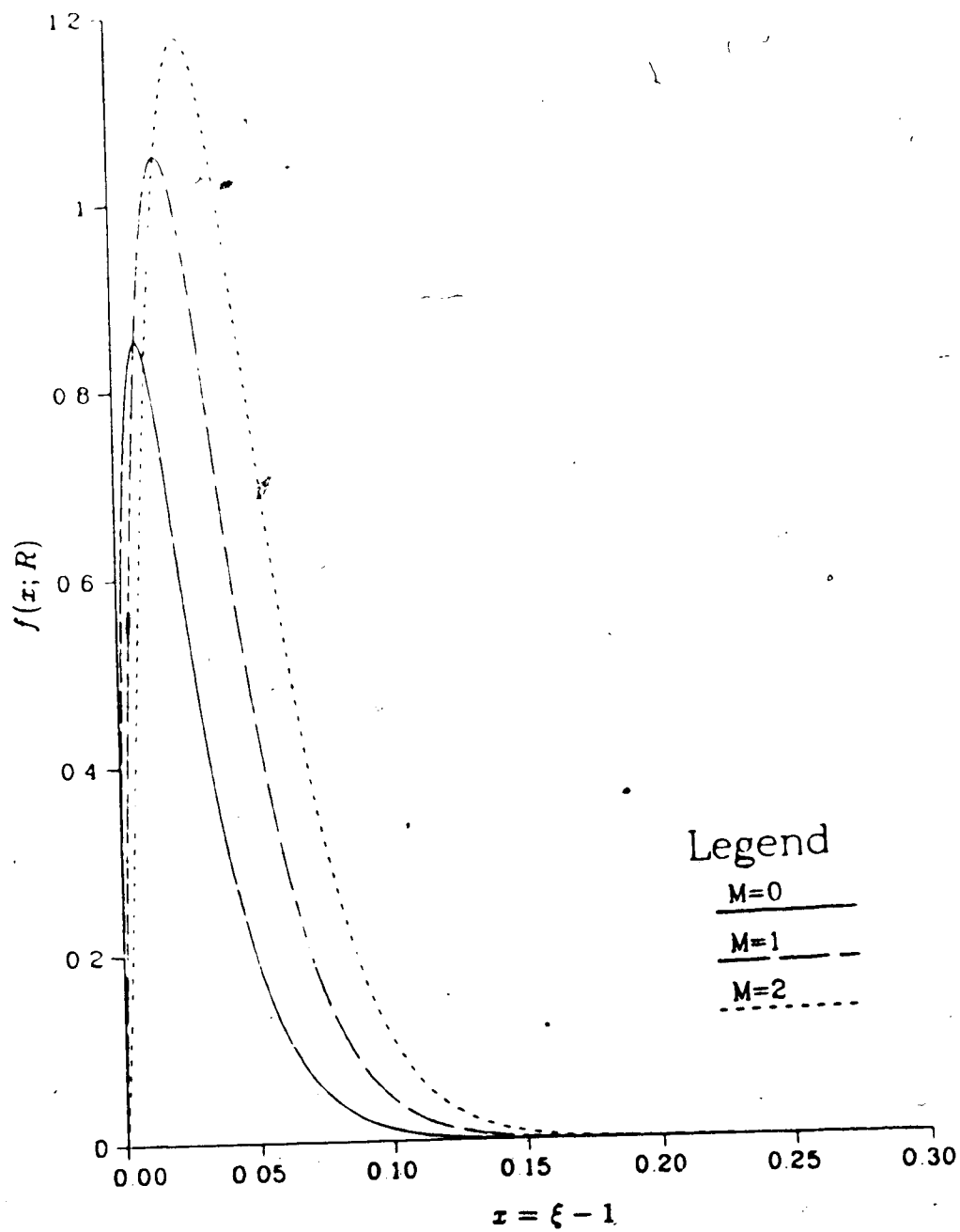


Figure 5.11  $f(x; R)$  vs.  $x$  for  $(0, 0, m)$   
at  $R = 4.40$  a.u.



## B. Frequencies of Infra-Red Spectral Transitions

At this point we may estimate roughly the frequencies of the allowed IR transitions of our model of the isolated  $[\text{FHF}]^-$  ion.

Since the  $[\text{FHF}]^-$  ion belongs to the  $D_{\infty h}$  point symmetry group, (and under normal conditions all transitions initiate from the ground vibrational state of  $\sigma_g$  symmetry), for the non-vanishing of the IR transition moment,

- (1). only  $g \rightarrow u$  transitions are allowed,
- (2). only transitions with  $\Delta m = 0$  or  $\pm 1$  are allowed.

These two selection rules mean that the allowed transitions are of the type  $a\nu_2 + b\nu_3 + c\nu_1$  ( $a, b, c$  integers), where *either a or b but not both* may be even (including zero) and  $c = 0, 1, 2, \dots$

What we have at this stage are only the results of SCF calculations of the proton dynamics so that we cannot compute the values for transitions involving  $\nu_1$  (symmetric stretching of F...F) mode. Instead, we limit ourselves to the computation of  $a\nu_2 + b\nu_3$  (on which framework Franck-Condon progressions of  $c\nu_1$  can occur.)

It must also be pointed out that the SCF states are *not* the exact protonic states which will be known only after we perform Configuration Interaction (CI) calculations (see Chapter 6). Thus the theoretical vibrational frequencies that are given below will be modified somewhat when the exact protonic (CI) states are calculated. It is expected that the CI correction would be the smallest for the ground protonic state (of the order of  $10 \text{ cm}^{-1}$ ) and would progressively increase for the higher excited states. (The SCF approximation becomes poor at high energies with the interaction between the SCF states growing both in number and magnitude.) Furthermore, in the cases of 'avoided crossings' of protonic energy

level curves (see the next Chapter) the  $\nu_1$  dynamics may yield results quite different from the predictions of the adiabatic approximation.

Since all the experimental IR spectra obtained to date have frequencies no higher than  $5000\text{-}6000\text{ cm}^{-1}$ , the only transitions of the form  $a\nu_2 + b\nu_3$  that we would be interested in from a spectroscopic point of view are  $\nu_3$ ,  $\nu_2$ ,  $3\nu_3$ ,  $3\nu_2$ ,  $2\nu_3 + \nu_2$ ,  $\nu_3 + 2\nu_2$ .

For a precise evaluation of the transition energy for  $a\nu_2 + b\nu_3$ , we need to know the initial and final total vibrational energies. That is,  $\Delta E$  for the transition  $a\nu_2 + b\nu_3$  is given by,

$$E^{total}(n_{\nu_2} = a, n_{\nu_3} = b, n_{\nu_1} = 0) - E^{total}(n_{\nu_2} = 0, n_{\nu_3} = 0, n_{\nu_1} = 0).$$

However, since we have not analysed the  $\nu_1$  dynamics, the  $\Delta E$ 's have to be determined (approximately) in some other fashion, using the SCF energy level curves.

Clearly, any attempt to estimate the  $\Delta E$  by a vertical transition from the minimum of the  $(0,0,0)$  ground state curve,  $R_e^0$ , would lead to erroneous values for the frequencies (especially for any transitions involving the anti-symmetric stretching mode). This follows from the significant displacements of the minima of the higher energy level curves. Instead we determine the  $\Delta E$  for the transition by the difference in energy between the two SCF levels, evaluated at their respective minima. i.e. for the transition  $a\nu_2 + b\nu_3$ ;

$$\Delta E = E^{(SCF)}(n_{\nu_2} = a, n_{\nu_3} = b)_{R=R'_e} - E^{(SCF)}(n_{\nu_2} = 0, n_{\nu_3} = 0)_{R=R_e^0}$$

where  $R'_e$  and  $R_e^0$  are the minima of the SCF energy level curves  $(a, b)$  and  $(0, 0)$ , respectively. This would give a reasonably accurate estimate for the transition if at the same time we also make a correction for the difference in zero-point energies of the lowest *total* vibrational state in each SCF level curve (i.e. the difference

between  $(E^{total}(n_{\nu_2} = a, n_{\nu_3} = b, n_{\nu_1} = 0) - E^{(SCF)}(a, b)_{R'_e})$  and  $(E^{total}(n_{\nu_2} = 0, n_{\nu_3} = 0, n_{\nu_1} = 0) - E^{(SCF)}(0, 0)_{R'_e})$ . ) This zero-point energy is estimated here for transitions involving  $a = 0$  by using the values calculated by Barton and Thorson [29] in their work on non-bending  $[\text{FHF}]^+$ . For transitions with  $b = 0$ , the zero-point energy differences are taken to be half as much as those for  $a = 0$ , and for combination tones ( $a \neq 0, b \neq 0$ ) intermediate values are assumed.

It should again be emphasized at this point that our eventual goal is to understand the crystalline  $\text{KHF}_2$  spectrum with a model of the isolated  $[\text{FHF}]^-$  ion. It is a major assumption of this work that the *main* spectral features and the *overall* structure observed in the IR spectrum are the result of vibrational dynamics *within* the isolated bifluoride system. Effects of the crystal environment have not been included in our model. It would be injudicious at this stage to attempt to obtain quantitative agreement with the experimental frequencies for the gaseous phase free ion (let alone the crystalline spectrum) not only because the dynamical analysis is incomplete at this stage, but also (as the work by Janssen et al. shows) the vibrational frequencies are dependent on the level of electronic calculation of the potential surface.

The vibrational frequencies evaluated in this work (TW) are listed in Table 5.2. Below each TW value, the zero-point energy difference correction is included in parentheses. Also listed in Table 5.2 are the values from previous theoretical calculations by Lohr and Sloboda (LS) [93], Barton and Thorson (BT) [29], Almlöf (AL) [94], and two sets of values by Janssen et al. (JASB1 and JASB2) [71]. (See Chapter 1 for brief descriptions of the methods used in previous theoretical calculations.) Experimental values by Coté and Thompson (CT) [64]— for solid  $\text{KHF}_2$ — and by Kawaguchi and Hirota (KH) [63,141]— for the free  $[\text{FHF}]^-$  ion in the gaseous state— are also listed. (Note that the values quoted

Table 5.2

Frequencies for the IR-Allowed Lower Transitions in  $\text{cm}^{-1}$ 

	$\nu_3$ (0,1,0)	$\nu_2$ (0,0,1)	$3\nu_3$ (0,3,0)	$3\nu_2$ (1,0,1)	$2\nu_2 + \nu_3$ (1,1,0)	$\nu_2 + 2\nu_3$ (0,2,1)
TW	1601 (-65)	1371 (-30)	5267 (-100)	4176 (-60)	4179 (-80)	4578 (-80)
LS	1669	1378	6159	4118	4122	4897
BT	1520	-	5103	-	-	-
AL	1497	-	5157	-	-	-
JASB1	1698	1449	-	-	-	-
JASB2	1427	1363	-	-	-	-
KH	1331	1286	-	-	-	-
CT	1450	1225 -1274	5090	3651 -3828	-	-

Table 5.3

Frequencies for the IR-Allowed Higher Transitions in  $\text{cm}^{-1}$ 

	Transition	Computed value (TW)
$4\nu_2 + \nu_3$	$\{(0, 0, 0) \rightarrow (2, 1, 0)\}$	6838
$5\nu_2$	$\{(0, 0, 0) \rightarrow (2, 0, 1)\}$	7028
$3\nu_2 + 2\nu_3$	$\{(0, 0, 0) \rightarrow (1, 2, 1)\}$	7065
$2\nu_2 + 3\nu_3$	$\{(0, 0, 0) \rightarrow (1, 3, 0)\}$	7556
$\nu_2 + 4\nu_3$	$\{(0, 0, 0) \rightarrow (0, 4, 1)\}$	8174
$5\nu_2 + 2\nu_3$	$\{(0, 0, 0) \rightarrow (2, 2, 1)\}$	9637
$7\nu_2$	$\{(0, 0, 0) \rightarrow (3, 0, 1)\}$	9910

by Kawaguchi and Hirota in reference [63] are in error and have been corrected in reference [141].) Table 5.3 lists frequencies of some of the higher transitions computed in this work (TW). We see that our value for  $\nu_3$ , like all of the previous theoretical values, is higher than the experimental result in the gas phase (KH). (Except for JASB2, all the theoretical values are also somewhat higher than the experimental frequency in the solid phase given by CT.)

There is less variation among the theoretical values for  $\nu_2$  by TW, LS, and JASB2; all of which are about 50-100  $\text{cm}^{-1}$  higher than the experimental values in both gas and solid phase.

The recently measured (KH) value of  $\nu_3 = 1331 \text{ cm}^{-1}$  for the gas phase free ion  $[\text{FHF}]^-$  shows, reasonably enough, a decrease in the curvature of the potential surface in the protonic stretching direction (compared to the solid state  $\text{KHF}_2$  environment). It is interesting to note that this value is close to  $\nu_3$  measured for  $[\text{FHF}]^-$  isolated in an Ar matrix; 1364  $\text{cm}^{-1}$  [56], and 1377  $\text{cm}^{-1}$  [142].

The theoretical values for  $\nu_2$  and especially  $\nu_3$  should move closer to the gas phase free ion frequency with the use of *ab initio* potential surfaces at higher levels of sophistication (i.e. more extensive basis set). In this regard, although Janssen et al.'s results for  $\nu_3$  do not show convergence with respect to the basis set, the trend does seem to be in the direction of lower frequencies (i.e. moving towards the gas phase frequency of KH.)

Almlöf as well as Lohr and Sloboda used a local polynomial representation of their potential surfaces. Such a polynomial model, because of the unphysical characteristics at high coordinate values, leads to errors in the computed frequencies for the higher transitions. In comparison, the global potential model  $\text{CIDR}_{\text{fit}}$  used in this work behaves physically at higher energies.

A more serious source of error in Lohr and Sloboda's results (particularly for  $\nu_3$ ,  $\nu_2 + 2\nu_3$ ,  $3\nu_3$ ) is due to evaluation of the frequencies as vertical transition

energy differences (at  $R=4.3313$  a.u.). As we showed earlier, because of the significant displacement of the minima of the excited SCF energy level curves, this leads to overestimation of the frequencies. For example, their value for  $3\nu_3$  is about  $1000\text{ cm}^{-1}$  higher than the other theoretical or experimental frequencies.

Our estimated values for the transition frequencies give valuable information on the anharmonicity in the vibrational modes. If the protonic motion were perfectly harmonic, then the ratio  $(a\nu_2 + b\nu_3)/(a \times \nu_2 + b \times \nu_3)$  should be exactly 1.0. Consider the following ratios from our results:

$$3\nu_3/3 \times \nu_3 = 1.10$$

$$3\nu_2/3 \times \nu_2 = 1.015$$

$$5\nu_2/5 \times \nu_2 = 1.025$$

$$7\nu_2/7 \times \nu_2 = 1.033$$

$$(2\nu_2 + \nu_3)/(2\nu_2) + (\nu_3) = 0.956$$

$$(\nu_2 + 2\nu_3)/(\nu_2) + (2\nu_3) = 0.961$$

These ratios show that the  $\nu_3$  mode (anti-symmetric stretching) is much more anharmonic than the  $\nu_2$  (bending) mode. This, of course, is exactly what we would have expected, for as our modelling with the potential surface with a Taylor polynomial in  $(z, \rho)$  showed in Chapter 2, the quartic term in the  $z$ -coordinate is relatively much larger than the quartic term in the  $\rho$ -coordinate. (See equation 2.5 and Table 2.1.)

We see that the anharmonicity in the  $\nu_2$  vibrational mode increases with increasing excitation in that mode. This is because in higher excited states the proton samples a greater range of the coordinate space. As the magnitude of

the coordinate value increases, the anharmonic terms in the potential become relatively more important.

We note that the frequency for the transition  $2\nu_2 + \nu_3$  is lower than the sum of  $2\nu_2$  and  $\nu_3$ . The negative biquadratic coupling term  $z^2\rho^2$  in the Taylor series representation of the potential surface is the major source of this depression of the combination tone frequency. This phenomenon is illustrated even more dramatically by the fact that  $(2\nu_2 + \nu_3) \sim 3\nu_2$ , despite  $\nu_3$  being  $200 \text{ cm}^{-1}$  higher than  $\nu_2$ , and the fact that  $(4\nu_2 + \nu_3)$  is actually lower than  $5\nu_2$ . Similarly,  $\nu_2 + \nu_3$  — which is a forbidden transition — is  $2870 \text{ cm}^{-1}$  while the sum of  $\nu_2$  and  $\nu_3$  is more than  $100 \text{ cm}^{-1}$  higher at  $2972 \text{ cm}^{-1}$ . All these observations clearly illustrate the strong anharmonic coupling which exists between the protonic vibrational modes.

### C. Isotope Effects

Figure 5.12 shows the variation of the SCF energy levels  $(0,0,0)$  (i.e. ground level),  $(0,1,0) (\equiv \nu_3)$ , and  $(0,0,1) (\equiv \nu_2)$  for the isotopic systems  $[\text{FDF}]^-$  and  $[\text{F}\mu\text{F}]^-$ . These SCF states were calculated from the same programs as were the protonic states, the only change made being the value for the reduced mass.

It can be seen that the SCF energy curves for  $[\text{F}\mu\text{F}]^-$  are situated higher (and have greater zero-point energies) than the corresponding  $[\text{FHF}]^-$  curves. On the other hand, the SCF energy curves of  $[\text{FDF}]^-$  are situated lower (and have smaller zero-point energies) and also have narrower inter-curve spacing than the  $[\text{FHF}]^-$  analogues. This is a direct result of the change in the reduced mass of the light particle, from deuteron, through proton, to muon. (In the example of the simple harmonic oscillator, the zero-point energy, and the energy level spacing is proportional to  $(\text{reduced mass})^{-1/2}$ .)



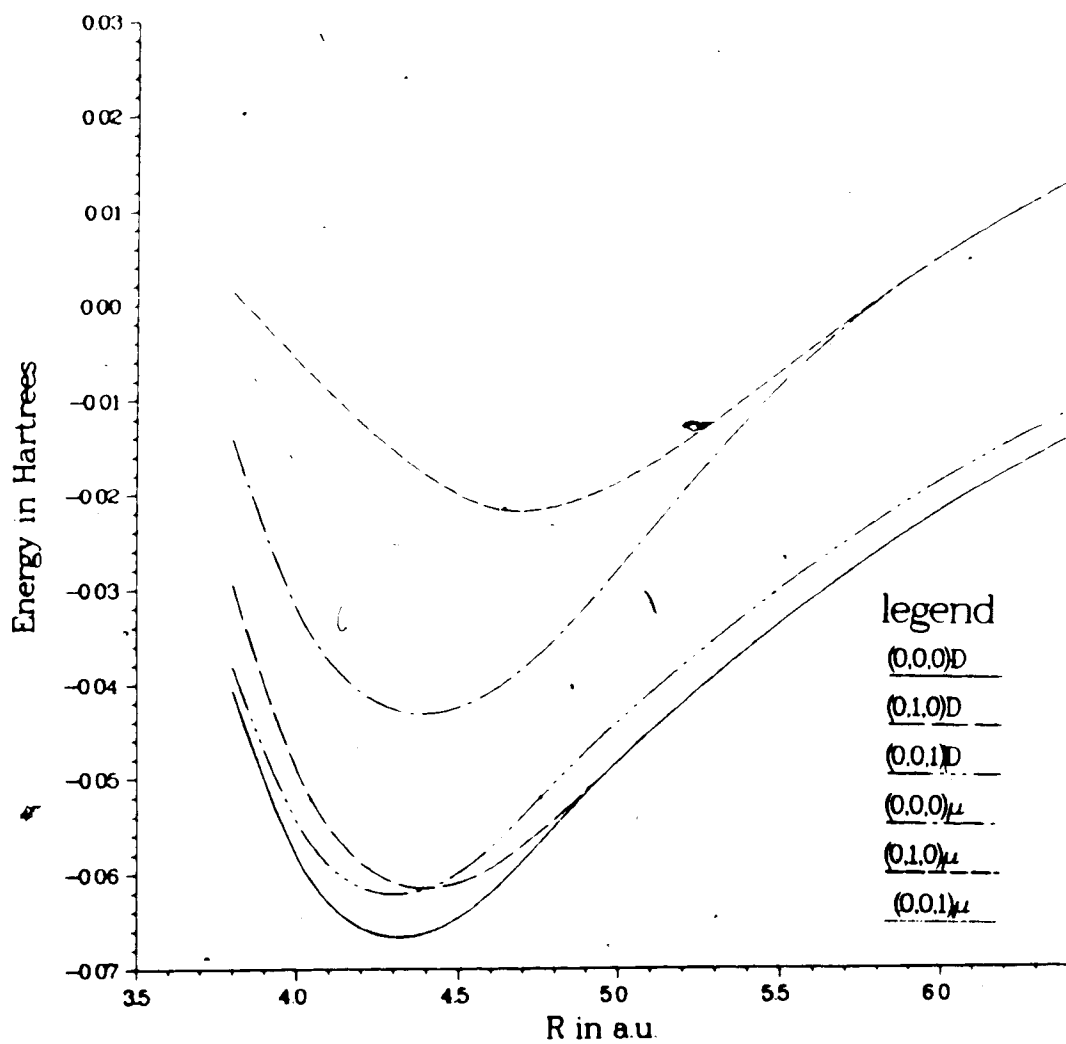


Figure 5.12. SCF Energy vs. R for  $[FDF]^-$  and  $[F\mu F]^-$

It should be noted that regardless of the mass, the proton, the deuteron, and the muon all move on the same potential surface,  $CIDR_{fit}(\xi, \eta, \zeta; R)$ . As the isotopic particle becomes lighter it samples a greater region of the potential surface and the wave functions extend over a greater range of the coordinate space. This is illustrated by Figures 5.13 and 5.14 which show the functions  $\{f(x; R)\}$  and  $\{g(\eta; R)\}$  of the state  $(0, 0, 1)_{R=4.40}$  for the systems  $[FDF]^-$ ,  $[FHF]^-$ , and  $[F\mu F]^-$ . This also means that the degree of anharmonicity exhibited by these systems will be in the order,  $[F\mu F]^- > [FHF]^- > [FDF]^-$ . This is confirmed by considering the vibrational frequencies given in Table 5.4. (In computing these values the zero-point energy difference corrections have not been made.)

From these frequencies,

$$3\nu_{3,D}/3 \times \nu_{3,D} = 1.085, \quad \text{and}$$

$$3\nu_{2,D}/3 \times \nu_{2,D} = 1.012,$$

while,

$$3\nu_{3,\mu}/3 \times \nu_{3,\mu} = 1.110, \quad \text{and}$$

$$3\nu_{2,\mu}/3 \times \nu_{2,\mu} = 1.032,$$

Comparing these ratios with the corresponding ones for  $[FHF]^-$  we see that the order of anharmonicity is indeed as was predicted earlier. Furthermore, it should be noted that in each case, the anti-symmetric stretching mode is *more* anharmonic than the bending mode.

We also find  $(\nu_{3,H}/\nu_{3,D}) = 1.412$  and  $(\nu_{2,H}/\nu_{2,D}) = 1.392$  compared with  $(m_{r,[FDF]^-}/m_{r,[FHF]^-})^{1/2} = 1.396$ , again showing the greater anharmonicity in the  $\nu_3$  mode. In comparison, Barton and Thorson and Ketelaar and Vedder obtain

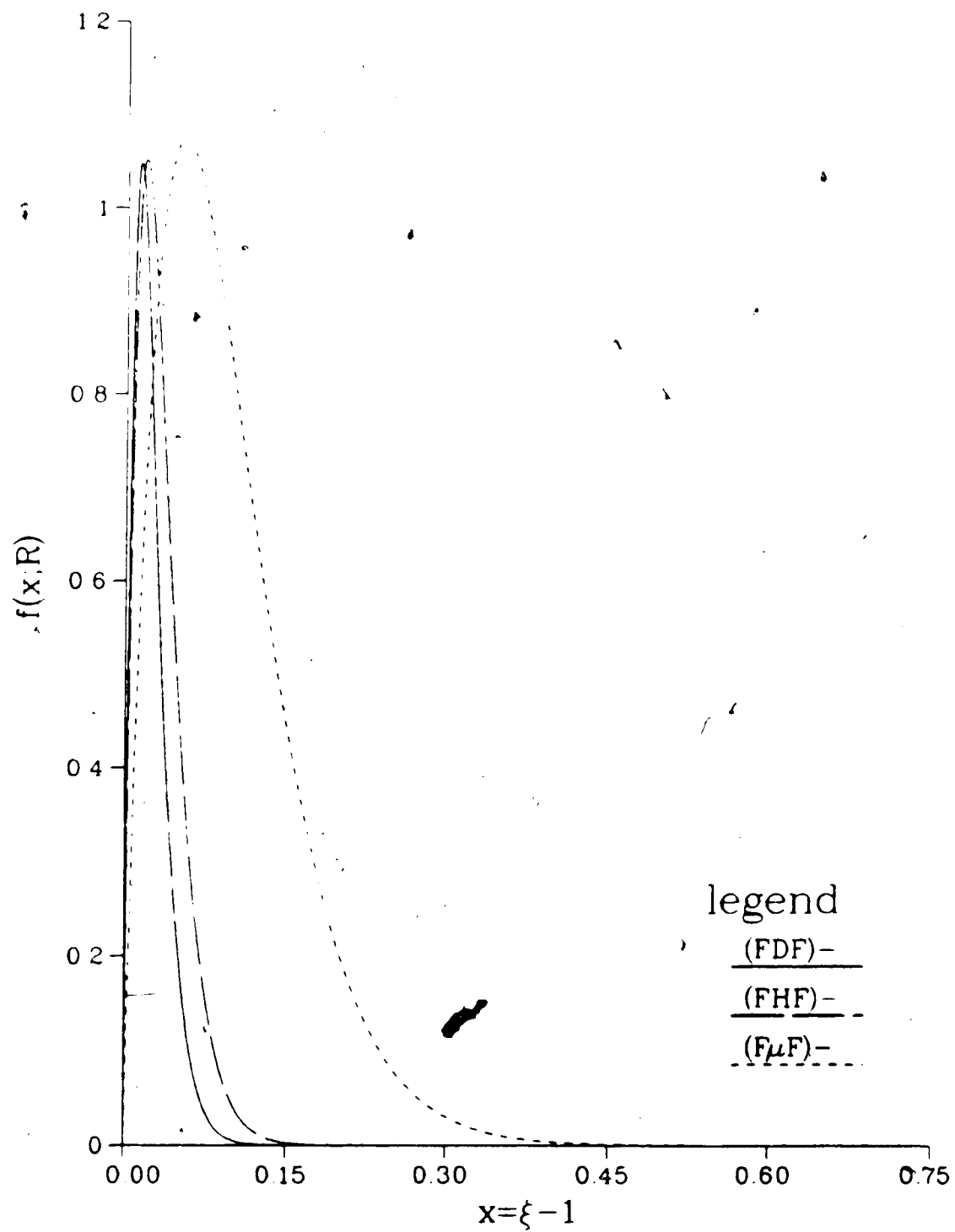


Figure 5.13  $f(x; R)$  vs.  $x$  for  $(0, 0, 1)$  at  $R = 4.40$  a.u.

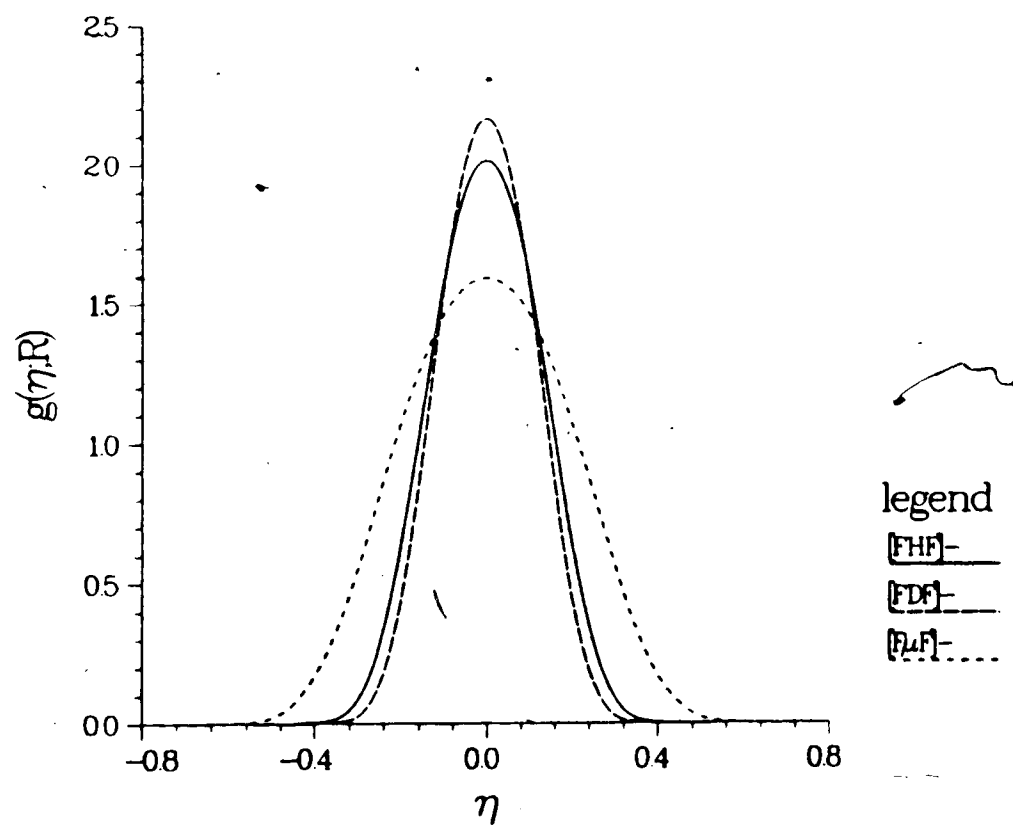


Figure 5.14 •  $g(\eta; R)$  vs.  $\eta$  for  $(0,0,1)$  at  $R = 4.40$  a.u.

Table 5.4

IR Frequencies for the Isotopic Systems in  $\text{cm}^{-1}$ (1).  $[\text{FDF}]^-$ 

	$\nu_{3,D}$	$\nu_{2,D}$	$3\nu_{3,D}$	$3\nu_{2,D}$
TW	1134	985	3693	2991
BT	1061	-	3511	-
AL	1038	-	4088	-
JASB2	983	974	-	-
DA	995	884	-	-
KV	1023	-	4115	-

(DA and KV refer to the experimental work done by Dawson et al. [47-48] and Ketelaar and Vedder [45-46] on  $\text{KDF}_{2(s)}$ .)

(2).  $[\text{F}\mu\text{F}]^-$ 

	$\nu_{3,\mu}$	$\nu_{2,\mu}$	$3\nu_{3,\mu}$	$3\nu_{2,\mu}$
TW	4697	3884	15582	12030

1.43 and 1.42, respectively (for the ratio  $\nu_{3,H}/\nu_{3,D}$ ), while Janssen et al. obtain 1.45 (from JASB2). Hunt and Andrews [142] observed 1.427 for  $[\text{FHF}]^-$  isolated in solid Argon.

Previous workers have observed a small negative shift in the equilibrium F...F distance on deuteration. McGaw and Ibers [23] observed a value of  $-0.0024 \text{ \AA}$  for  $\text{KHF}_2 \rightarrow \text{KDF}_2$  while McDonald [21] observed  $-0.0046 \text{ \AA}$  for  $\text{NaHF}_2 \rightarrow \text{NaDF}_2$ . We estimate this difference to be  $-0.0051 \text{ \AA}$  (from  $R_{e,[FDF]}^0 - R_{e,[FHF]}^0$ ), compared with estimates calculated to be  $-0.007 \text{ \AA}$ ,  $-0.0058 \text{ \AA}$ , and  $-0.006 \text{ \AA}$ , by Barton and Thorson, Almlöf [94], and Jiang and Anderson [95], respectively.

On the other hand, we predict an expansion in the F...F equilibrium distance in going from  $[\text{FHF}]^-$  to  $[\text{F}\mu\text{F}]^-$  of  $+0.0325 \text{ \AA}$  (compared with  $+0.0270 \text{ \AA}$  estimated by Noakes [138]).

#### D. Summary

In this Chapter, the results of approximately 300 calculations on protonic SCF states  $\{(n_\xi, n_\eta, m)_R\}$  were presented. The SCF energy vs. R curves gives insight into the nature of the protonic vibrational dynamics in the  $[\text{FHF}]^-$  ion and are key features of this work.

The protonic SCF states are also labelled according to the 'spectroscopic' quantum numbers,  $(n_{\nu_2}, n_{\nu_3})$ . These SCF energy curves obey a certain non-crossing rule proposed by J. D. Power. However, configuration interaction will remove the crossings between states with the same symmetry. Several interesting phenomena are due to the properties of the potential surface on which the proton moves. The F...F distance will expand when the  $[\text{FHF}]^-$  ion is excited in

the anti-symmetric stretching mode while it will contract when the ion is excited in the bending mode.

Vibrational frequencies are calculated at the SCF level for IR allowed transitions  $a\nu_2 + b\nu_3$ , using estimates of zero-point energy difference corrections. This gives  $\nu_3 = 1536 \text{ cm}^{-1}$  and  $\nu_2 = 1341 \text{ cm}^{-1}$ . The effects of the greater anharmonicity in the  $\nu_3$  mode compared with the  $\nu_2$  mode, as well as the significant coupling between these modes were observed. Several isotope effects were also computed using the systems  $[\text{FDF}]^-$  and  $[\text{F}\mu\text{F}]^-$ .

## 6. AN OUTLINE OF FURTHER WORK

In this Chapter, we survey in broad terms the work necessary to complete the analysis of the vibrational dynamics. In Section A, the discussion will be on the Configuration Interaction (CI) method as applied to our problem, followed by the mathematical formulation of this scheme. Section B will lay out the results of limited CI calculations performed in this thesis. In Section C we will turn our attention to the treatment of  $\nu_1$ -dynamics, considering both cases where the adiabatic approximation is valid and those cases where it may fail. Finally, in Section D, we consider some possible extensions of this work.

### A. Configuration Interaction Calculation of Protonic Eigenstates

#### 1. CI Expansions in SCF Functions as Basis States

The protonic eigenfunctions computed by the self-consistent field approximation are not the exact eigenstates of the protonic Schrödinger equation (3.5). They offer important conceptual understanding of the proton dynamics, since they allow us to continue the idea of separable *modes* associated with the degrees of freedom of the proton motion and characterized by the nodal quantum numbers  $(n_\xi, n_\eta, m)$  and mode excitation ('spectroscopic') quantum numbers  $(n_{\nu_2}, n_{\nu_3})$ ; but this approximation ignores any dynamical *correlation* of proton motions in the separated degrees of freedom. (The SCF approximation implies that the dynamics of the protonic vibration in the  $\xi$ -coordinate, for example, is independent of what its  $\eta$ -coordinate value is at that time.)

Such correlation arises from the fact that the true potential is not exactly separable in the coordinate system being used. In the SCF approximation, the



effective (SCF) potential for motion in each degree of freedom is an average over the motion in the remaining degrees of freedom. This effective potential is different for each distinct state of motion in the other degrees of freedom, but at best it is still an *average*; by contrast the true potential depends at each point on the instantaneous values of *all* proton coordinates.

We construct more accurate approximations to the exact protonic eigenstates  $\chi_{n_p}(\xi, \eta, \phi; R)$  at each F...F separation  $R$  as expansions in the SCF wave functions  $\chi_{n_\xi, n_\eta, m}^{(SCF)}$ :

$$\chi_{n_p}^{(CI)}(\xi, \eta, \phi; R) = \sum_i C_i \chi_i^{(SCF)}(\xi, \eta, \phi; R), \quad (6.1)$$

where  $\{i\} \equiv \{(n_\xi, n_\eta, m)\}$ , and the mixing coefficients  $\{C_i\}$  are parametrically dependent on  $R$ .

Since the non-separable potential  $CIDR_{fit}(\xi, \eta; R)$  can connect any SCF states which have the same symmetry under  $D_{\infty h}$ , the summation in (6.1) extends over all SCF states with a given symmetry. As we have seen in Chapter 4, this symmetry for the SCF states is specified by the value of the azimuthal quantum number  $m$  and the (even/odd) parity of the  $\eta$ -motion nodal quantum number,  $n_\eta \equiv \nu_3$ .

This type of expansion for the exact solution is called Configuration Interaction (CI) by analogy with a corresponding scheme used in quantum chemical calculations of electronic eigenstates for many-electron systems. However, there are certain differences between them:

Firstly, as mentioned in Chapter 3, in most quantum chemical calculations the SCF equations include the effects of the Pauli principle arising from the indistinguishability of electrons; the resulting scheme, called the Hartree-Fock

SCF (HF-SCF) method, yields a set of 'one-electron orbitals' which are mutually orthogonal because they are solutions of the same SCF operator, called the Hartree-Fock operator. Our use of the SCF approximation to separate proton vibrational degrees of freedom entails no such questions, since of course there is no equivalence of the  $\xi$ - motion and  $\eta$ - motion SCF operators and their eigenstates, and hence no indistinguishable entities are involved.

Secondly, in many quantum chemical CI calculations, the basis states used for a CI expansion are 'SCF states' in a somewhat different sense than the precise one used here. In the construction of a HF-SCF wave function by solving for the eigenfunctions of the Hartree-Fock operator, a very large number of basis functions is normally used and as a result a large number of 'excited HF-SCF orbitals' is obtained which are not 'occupied' in the actual HF-SCF state itself. In most quantum chemical CI calculations the basis states used for CI expansion are generated by replacing one or more of the orbitals occupied in the lowest HF-SCF state with 'unoccupied' or 'excited' orbitals. As a result, these basis states are mutually orthogonal.

By contrast, the SCF states used as the expansion basis in equation (6.1) are the true SCF states for each specification of the nodal quantum numbers  $(n_\xi, n_\eta, m)$ ; the self-consistent fields for both  $\xi$ - and  $\eta$ - are different for each state and hence the SCF states themselves are not quite orthogonal (which introduces minor computational complications). In addition they do not formally constitute a complete set of basis functions. (However, we do not believe that this issue has any practical relevance, since the set we actually use is almost as certainly as complete in practice as that generated by any alternative scheme.)

Of course, there is no *a priori* requirement that the basis set for the CI expansion be the SCF wave functions. Any convenient and reasonably complete

set of basis states would serve the purpose. Nevertheless, as pointed out also by Bowman [74], using the SCF states as an expansion basis is a good strategy because firstly, as stated above they offer very simple conceptual understanding in terms of traditional 'mode' ideas, and it happens that in many cases a single SCF state will make a dominant contribution to the corresponding protonic state, justifying the SCF description in zeroth order; and secondly, the actual convergence of an expansion using such solutions may be faster, although this question is not directly tested here.

In performing the CI calculations, in addition to obtaining the states which are the exact (if converged) and adiabatic solutions of the protonic Hamiltonian, we will also obtain some information on how 'good' the application of the SCF approximation is in our case.

There are two indicators on the 'goodness' of the SCF approximation. Firstly, the energy difference  $|E^{(CI)} - E^{(SCF)}|$  (= 'correlation energy') will increase as the SCF description becomes less accurate. Secondly, the amount of mixing in the CI expansion (6.1) will increase (i.e. more than one coefficient  $C_i$  will have significant and nearly equal magnitude) as the SCF approximation breaks down. For a mode-type vibrational description to hold, we require that a particular ' $C_i$ ' in the expansion (6.1) to be dominant over the others, so that we can continue to label the (exact) CI protonic states by the SCF quantum numbers, i.e. as  $\chi_{(n_\xi, n_\eta, m)}^{(CI)}$ . Although in theory the expansion (6.1) could be of infinite size, in practice we truncate the basis set at a finite manageable size. How fast this CI expansion converges (i.e. how few basis functions are needed to achieve this convergence) is also an indicator of a satisfactory SCF-level description.

We expect that the correlation energy (i.e. the CI correction to the protonic state energy) would increase as the energy of the state increases. This is because with increasing energy, the proton samples a wider range of coordinate space,

the anharmonic coupling terms in the potential become more important, and the SCF approximation becomes worse. Furthermore, correlation energy would also in general be larger for protonic states at large  $R$  than they are at near-equilibrium  $R$  values.

We would expect the SCF approximation to break down in the case of degeneracies and near-degeneracies of SCF states of the same symmetry i.e. the avoided crossings mentioned in Chapter 5. Provided that there are no other SCF states nearby (of the same symmetry), including just the two crossing states in a CI calculation should give accurate results. (This was demonstrated by Thompson and Truhlar [80] in cases of 'Fermi resonances' of a model coupled oscillator problem.)

Finally, we also expect that the magnitude of the CI correction to a particular state at a given  $R$  value would, for isotopic systems, increase in the order  $[FDF]^- < [FHF]^- < [F\mu F]^-$ . This is due to the fact that the lighter particle has a greater amplitude of vibration, and thus the coupling terms in the potential play a correspondingly more important role.

## 2. Mathematical Formulation of the CI Scheme

Within the space spanned by  $N$  SCF states  $\{\chi_{n\xi, n\eta, m}^{(SCF)}\}$  of a given  $D_{\infty h}$  symmetry type, the requirement that expansions of the type (6.1) be eigenstates of the protonic Schrödinger equation leads directly to the secular equation

$$|H_{ij} - ES_{ij}| = 0 \quad (i, j = 1, 2, \dots, N), \quad (6.2a)$$

where the indices  $i, j$  indicate individual SCF basis states in the expansion, and

$$H_{ij} = \left\langle \chi_i^{(SCF)} \left| H_{vib} + \left( \frac{1}{2\mu} \right) \left( \frac{\partial^2}{\partial R^2} \right) \right| \chi_j^{(SCF)} \right\rangle, \quad (6.2b)$$

$$S_{ij} = \left\langle \chi_i^{(SCF)} \mid \chi_j^{(SCF)} \right\rangle. \quad (6.2c)$$

The solutions to the energy obtained by solving (6.2),  $E_{(n_p=)1} < E_2 < E_3, \dots$  are the energies of the CI ground state, first excited state, ... and so on. For each solution  $E_k$ , there will be a vector of  $N$  coefficients,  $\{C_{ik}; i = 1, 2, \dots, N\}$  giving the appropriate linear combination of  $N$  SCF states for the  $k^{\text{th}}$  CI state, and normalized so that

$$\left\langle \chi_{n_p}^{(CI)}(\xi, \eta, \phi; R) \mid \chi_{n_p}^{(CI)}(\xi, \eta, \phi; R) \right\rangle = 1 \quad (6.3)$$

Therefore the CI calculation entails evaluating the matrix elements  $S_{ij}$  and  $H_{ij}$  between the SCF total wave functions.

Recalling from Chapter 3 that

$$\chi_i^{(SCF)} = C_{NI} \alpha_i(\xi; R) \beta_i(\eta; R) (2\pi)^{-1/2} e^{im_i \phi},$$

where  $C_{NI}$  is the normalisation constant for  $\chi_i^{(SCF)}$  (excluding the function  $(2\pi)^{-1/2} e^{im_i \phi}$ ),

$$\text{with } \alpha_i(\xi; R) = f_i(\xi; R) (\xi^2 - 1)^{-1/2} \quad \text{and}$$

$$\beta_i(\eta; R) = g_i(\eta; R) (1 - \eta^2)^{-1/2}$$

Using normalization condition (3.15) this leads to,

$$S_{ij} = (C_{NI} C_{NJ}) \left(\frac{R}{2}\right)^3 \int_{-1}^{+1} d\eta \frac{g_i g_j}{(1 - \eta^2)} \int_0^{+\infty} dx f_i f_j + (C_{NI} C_{NJ}) \left(\frac{R}{2}\right)^3 \int_0^{+\infty} dx \frac{f_i f_j}{x(x+2)} \int_{-1}^{+1} d\eta g_i g_j \quad (6.4)$$

where  $x = \xi - 1$ .

$$\text{Also, } H_{ij} = I_1 + I_2 + I_3 \quad (6.5)$$

where

$$I_1 = \frac{-C_{NI}C_{NJ}}{A} \left(\frac{R}{2}\right)^3 \left( \int_{-1}^{+1} d\eta \frac{g_i(\eta; R)g_j(\eta; R)}{(1-\eta^2)} \right) \left\{ \int_{+1}^{+\infty} d\xi \left[ \frac{A}{(\xi^2-1)} \right. \right. \\ \left. \left. \int_{-1}^{+1} d\eta (\xi^2 - \eta^2) [V - E_j^{(SCF)}] [g_j(\eta; R)]^2 \frac{\epsilon_{g_j}}{(\xi^2-1)} \right] [f_i(\xi; R)f_j(\xi; R)] \right\}, \quad (6.6a)$$

$$I_2 = \frac{-C_{NI}C_{NJ}}{A} \left(\frac{R}{2}\right)^3 \left( \int_{+1}^{+\infty} d\xi \frac{f_i(\xi; R)f_j(\xi; R)}{(\xi^2-1)} \right) \left\{ \int_{+1}^{+\infty} d\xi \left[ \frac{A}{(1-\eta^2)} \right. \right. \\ \left. \left. \int_{+1}^{+\infty} d\xi (\xi^2 - \eta^2) [V - E_j^{(SCF)}] [f_j(\xi; R)]^2 \frac{\epsilon_{f_j}}{(1-\eta^2)} \right] [g_i(\eta; R)g_j(\eta; R)] \right\}, \quad (6.6b)$$

and,

$$I_3 = C_{NI}C_{NJ} \left(\frac{R}{2}\right)^3 \int_{+1}^{+\infty} d\xi \frac{f_i(\xi; R)f_j(\xi; R)}{(\xi^2-1)} \left\{ \int_{-1}^{+1} d\eta (\xi^2 - \eta^2) V [g_i(\eta; R)g_j(\eta; R)] \right\} \quad (6.6c)$$

(where  $A = R^2 m_r / 2$ )

Note that  $H_{ii} = E_i^{(SCF)}$ ,  $S_{ii} = 1$ ,  $H_{ij} = H_{ji}$ , and  $S_{ij} \neq 0$  for  $i \neq j$ .

The protonic Hamiltonian operator and the identity operator are invariant under the symmetry operations of the  $[FHF]^-$  system. Therefore the matrix elements  $H_{ij}$  and  $S_{ij}$  will vanish unless  $\chi_i^{(SCF)}$  and  $\chi_j^{(SCF)}$  are of the same symmetry under  $D_{\text{oh}}$ .

Thus configuration interaction will occur only *inside* each of the blocks  $\sigma_g$ ,  $\sigma_u$ ,  $\pi_g$ ,  $\pi_u$ ,  $\delta_g$ ,  $\delta_u$ , and never between two of them. (Of course, if we are interested only in the IR spectroscopic frequencies, the situation can be simplified still further by limiting ourselves to the  $\sigma_g$ ,  $\sigma_u$ , and  $\pi_u$  blocks.)

## B. Some Results from CI Calculations

As was stated in Chapter 1, it is not our intention to perform comprehensive CI calculations in this thesis. However, some results of limited CI

among  $\pi_u$  protonic states will be presented. Not only did this set up the algorithms and the computational apparatus that will be needed for more extensive CI calculations and help us to prepare a strategy for the complete solution of the  $[\text{FHF}]^-$  vibrational dynamics, but also it will give us some information on whether our application of the SCF approximation using the prolate spheroidal coordinate system to the protonic vibrational dynamics was satisfactory.

Calculation of the matrix elements  $S_{ij}$  and  $H_{ij}$  is one of the instances where having numerical SCF wave functions is computationally more efficient and convenient than expansions of the SCF wave functions such as a basis set of HO functions. In our case, the stored wave functions can be used, with no other description than their range, in a simple procedure such as Simpson's rule or the trapezoidal rule to evaluate all the necessary integrals. Standard computational algorithms were used to diagonalize the secular determinant and obtain the eigenvalues  $\{E_i^{(CI)}\}$ .

In computing the  $S_{ij}$ , it was observed that for *different* SCF wave functions  $|n_\xi, n_\eta, m\rangle$  and  $|n'_\xi, n'_\eta, m\rangle$ , the value of  $\int_{+1}^{+\infty} d\xi \alpha_i \alpha_j$  when  $n_\xi = n'_\xi$  (but  $n_\eta \neq n'_\eta$ ), and the value of  $\int_{-1}^{+1} d\eta \beta_i \beta_j$  when  $n_\eta = n'_\eta$  (but  $n_\xi \neq n'_\xi$ ), are close to 1.0 (to which they would be equal if  $n_\xi = n'_\xi$  and  $n_\eta = n'_\eta$ ). Furthermore,  $\int_{-1}^{+1} d\eta \beta_i \beta_j$  in the first case, and  $\int_{+1}^{+\infty} d\xi \alpha_i \alpha_j$  in the second case are quite small. (See for example, Table 6.1) This may be taken as a rough indicator that the SCF approximation to separate the vibrational motion is reasonably successful.

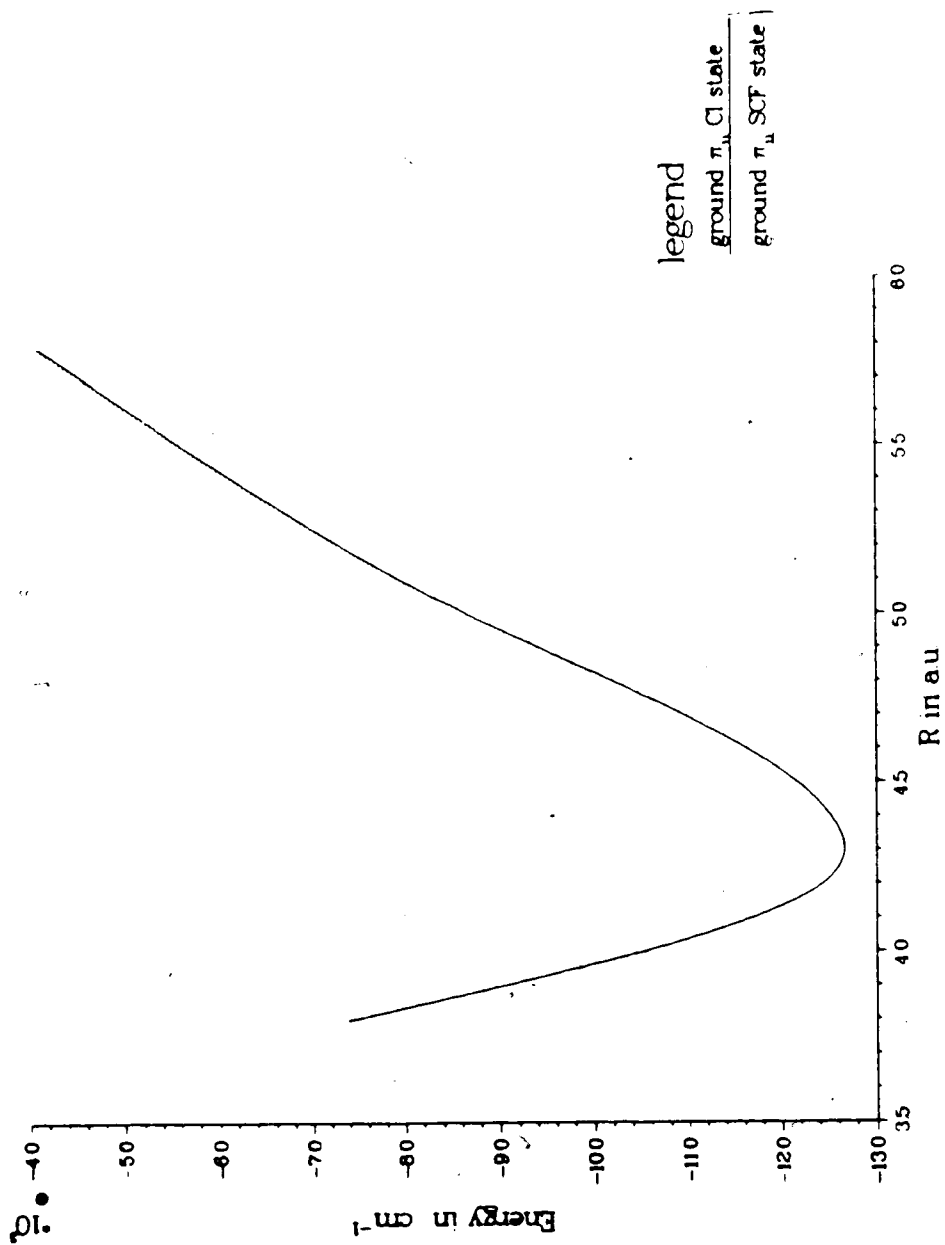
Figure 6.1 shows the variation with  $R$  of the lowest  $\pi_u$  SCF (i.e. (0,0,1)) and CI energy levels (in  $\text{cm}^{-1}$ ). It can be seen that the CI correction is very small for the entire range of  $R$ . (Also, the CI mixing coefficients for the (0,0,1) SCF state is nearly 1.0 for the entire range.) This clearly demonstrates that the SCF approximation has worked very well in using prolate spheroidal coordinates for the lowest  $\pi_u$  state, at least.

Table 6.1

## SCF Overlap Integrals

$(n_\xi, n_\eta, m), (n'_\xi, n'_\eta, m)$	$\int_{-1}^{+1} d\eta \beta_i \beta_j$	$\int_{+1}^{+\infty} d\xi \alpha_i \alpha_j$
$(0, 0, 1), (0, 0, 1)$	1.0000	1.0000
$(0, 0, 1), (1, 0, 1)$	0.9984	0.0310
$(0, 0, 1), (2, 0, 1)$	0.9935	0.0021
$(0, 0, 1), (3, 0, 1)$	0.9846	0.0002
$(0, 0, 1), (0, 2, 1)$	-0.005	0.9878
$(0, 0, 1), (0, 4, 1)$	-0.001	0.9345



Figure 6.1 Ground  $\pi_u$  CI and SCF States

The difference between the energy at the  $R_{min}$  of the (0,0,1) SCF curve and that at the  $R_{min}$  of the lowest  $\pi_u$  CI curve is only  $3.9 \text{ cm}^{-1}$ . Since one expects that the lowest  $\sigma_g$  and  $\sigma_u$  CI energy level curves have energies at their  $R_{min}$  lowered by approximately the same amount w.r.t. the corresponding SCF energy level curves (i.e. (0,0,0) and (0,1,0), respectively), this means that the CI corrections to our values of the fundamentals  $\nu_2$  and  $\nu_3$  (calculated in Chapter 5) would be insignificantly small. Therefore our values  $\nu_2 = 1341 \text{ cm}^{-1}$  and  $\nu_3 = 1536 \text{ cm}^{-1}$  (*within the zero-point energy difference corrections*) are probably very close to the final results at the completion of the analysis.

Estimating the IR frequencies for the transitions to most of the higher states from the CI calculations, however, is not so simple. This is because in most of these cases, avoided crossings occur in the vicinity of the minima of the energy level curves. This problem will be discussed in more detail in Section C.

Figure 6.2 shows the avoided crossing at  $R \sim 4.46 \text{ a.u.}$  between the first and second excited  $\pi_u$  CI energy level curves (i.e. the crossing between the corresponding SCF energy level curves (1,0,1) and (0,2,1)). Two sets of CI curves are displayed: firstly the CI levels constructed with just the two crossing SCF levels, (1,0,1) and (0,2,1); and secondly, the CI levels obtained from adding six more SCF states to the basis set. One observes that there is only a very small difference between the two sets of CI curves. This shows that, at least in the absence of any other close-lying SCF states, an adequately accurate representation of the exact state at an avoided crossing may be obtained by mixing in just the two crossing SCF states. The energy gap at this avoided crossing is  $\sim 440 \text{ cm}^{-1}$ . There is a further avoided crossing between the first and second excited  $\pi_u$  CI energy levels at  $R \sim 5.29 \text{ a.u.}$  where the energy gap is  $\sim 880 \text{ cm}^{-1}$ .

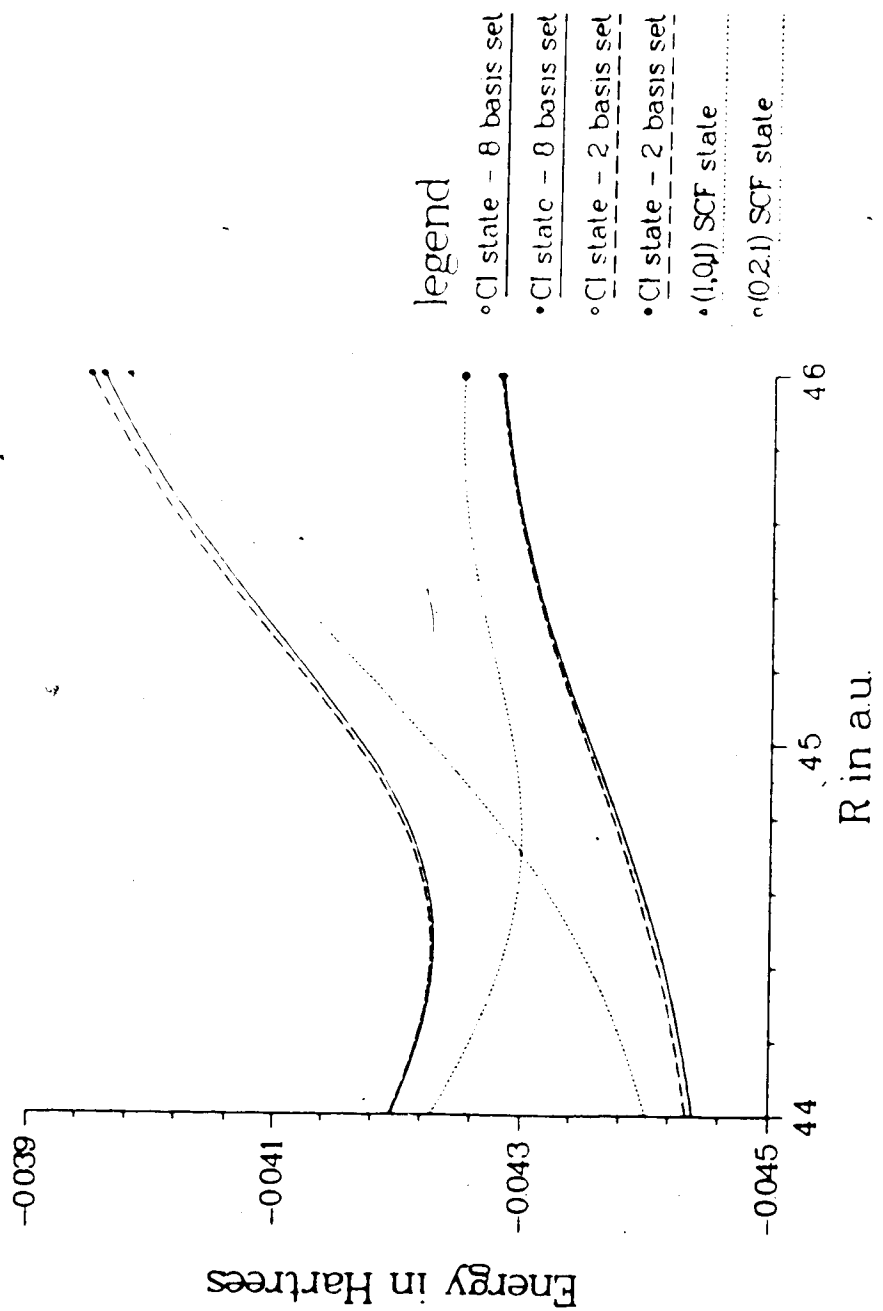


Figure 6.2 Avoided Crossing at R=4.46 a.u. between  $\pi_v$  CI States

Table 6.2

Composition of the First Excited  $\pi_u$  CI State

$$\chi_1^{(CI)} = C_1 \chi_{(1,0,1)}^{(SCF)} + C_2 \chi_{(0,2,1)}^{(SCF)} + 6 \text{ other states}$$

$R$ (a.u.)	$C_1$	$C_2$
3.80	0.99	-0.06
4.20	0.99	-0.11
4.40	0.93	-0.36
4.50	0.58	-0.81
4.60	0.30	-0.95
5.00	0.28	-0.96
5.40	0.87	-0.47
5.80	0.93	-0.33

Representing the first excited  $\pi_u$  CI state by,

$$\chi_1^{(CI)} = C_1 \chi_{(1,0,1)}^{(SCF)} + C_2 \chi_{(0,2,1)}^{(SCF)} + \text{six others}$$

at each  $R$  value, Table 6.2 gives the relative amount of interaction between the two major component SCF states.

Table 6.3 shows the effect of increasing the basis set size has on convergence of the five lowest  $\pi_u$  CI states at  $R = 4.40$  a.u. The SCF states in the basis set are, (in order of addition to the expansion), (0,0,1), (1,0,1), (0,2,1), (1,2,1), (2,0,1), (0,4,1), (2,2,1), (3,0,1), (1,4,1), (0,6,1), and (3,2,1). The major components of the CI states at this  $R$  value are, in order of increasing energy, (0,0,1), (1,0,1), (0,2,1), (1,2,1), and (2,0,1). We see that with an 11-member basis set, the ground CI state has converged to the order of  $0.001 \text{ cm}^{-1}$ , the first and second excited CI states have converged to the order of  $0.1 \text{ cm}^{-1}$ , and the third and fourth excited CI states have converged upto  $5 \text{ cm}^{-1}$ . This relatively rapid CI convergence is again an indication of the success of the SCF approximation.

Finally, Figure 6.3 shows the variation with  $R$  of the five lowest  $\pi_u$  CI energy levels and the six SCF energy levels from which they have been constructed.

Table 6.3

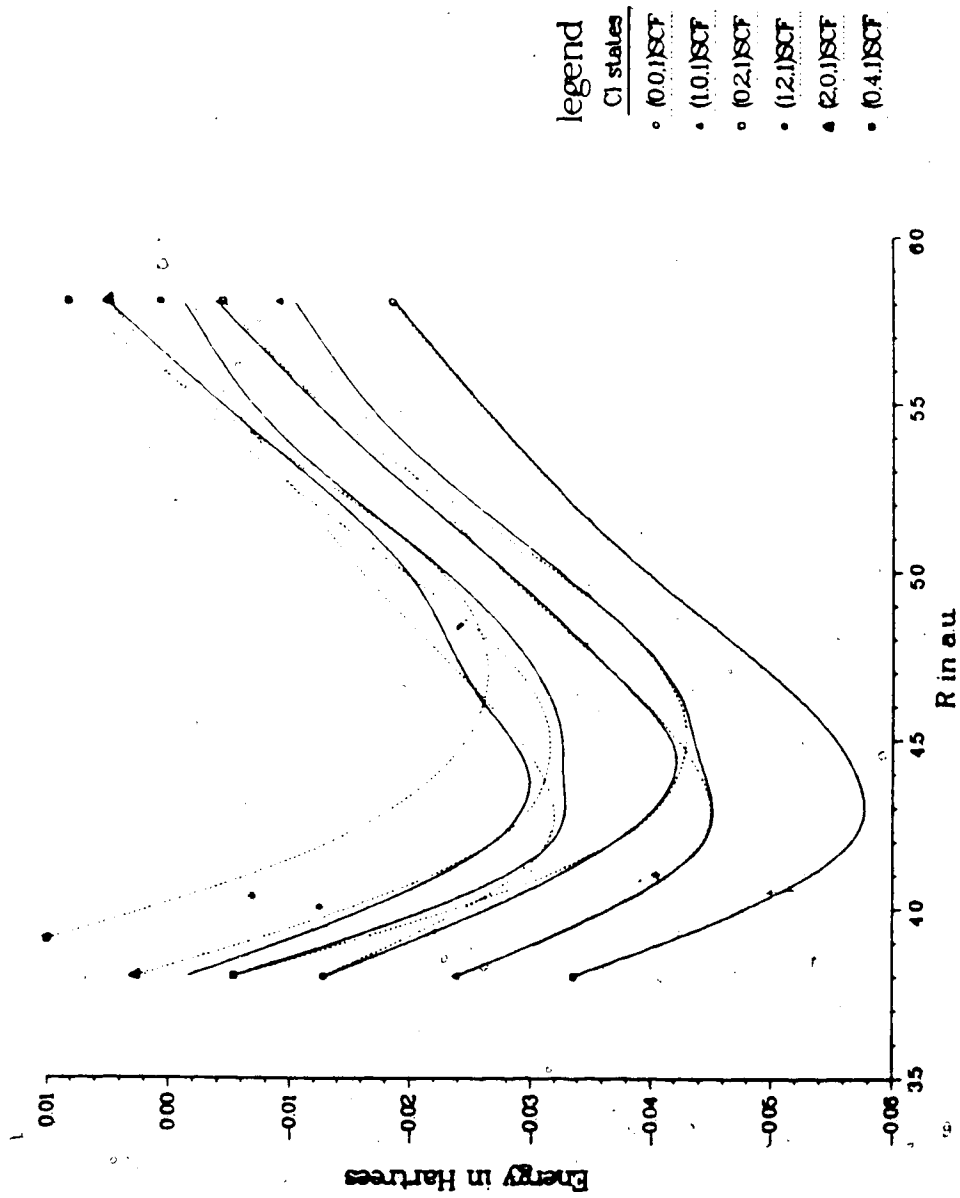
CI Convergence of the Lowest 5  $\pi_u$  States at R=4.40 a.u.

( $\Delta E$  = change in energy w.r.t. the corresponding SCF state ( $\text{cm}^{-1}$ ))

$\pi_u$ CI State	Basis Set Size	$\Delta E$ ( $\text{cm}^{-1}$ )
Ground	6	-4.02
	8	-4.29
	9	-4.30
	10	-4.32
	11	-4.32
1 <sup>st</sup> Excited	6	-73.24
	8	-82.83
	9	-86.47
	10	-87.49
	11	-87.69
2 <sup>nd</sup> Excited	6	72.47
	8	70.55
	9	56.33
	10	55.98
	11	55.68

(Table 6.3 continued)

$\pi_u$ CI State	Basis Set Size	$\Delta E$ (cm <sup>-1</sup> )
3 <sup>rd</sup> Excited	6	-307.13
	8	-310.18
	9	-314.97
	10	-322.56
	11	-326.50
4 <sup>th</sup> Excited	6	237.26
	8	237.19
	9	237.17
	10	220.92
	11	219.69

Figure 6.3 CI Energy vs. R for  $\pi_n$  States



### C. Treatment of $\nu_1$ - Mode Dynamics

#### 1. $\nu_1$ - Dynamics in Adiabatic Approximation

As was stated in Chapter 3 the problem of the FHF motion is greatly simplified if the *adiabatic* approximation is valid. The vibrational eigenfunctions for the entire system, which are solutions to equation (3.4), may then be approximated as products of the form (c.f. equation (3.7))

$$\Psi_n(\vec{r}; R) \simeq \Psi_{n_{\nu_1}, n_p}^{AD}(\vec{r}; R) = \Phi_{n_{\nu_1}, n_p}(R) \chi_{n_p}(\vec{r}; R) \quad (6.7)$$

$\chi_{n_p}(\vec{r}; R)$  is a single protonic eigenstate, i.e. an eigensolution of the protonic Schrödinger equation (3.5), which we construct here by configuration interaction from the protonic SCF states as described in the preceding sections of this chapter.

The  $R$ - motion wave function  $\Phi_{n_{\nu_1}, n_p}(R)$  is then simply an eigenfunction of the one-dimensional Schrödinger equation (c.f. equation (3.8))

$$\left\{ \frac{-1}{2\mu} \frac{d^2}{dR^2} + \bar{E}_{n_p}(R) \right\} \Phi_{n_{\nu_1}, n_p}(R) = E_{n_{\nu_1}, n_p}^{total} \Phi_{n_{\nu_1}, n_p}(R) \quad (6.8)$$

$E_{n_{\nu_1}, n_p}^{total}$  is the total vibrational energy for the  $[FHF]^-$  system in the  $(\nu_1, \nu_2, \nu_3)$  state. The protonic eigenvalue curve  $E_{n_p}(R)$  plays the role of an effective potential for the  $\nu_1$ - motion. In the discussion of Chapter 5 and the earlier sections of this Chapter, we have implicitly assumed that the eigenvalue curves  $E_{n_p}^{(CI)}$  or the SCF eigenvalue curves  $E_{n_p}^{(SCF)}$  would eventually play such a role. (More sophisticated analysis of finer details in the adiabatic separation scheme leads to small corrections to this effective potential arising from non-adiabatic interactions, so that it may be slightly more accurate to use a corrected effective potential,  $U_{n_p}(R)$  in place of  $E_{n_p}(R)$  itself; in any case the form of equation (6.8) is the same.)

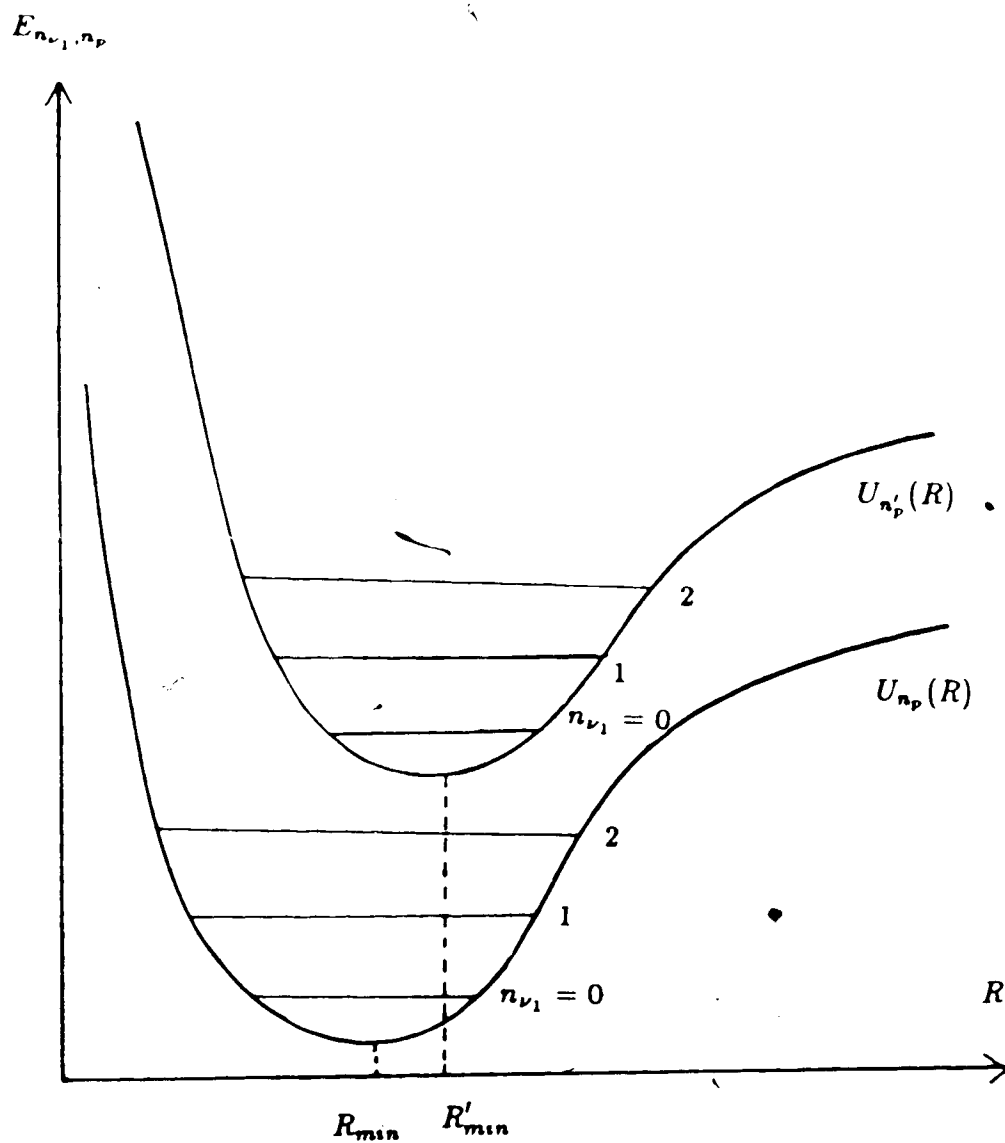


Figure 6.4 The Total Vibrational States under the Adiabatic Approximation

Solution of the eigenvalue problem posed by equation (6.8) is straightforward. Each effective potential function ( $U_{n_p}(R)$  or  $E_{n_p}(R)$ ) then supports a number of  $\nu_1$ -mode eigenstates, as depicted in Figure 6.4. Again, it is convenient to use the quantal momentum or Milne's method (see Chapter 4) to solve the equations. Rewriting equation (6.8) in the form

$$\left[ \frac{d^2}{dR^2} + k^2(R) \right] \Phi_{n_{\nu_1}, n_p}(R) = 0, \quad (6.9a)$$

where

$$k^2(R) = (2\mu) \left[ E_{n_{\nu_1}, n_p}^{total} - U_{n_p}(R) \right]. \quad (6.9b)$$

Milne's method as outlined in Section A of Chapter 4 can be applied directly. The eigenfunctions have the form

$$\Phi_{n_{\nu_1}, n_p}(R) = C [q_{Rc}(R)]^{-1/2} \sin \theta(R), \quad (6.10a)$$

where  $C$  is a normalization constant defined by

$$C^2 \int_0^{+\infty} dR \left[ \Phi_{n_{\nu_1}, n_p}(R) \right]^2 = 1, \quad (6.10b)$$

and the phase  $\theta(R)$  is given by

$$\theta(R) = \int_0^R dR' q_{Rc}(R'). \quad (6.10c)$$

The eigenvalues  $E_{n_{\nu_1}, n_p}^{total}$  are determined from the quantization condition

$$\int_0^{+\infty} dR q_{Rc}(R) = (n_{\nu_1} + 1)\pi, \quad n_{\nu_1} = 0, 1, 2, \dots \quad (6.11a)$$

Integration of the Riccati equation for  $q(R)$  is initiated at the minimum of  $-k^2(R)$ ,  $R = R_{min}$  using the 'classical' initial conditions

$$q(R = R_{min}) = k(R = R_{min}) \quad (6.11b)$$

(Application of Milne's method to this problem is much easier than for the application to proton motion treated in Chapter 4, since there are no problems associated with the behaviour at the origin or with double minima.)

We may expect that this level of approximation will give accurate vibrational eigenvalues and eigenfunctions for vibrational states associated with clearly non-degenerate protonic states such as those approximated by the SCF descriptions  $(0,0,0)$  (ground protonic level),  $(0,0,1)$  (single excitation of  $\nu_2$ ),  $(0,1,0)$  (single excitation of  $\nu_3$ ), etc. However, for those cases where two or more protonic eigenvalue curves are nearly degenerate over some domain of the coordinate  $R$ , exhibiting the effects of configuration interaction in avoided crossings, etc., the problem of  $\nu_1$ -dynamics is not so simple. As we have seen in earlier sections of this chapter, this more complex situation occurs for most of the higher excited protonic levels in the system (e.g. the mixing of SCF  $\pi_u$  levels  $(1,0,1)$  ( $3\nu_2$ ) and  $(0,2,1)$  ( $2\nu_3 + \nu_2$ ). We discuss these cases in the next sub-section.

## 2. Breakdown of the Adiabatic Separation and Coupled $\nu_1$ -Dynamics

As illustrated in Section B of this chapter for protonic states of  $\pi_u$  symmetry (c.f. Figure 6.3), two or more protonic eigenstates with a given  $D_{\infty h}$  symmetry may be nearly degenerate over some domain of the coordinate  $R$ . Usually this situation occurs when two SCF eigenvalue curves cross at some point  $R_c$ : the corresponding exact protonic eigenvalue curves (computed in this scheme using CI) do not cross, but exhibit an *avoided crossing* as shown. This situation is actually very frequent in the  $[\text{FHF}]^-$  system for states involving more than one or two quanta of proton excitation; as discussed in Section B, it arises from the strongly non-separable potential surface interactions between the bending and stretching coordinates. In the qualitative terminology usually employed to describe such interactions in vibrational spectra, such states exhibit a strong 'Fermi resonance'.

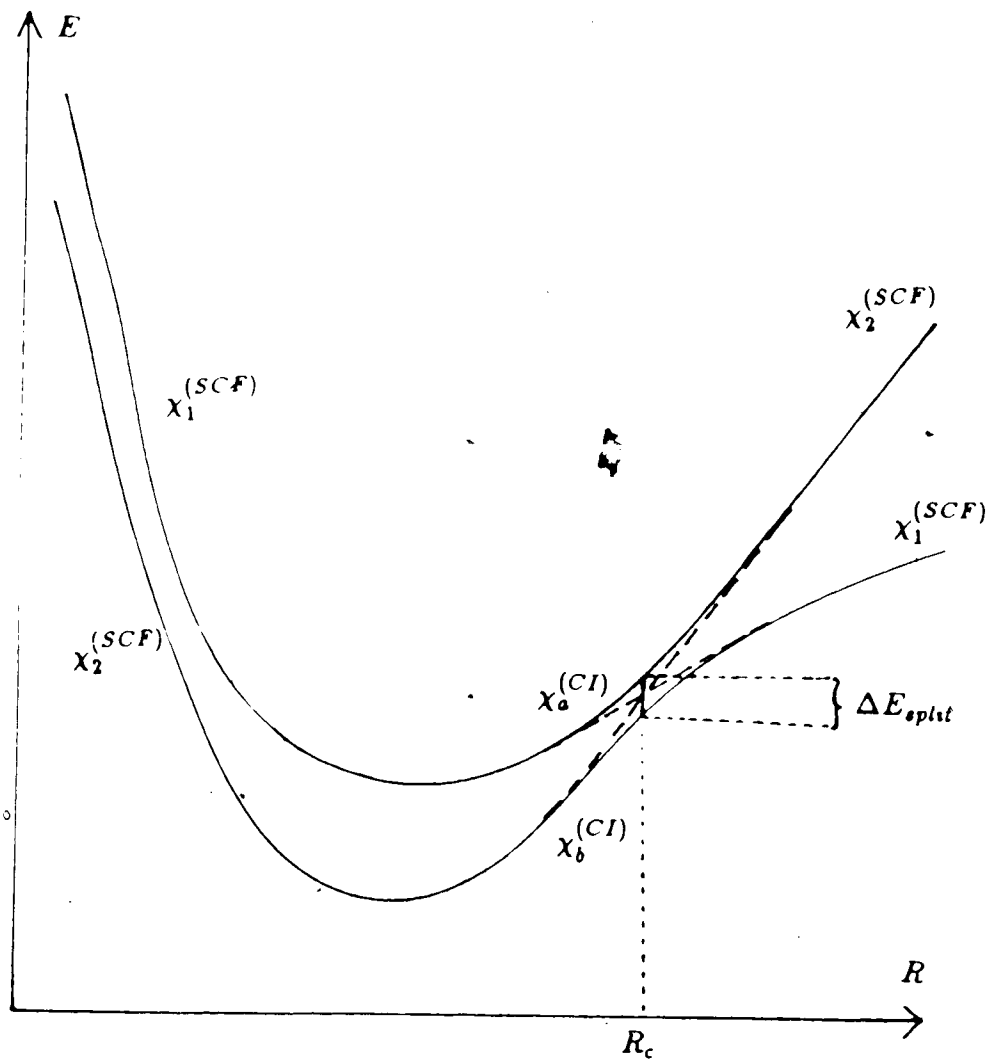


Figure 6.5 An Avoided Crossing with  $\Delta E_{split} \leq \nu_1$

The essential point is that because the proton eigenvalue curves are still very nearly degenerate (splittings as small as 200-400  $\text{cm}^{-1}$ ), the adiabatic separation will break down and the nearly degenerate protonic states will be dynamically coupled by the F...F motion. (The study by Barton and Thorson [29] justifying the adiabatic separation did not encounter this situation because they did not include any treatment of the proton bending mode; the non-adiabatic couplings that they considered involved stretching mode protonic states which were always separated by energies greater than 2000  $\text{cm}^{-1}$ .)

One way of understanding the situation is as follows: (see Figure 6.5) Consider an avoided crossing at  $R = R_c$  between two exact protonic energy curves  $E_a^{(CI)}(R)$  and  $E_b^{(CI)}(R)$ . The corresponding wave functions of these states (at each value of  $R$ ) are given by  $\chi_a^{(CI)}(\xi, \eta, \phi; R)$  and  $\chi_b^{(CI)}(\xi, \eta, \phi; R)$ , respectively. Assume that throughout the entire range of  $R$  the CI wave functions consist of just two SCF components,  $\chi_1^{(SCF)}(\xi, \eta, \phi; R)$  and  $\chi_2^{(SCF)}(\xi, \eta, \phi; R)$  of energies  $E_1^{(SCF)}(R)$  and  $E_2^{(SCF)}(R)$ , respectively. (i.e. there are no other SCF states of the same symmetry near enough.)  $E_1^{(SCF)}(R)$  and  $E_2^{(SCF)}(R)$  of course, cross at  $R = R_c$ . Interaction of these two SCF states removes this degeneracy at  $R_c$  by an amount  $\Delta E_{split}$ .

Let us examine first the upper protonic energy curve,  $E_a^{(CI)}(R)$ . On this curve, far to the left of the avoided crossing,  $\chi_a^{(CI)}$  is essentially  $\chi_1^{(SCF)}$  while far to the right of the avoided crossing, it is essentially  $\chi_2^{(SCF)}$ . Thus, as one moves past  $R = R_c$ , the protonic eigenfunction changes from  $\chi_1^{(SCF)}$  to  $\chi_2^{(SCF)}$ . These changes in the protonic wave function take place during a time  $t_p \sim h/\Delta E_{split}$ . On the other hand, we may estimate that the F...F motion will move the system through such a region in a time  $t_F \sim h/\nu_1$ . When  $t_p \geq t_F$ , (i.e.  $\Delta E_{split} \leq \nu_1$ ), it can no longer be claimed that the protonic wave function adjusts itself instantaneously to

any change in the heavy nuclear (F) configuration. That is, the protonic motion can no longer be quantized for a fixed F...F configuration. Clearly, *the adiabatic approximation has broken down.*

In the [FHF]<sup>-</sup> system  $\nu_1 \sim 600 \text{ cm}^{-1}$ ; we may therefore assume as a rough guideline that any protonic energy levels which are separated by an energy spacing less than or comparable to  $\sim 600 \text{ cm}^{-1}$  in an accessible domain of the coordinate  $R$  will experience significant dynamical couplings associated with the  $\nu_1$ -motion.

To determine vibrational eigenvalues and eigenfunctions for equation (3.4) in such cases, instead of the simple adiabatic approximation (6.7), the wave function must be written out as an expansion in the relevant (nearly degenerate) protonic states (c.f. also equation (3.6)):

$$\Psi_n^{total}(\vec{r}, R) = \sum_{n'_p} \Phi_{n,n'_p}(R) \chi_{n'_p}(\vec{r}; R). \quad (6.12)$$

Substitution of (6.12) into the vibrational Schrödinger equation (3.4), followed by closure on the left with  $\chi_{n_p}^*(\vec{r}; R)$ , leads to a system of coupled multi-channel differential equations for the amplitude coefficients  $\{\Phi_{n,n_p}(R)\}$ :

$$\left\{ \left( \frac{-1}{2\mu} \right) \frac{d^2}{dR^2} + E_{n_p}(R) - E_n^{total} \right\} \Phi_{n,n_p}(R) - \left( \frac{1}{2\mu} \right) \sum_{n'_p} [2P_{n_p,n'_p}(R) \frac{d}{dR} + B_{n_p,n'_p}(R)] \Phi_{n,n'_p}(R) = 0, \quad (6.13)$$

where the non-adiabatic coupling matrix elements  $P_{n_p,n'_p}(R)$  and  $B_{n_p,n'_p}(R)$  are defined

$$P_{n_p,n'_p}(R) = \left\langle \chi_{n_p}(\vec{r}; R) \left| \frac{\partial}{\partial R} \right| \chi_{n'_p}(\vec{r}; R) \right\rangle \quad (6.14a)$$

and

$$B_{n_p,n'_p}(R) = \left\langle \chi_{n_p}(\vec{r}; R) \left| \frac{\partial^2}{\partial R^2} \right| \chi_{n'_p}(\vec{r}; R) \right\rangle \quad (6.14b)$$

The integration in (6.14a,b) are performed over  $\xi$ ,  $\eta$ ,  $\phi$  and connect states with the same  $D_{\text{oh}}$  symmetry.

The simple one-channel description given by the adiabatic approximation (c.f. Section C.1 above) is recovered if we neglect all the coupling terms in the summation in the second term in equation (6.13). In the case of a close avoided crossing such as those shown in Figure (6.3), for example, such neglect is not justified, because these coupling matrix elements exhibit maxima in the neighbourhood of an avoided crossing, due mainly to the CI mixing or crossover between the two strongly interacting SCF protonic configurations.

As was shown by Barton and Thorson [29], the calculation of the non-adiabatic coupling matrix elements defined in equations (6.14) requires some care; the difficulties they treat arise from the fact that the 'molecular' coordinates  $(\vec{r}, R)$  used to define the vibrational Hamiltonian (equation (3.3)) are not appropriate in the dissociation limit. In the cases of avoided crossing which concern us here, however, the dominant contributions to the coupling matrix elements arise from strong CI mixing of two SCF states, and the finer corrections discussed by Barton and Thorson do not affect these contributions. Further discussion of the details of these couplings is beyond the scope of this thesis.

In the solution of the coupled multi-channel equations (6.13) discrete eigenvalues arise when boundary conditions requiring that all the amplitude coefficients  $\{\Phi_{n,n_p}(R)\}$  be regular in the limits  $R \rightarrow 0$  and  $R \rightarrow \infty$  are imposed. Analysis of the resulting amplitudes associated with each of the coupled protonic state 'channels' can show whether a qualitative interpretation of a particular eigenstate in terms of dominant contributions from a single protonic state is justified (thus retaining the concept of vibrational 'modes'.) Convergence of such computations can be tested by adding more coupled channels to the calculations for a



particular vibrational level. It may happen that more than two protonic states may be coupled significantly by the  $\nu_1$ - motion; for example, as can be anticipated from Figure 6.3 it may happen that the CI  $\pi_u$  states involving the SCF zero-order state (1,2,1) ( $\equiv 3\nu_2 + 2\nu_3$ ), and possibly also (2,0,1) ( $\equiv 5\nu_2$ ) may play some dynamical role in the coupling even though the two lower levels (1,0,1) ( $\equiv 3\nu_2$ ) and (0,2,1) ( $2\nu_3 + \nu_2$ ) are those dominantly involved. At the present time it would be premature to speculate about these questions, although it may be that the rather complex structure of the IR bands seen by Côté and Thompson in the region 3700-4500  $\text{cm}^{-1}$  may conceivably have an interpretation in terms of these avoided crossings or 'Fermi resonance' effects.

## D. Future Work

### 1. Frequencies and Relative Intensities of IR Transitions

When the solution of the  $\nu_1$ - dynamics is completed one is in a position to compute the quantitative vibrational frequencies and the relative intensities for the isolated bifluoride system.

For a transition  $n = n \rightarrow n = n'$  the frequency is then given simply by

$$h\nu_{nn'} = \Delta E = E_{n'}^{total} - E_n^{total} \quad (6.15)$$

Assuming that only the ground state is populated, the relative (integrated) intensities of two IR transitions  $0 \rightarrow n'$  and  $0 \rightarrow n$  are given by the ratio

$$R.I.(0 \rightarrow n'/0 \rightarrow n) = \left( \frac{\nu_{n'0}}{\nu_{n0}} \right) \left[ \frac{|T_{n'0}|^2}{|T_{n0}|^2} \right] \quad (6.16a)$$

where  $\nu_{n0}$ ,  $\nu_{n'0}$  are the frequencies of the two transitions and the electric dipole transition matrix elements are defined

$$T_{n0} = \langle \Psi_n^{total} | \vec{\mu}_e(\vec{r}, R) | \Psi_0^{total} \rangle, \quad (6.16b)$$

$\vec{\mu}_e(\vec{r}, R)$  being the instantaneous electric dipole moment for the vibrational configuration  $(\vec{r}, R)$ . Since  $[\text{FHF}]^-$  has  $D_{\infty h}$  symmetry in its equilibrium configuration,  $\vec{\mu}_e(\vec{r}, R)$  is zero except when the proton displacement  $\vec{r}$  is non-zero. Non-vanishing components of the dipole moment are of two distinct symmetry types: those *parallel* to the F...F axis, which transform like  $z$  ( $\sigma_u$  type), and those *perpendicular* to the F...F axis, which transform like  $(x, y)$  ( $\pi_u$  type). These two distinct types of moments form two separate families of non-vanishing transition matrix elements, which can be treated on separate theoretical footings. For the parallel moment we can write

$$\mu_{\parallel}(\vec{r}, R) = D_{\parallel}(\xi, \eta, R) \left( \frac{R}{2} \xi \eta \right) \quad (6.17a)$$

and for the perpendicular moment,

$$\mu_{\perp}(\vec{r}, R) = D_{\perp}(\xi, \eta, R) \left( \frac{R}{2} [(\xi^2 - 1)(1 - \eta^2)]^{1/2} \right) \exp(i\phi) \quad (6.17b)$$

where the two functions  $D_{\parallel}$  and  $D_{\perp}$  have strictly  $D_{\infty h}$  symmetry. IR transitions to states of  $\pi_u$  symmetry involve only  $\mu_{\perp}$  while those to states of  $\sigma_u$  symmetry involve only  $\mu_{\parallel}$ . As a comparative standard for the  $\sigma_u$  transitions we can use the  $\nu_3$  fundamental, while for the  $\pi_u$  transitions we can use the  $\nu_2$  fundamental.

Of course we cannot realistically compute either of the functions  $D_{\parallel}$  or  $D_{\perp}$  from theory. Hence there is no way to relate intensities of the  $\pi_u$  series to those of the  $\sigma_u$  series of transitions (except by observation), and it is not a legitimate exercise to make more than the most primitive possible assumptions about these

functions. The simplest possible form is that they are just constants  $D_{\parallel}^0$  and  $D_{\perp}^0$ , respectively. Then, except for the frequency factors, the relative intensities of all  $\sigma_u$ , and  $\pi_u$  are determined by the relative magnitudes of the squares of the purely *mechanical* matrix elements  $\langle \Psi_{n\sigma_u}^{total} | z | \Psi_0^{total} \rangle$ , and  $\langle \Psi_{n\pi_u}^{total} | x + iy | \Psi_0^{total} \rangle$ , respectively.

In the study by Barton and Thorson [29] of the non-bending  $[\text{FHF}]^-$  system, the relative intensity was found to be controlled almost completely by the mechanical properties of this non-separable, non-harmonic oscillator, and not by any electrical anharmonicity in the dipole moment function. This claim is important in relation to the concept of the adiabatic or nearly adiabatic separation of the  $\nu_1$ - motion from the proton degrees of freedom because it implies that the Franck-Condon principle is fundamental to understanding the intensities of progressions in the  $\nu_1$ - mode and that the mechanics of the non-harmonic  $\nu_3$ - motion controls relative intensities of the overtones of  $\nu_3$ . In view of the success of Barton and Thorson's predictions of relative intensities for their limited model of this system, relative intensity calculations are probably well worth doing as a further demonstration of the validity of the dynamical analysis of our model.

## 2. Other Potential Surfaces and H-bonded Systems

Continuing the vibrational analysis in the manner described in the preceding sections will finally yield the complete quantitative spectrum for our model of the  $[\text{FHF}]^-$  system. We expect that the global structure of this theoretical spectrum will agree with the experimental one for  $\text{KHF}_{2(g)}$ . If our completely *ab initio* model of the  $[\text{FHF}]^-$  ion closely simulates the actual experimental spectrum, it would then be a legitimate enterprise subsequently to adjust a limited number of parameters in the potential surface in order to improve *quantitative* agreement

with the experimental details (for example, the frequency  $\nu_3$ ). (By following such a procedure we would be introducing the effects of the environment indirectly through the potential surface of the  $[\text{FHF}]^-$  ion.) If by such empirical processes one can achieve greater coincidence of the frequency values *without* altering the overall structure of the spectrum, then we would have a high level of confidence that we do in fact understand the vibrational spectrum of the  $[\text{FHF}]^-$  ion in the solid state environment using this isolated ion model.

Apart from understanding the crystal spectrum, the other main value of this study is its tests of purely theoretical questions regarding the feasibility of such analyses of vibrational dynamics. We are showing that concepts of separability can be retained and used in an accurate, quantitative way, and that such methods offer predictive as well as interpretive power in the understanding of this type of strongly non-harmonic and non-separable system. The test of such a claim, of course, lies in the applications to other experimental systems.

Obvious systems to which our theoretical model could be extended are the other bihalide ions such as  $[\text{ClHCl}]^-$ ,  $[\text{BrHBr}]^-$ , and  $[\text{IHI}]^-$ . For these heavy atom systems calculating *ab initio* potential surfaces at the CID level could be quite expensive. Therefore, the question arises as to whether results of *ab initio* electronic calculations done at a less sophisticated level may be reliably used. It may appear that the recent work by Janssen et al. answers this question in the negative (at least as far as quantitative results are concerned). On the other hand, these ions, unlike  $[\text{FHF}]^-$ , are relatively weak H-bonded ( $\Delta H \sim 10 - 12$  kcal/mol) systems (i.e. are more 'normal' strength H-bonds) and it may very well be the case that the vibrational frequencies do not show the same high sensitivity to the level of electronic calculation that  $[\text{FHF}]^-$  does. Even if they do show high sensitivity, one might still use these less sophisticated *ab initio* surfaces (at the SCF level,

say) in order to understand the major spectral features. (There is some support for such a claim, even for a simple non-bending model of  $[\text{FHF}]^-$  itself, from the work by Almlöf, and Barton and Thorson.)

For this reason, one of the immediate post-thesis projects will be performing vibrational SCF calculations for  $[\text{FHF}]^-$  (using the same vibrational SCF and SCF-CI programs that were used to generate the results in this thesis) with an *ab initio* surface at the Hartree-Fock level (also calculated by M. Klobukowski). Comparison of the results with the two different surfaces should make it clearer what the effect of the quality of the electronic calculation has on the overall vibrational spectrum, and augment the information given by Janssen et al.

Our method may also be applied to mixed bihalide ions,  $[\text{FHX}]^-$ ; X=Br, Cl, I. (These also belong to the category of 'normal' H-bonds.) In these examples, because of the loss of symmetry, the SCF approximation in  $(\xi, \eta)$  coordinates may be less appropriate, and the solution of the SCF equations computationally more complicated.

Finally, this adiabatic-SCF model (with limited CI) may be applied to other H-bonded (multi-mode) systems. This scheme may be preferable in certain cases to the pure SCF-CI method because of the more physical nature, and the more information this model gives, even if at times it may be computationally less simple. The only major limitation would be the ready availability of full-dimensional potential surfaces.

## E. Summary

In this chapter, a strategy for completing the analysis of the vibrational dynamics was outlined.

Results of limited CI computations among the  $\pi_u$  SCF states were presented. The CI correction to the fundamentals is very small. With an 11-member basis set, the ground protonic state converged up to  $0.001 \text{ cm}^{-1}$ , and the fourth excited state converged up to  $5 \text{ cm}^{-1}$ . The SCF separation scheme in  $(\xi, \eta)$  coordinates seems to be working satisfactorily. The SCF approximation as expected breaks down at avoided crossings, where there is extensive mixing between the two crossing SCF states.

A computational procedure was outlined for the solution of the  $\nu_1$ -dynamics. For those avoided crossings where the adiabatic approximation is not valid, coupled multi-channel equations in R-coordinate must be solved. Finally, some extensions of this study on  $[\text{FHF}]^-$  were suggested.

## BIBLIOGRAPHY

1. W. M. Latimer and W. H. Rodebush, *J. Am. Chem. Soc.*, 42, 1419 (1920)
2. G. C. Pimentel and A. L. McClellan, *The Hydrogen Bond* (W. H. Freeman, 1960)
3. S. N. Vinogradov and R. innell, *Hydrogen Bonding* (Van Nostrand Reinhold, 1972)
4. M. D. Joesten and L. J. Schaad, *Hydrogen Bonding* (Marcel Dekker, 1974)
5. P. Schuster, G. Zundel and C. Sandorfy (ed.), *The Hydrogen Bond: Recent Developments in Theory and Experiments* (North Holland, 1976), vols. 1,2,3 (esp. chas 2,3,6,12,13)
6. C. A. Coulson, *Research*, 10, 149 (1957)
7. J. Emsley, *Chem. Soc. Rev.*, 9, 91 (1980)
8. D. Hadzi and H. W. Thompson (ed.), *Hydrogen Bonding* (Pergamon, 1959) (esp. pg.s 85-106)
9. P. A. Kollman and L. C. Allen, *Chem. Rev.*, 72, 283 (1972)
10. F. L. Boschke (ed.), *Topics in Current Chemistry*, vol. 120, (Springer Verlag, 1984)
11. S. A. Harrell and D. H. McDaniel, *J. Am. Chem. Soc.*, 86, 4497 (1964)
12. T. C. Waddington, *Trans. Farad. Soc.*, 54, 25 (1958)
13. H. P. Dixon, H. D. B. Jenkins, and T. C. Waddington, *J. Chem. Phys.*, 57, 4388 (1972)
14. D. G. Tuck, *Prog. Inorg. Chem.*, 9, 161 (1968)
15. M. Heni and E. Illenberger, *J. Chem. Phys.*, 83, 6056 (1985)
16. A. B. Sannigrahi and S. D. Peyerimhoff, *J. Mol. Struct. (THEOCHEM)*, 122, 127 (1985)

17. M. J. Frisch, J. E. Del Bene, J. S. Binkley, H. F. Schaeffer III, J. Chem. Phys., 84, 2279 (1986)
18. S. W. Peterson, and H. A. Levy, J. Chem. Phys., 20, 704 (1952)
19. J. A. Ibers, J. Chem. Phys., 40, 402 (1964)
20. R. Kruh, K. Fuwa, and T. E. McEever, J. Am. Chem. Soc., 78, 4256 (1956)
21. T. R. R. McDonald, Acta. Cryst., 13, 113 (1960)
22. L. K. Frevel and H. W. Rinn, Acta. Cryst., 15, 286 (1962)
23. B. L. McGaw and J. A. Ibers, J. Chem. Phys., 39, 2677 (1963)
24. W. Van Gool, J. Bruinink, and P. H. Bottelberghs, J. Inorg. Nucl. Chem., 34, 3631 (1972)
25. H. L. Carell and J. Donohue, Israel J. Chem., 10, 195 (1972)
26. R. M. Bozorth, J. Am. Chem. Soc., 45, 2128 (1923)
27. J. M. Williams and L. F. Schneemeyer, J. Am. Chem. Soc., 95, 5780 (1973)
28. Y. Marechal, Mol. Interactions, 1, 231 (1980)
29. S. A. Barton and W. R. Thorson, J. Chem. Phys., 71, 4263 (1979)
30. S. Besnainou, Adv. Mol. Relax. Inter. Pro., 16, 81 (1980)
31. Y. Marechal, J. Mol. Struct., 47, 291 (1978)
32. Y. Marechal, Chem. Phys., 52, 245 (1980)
33. Y. Marechal, Chem. Phys., 79, 69 (1983)
34. G. Auvert and Y. Marechal, J. de Physique, 8, 735 (1979)
35. Y. Marechal, Chem. Phys., 79, 85 (1983)
36. L. Soulard and F. Fillaux, Chem. Phys., 100, 355 (1985)
37. C. A. Coulson and G. N. Robertson, Proc. Roy. Soc. Lond., A337, 167 (1974)
38. C. A. Coulson and G. N. Robertson, Proc. Roy. Soc. Lond., A342, 289 (1975)



39. C. A. Coulson and G. N. Robertson, *Phil. Trans. Roy. Soc. Lond.*, A286, 25 (1977)
40. N. D. Sokolov and V. A. Savel'ev, *Chem. Phys.*, 22, 383 (1977)
41. Y. Marechal and A. Witkowski, *J. Chem. Phys.*, 48, 3697 (1968)
42. A. Witkowski and M. Wójcik, *Chem. Phys.*, 1, 9 (1973)
43. S. Bratož and D. Hadzi, *J. Chem. Phys.*, 27, 991 (1957)
44. J. A. Salthouse and T. C. Waddington, *J. Chem. Phys.*, 48, 5274 (1968)
45. J. A. A. Ketelaar, *Rec. Trav. Chim.*, 60, 523 (1941)
46. J. A. A. Ketelaar and W. Vedder, *J. Chem. Phys.*, 19, 654 (1951)
47. P. Dawson, *J. Chem. Soc. Farad. Trans. 2*, 68, 1448 (1972)
48. P. Dawson, M. M. Hargreave, and G. R. Wilkinson, *Spectrochim. Acta A*, 31, 1055 (1975)
49. Z. Iqbal, *J. Chem. Phys.*, 59, 6183 (1973)
50. J. J. Rush, L. W. Schroeder, and A. J. Melveger, *J. Chem. Phys.*, 56, 2793 (1972)
51. R. Newman and R. M. Badger, *J. Chem. Phys.*, 19, 1207 (1951)
52. L. Couture and J. P. Mathieu, *C. R. Acad. Sci.*, 228, 555 (1949)
53. J. P. Mathieu and L. Couture, *C. R. Acad. Sci.*, 230, 1054 (1950)
54. R. D. Cooke, C. Pastorek, R. E. Carlson, and J. C. Decius, *J. Chem. Phys.*, 69, 5 (1978)
55. G. R. Wilkinson, *Nat. Bur. Stand. Spec. Publ.*, 30, 107 (1969)
56. B. S. Ault, *J. Phys. Chem.*, 82, 844 (1978)
57. J. E. Bertie, D. F. Thomas, and W. R. Thorson, *J. Chem. Phys.*, 73, 5399 (1980)
58. O. J. Chunnillall, W. F. Sherman, and G. R. Wilkinson, *J. Mol. Struct.*, 115, 205 (1984)

59. O. J. Chunnillall and W. F. Sherman, *J. Mol. Struct.*, **80**, 121 (1982)
60. E. Spinner, *Aust. J. Chem.*, **33**, 933 (1980)
61. K. M. Harmon, and R. R. Lovelace, *J. Phys. Chem.*, **86**, 900 (1982)
62. T. C. Waddington, J. Howard, K. P. Brierly, and J. Tomkinson, *J. Chem. Phys.* **64**, 193 (1982)
63. K. Kawaguchi and E. Hirota, *J. Chem. Phys.*, **84**, 2953 (1986)
64. G. L. Coté and H. W. Thompson, *Proc. Roy. Soc. Lond.*, **A210**, 206 (1951)
65. E. B. Wilson Jr., J. C. Decius, and P. C. Cross, *Molecular Vibrations* (Dover, 1980)
66. L. A. Woodward, *Introduction to the Theory of Molecular Vibrations and Vibrational Spectroscopy* (Clarendon Press, Oxford, 1972)
67. G. Herzberg, *Molecular Spectra and Molecular Structure* (Van Nostrand Reinhold, 1945, 1950) vols 1,2
68. (a) M. Born, and J. R. Oppenheimer, *Ann. der Phys.*, **84**, 457 (1927)  
(b) M. Born and K. Huang, *Dynamical Theory of Crystal Lattices* (Clarendon Press, Oxford, 1954), pg. 166 ff, 402
69. G. C. Carney, L. L. Sprandel, and C. W. Kern, *Adv. Chem. Phys.*, **37**, 305 (1978)
70. J. M. Bowman, *J. Chem. Phys.*, **68**, 608 (1978)
71. C. L. Janssen, W. D. Allen, H. F. Schaeffer III, and J. M. Bowman, *Chem. Phys. Lett.*, **131**, 352 (1986)
72. J. M. Bowman, K. M. Christoffel, and F. L. Tobin, *J. Phys. Chem.*, **83**, 905 (1979)
73. J. M. Bowman, *Acc. Chem. Res.*, **19**, 202 (1986)
74. F. L. Tobin and J. M. Bowman, *Chem. Phys.*, **47**, 151 (1980)
75. K. M. Christoffel and J. M. Bowman, *Chem. Phys. Lett.*, **85**, 220 (1982)

76. K. M. Christoffel and J. M. Bowman, *J. Chem. Phys.*, 74, 5057 (1981)
77. H. Romanowski and J. M. Bowman, *Chem. Phys. Lett.*, 110, 235 (1984)
78. H. Romanowski and J. M. Bowman, and L. B. Harding, *J. Chem. Phys.*, 82, 4155 (1985)
79. M. Cohen, S. Greita, and R. P. McEachran, *Chem. Phys. Lett.*, 60, 445 (1979)
80. T. C. Thompson and D. G. Truhlar, *J. Chem. Phys.*, 77, 3031 (1982)
81. N. Moiseyev, *Chem. Phys. Lett.*, 98, 233 (1983)
82. T. C. Thompson and D. G. Truhlar, *Chem. Phys. Lett.*, 75, 87 (1980)
83. R. B. Gerber, R. M. Roth, and M. A. Ratner, *Mol. Phys.*, 44, 1335 (1981)
84. R. B. Gerber and M. A. Ratner, *Chem. Phys. Lett.*, 68, 195 (1979)
85. R. M. Roth and M. A. Ratner, *Chem. Phys. Lett.*, 112, 322 (1984)
86. M. A. Ratner and R. B. Gerber, *J. Phys. Chem.*, 90, 20 (1986)
87. D. Farrelly and A. D. Smith, *J. Phys. Chem.*, 90, 1599 (1986)
88. A. Requena and R. Pena, *J. Quant. Spectrosc. Radiat. Transfer*, 29, 471 (1983)
89. F. M. Fernandez and E. A. Castro, *Chem. Phys.*, 58, 65 (1981)
90. H. Sellers, *J. Mol. Struct. (THEOCHEM)*, 92, 361 (1983)
91. F. R. Burden and H. M. Quiney, *Mol. Phys.*, 53, 917 (1984)
92. T. Saitoh, K. Mori, and R. Itoh, *Chem. Phys.*, 60, 161 (1981)
93. L. L. Lohr and J. R. Sloboda, *J. Phys. Chem.*, 85, 1332 (1981)
94. J. Almlöf, *Chem. Phys. Lett.*, 17, 49 (1972)
95. G. J. Jiang and G. R. Anderson, *J. Phys. Chem.*, 77, 1764 (1973)
96. T. R. Singh and J. L. Wood, *J. Chem. Phys.*, 48, 4567 (1968)
97. T. R. Singh and J. L. Wood, *J. Chem. Phys.*, 50, 3572 (1969)
98. J. A. Ibers, *J. Chem. Phys.*, 41, 25 (1964)

99. W. R. Thorson and J. B. Delos, *Phys. Rev.*, A18, 135 (1978)
100. E. R. Lippincott and R. Schröder, *J. Chem. Phys.*, 23, 1099 (1955)
101. E. R. Lippincott and R. Schröder, *J. Am. Chem. Soc.*, 78, 5171 (1956)
102. W. E. Milne, *Phys. Rev.*, 35, 863 (1930)
103. (a) B. I. Stepanov, *Zh. Fiz. Khim.*, 19, 507 (1945)  
(b) B. I. Stepanov, *Nature*, 157, 808 (1946)
104. D. H. McDaniel and R. E. Vallee, *Inorg. Chem.*, 2, 996 (1963)
105. P. Kebarle, A. Zolla, J. Scarborough, and M. Arshardi, *J. Am. Chem. Soc.*, 89, 6393 (1967)
106. R. L. Clair and T. B. McMahon, *Can. J. Chem.*, 57, 473 (1979)
107. T. H. Dunning, *J. Chem. Phys.*, 53, 2823 (1970)
108. Ø. Burrau, *Det. Kgl. Danske Vid. Selskab.*, 7, 1 (1927)
109. L. Pauling and E. B. Wilson, Jr., *Introduction to Quantum Mechanics* (McGraw-Hill, 1935), cha. 4
110. G. S. Ezra, *Chem. Phys. Lett.*, 101, 259 (1983)
111. R. S. Caswell and M. Danos, *J. Math. Phys.*, 11, 349 (1970)
112. T. A. Koopmans, *Physica*, 1, 104 (1934)
113. (a) L. A. Young, *Phys. Rev.*, 38, 1612 (1931)  
(b) L. A. Young, *Phys. Rev.*, 39, 445 (1932)
114. J. A. Wheeler, *Phys. Rev.*, 52, 1123 (1937)
115. R. A. Ballinger and N. H. March, *Proc. Phys. Soc.*, A67, 378 (1954)
116. C. E. Hecht and J. E. Mayer, *Phys. Rev.*, 106, 1156 (1957)
117. J. L. Peacher and J. G. Wills, *J. Chem. Phys.*, 46, 4809 (1967)
118. H. Ezawa, K. Nakamura, and Y. Yamamotu, *Proc. Jap. Acad.*, 46, 168 (1970)
119. (a) W. I. Newman and W. R. Thorson, *Phys. Rev. Lett.*, 29, 1350 (1972)

- (b) W. I. Newman and W. R. Thorson, *Can. J. Phys.*, 50, 2997 (1972)
120. J. G. Wills, *Can. J. Phys.*, 52, 664 (1974)
121. W. R. Thorson, *Can. J. Phys.*, 52, 2504 (1974)
122. J. C. Light and J. M. Yuan, *J. Chem. Phys.*, 58, 660 (1973)
123. J. M. Yuan, S. Y. Lee, and J. C. Light, *J. Chem. Phys.*, 61, 3394 (1974)
124. S. Y. Lee and J. C. Light, *Chem. Phys. Lett.*, 25, 435 (1974)
125. J. Killingbeck, *J. Phys. A*, 10, L99 (1977)
126. A. Alijah, J. T. Broad, and J. Hinze, *J. Phys. B*, 19, 2617 (1986)
127. B. Yoo and C. H. Greene, *Phys. Rev. A*, 34, 1635 (1986)
128. E. A. Solov'ev, *JETP Lett.*, 39, 100 (1984)
129. F. A. Robicheaux, U. Fano, M. Cavagnero, and D. A. Harmin, *Phys. Rev. A*, 35, 3619 (1987)
130. H. J. Korsch and H. Laurent, *J. Phys. B*, 14, 4213 (1981)
131. H. J. Korsch and H. Laurent, *J. Phys. B*, 15, 1 (1982)
132. H. J. Korsch, *Phys. Lett.*, 109A, 313 (1985)
133. R. E. Langer, *Phys. Rev.*, 51, 669 (1937)
134. J. M. Yuan and J. C. Light, 8, 305 (1974)
135. R. Bulirsch and J. Stoer, *Numer. Math.*, 8, 1 (1966)
136. *International Mathematics and Statistical Library Reference Manual*, edition 7, vol.2 (IMSL, Houston, Texas, 1979)
137. J. D. Power, *Phil. Trans. Roy. Soc.*, 274A, 663 (1973)
138. D. R. Noakes, private communication.
139. W. R. Thorson and J. H. Choi, unpublished results.
140. S. Huzinaga, *J. Chem. Phys.*, 42, 1293 (1965)
141. K. Kawaguchi and E. Hirota, *J. Chem. Phys.*, 87, 6838 (1987)
142. R. D. Hunt and L. Andrews, *J. Chem. Phys.*, 87, 6819 (1987)

## APPENDIX

### Series Solutions of the Differential Equation in $\xi$ - motion

Making the substitution  $x = \xi - 1$  in equation (3.22),

$$\left\{ \frac{d^2}{dx^2} + \frac{1-m^2}{x^2(x+2)^2} + \frac{1}{ax(x+2)} \int_{-1}^{+1} d\eta (\xi^2 - \eta^2) \frac{[V-E]g^2(\eta; R)}{(1-\eta^2)} + \frac{\epsilon_g}{x(x+2)} \right\} f(x; R) = 0 \quad (\text{A.1})$$

Expanding the SCF interaction potential term in a power series of  $x$ ,

$$\frac{1}{a} \int_{-1}^{+1} d\eta \frac{(\xi^2 - \eta^2)[V-E]g^2(\eta; R)}{(1-\eta^2)} = \sum_{k=0}^N V_k x^k \quad (\text{A.2})$$

where  $\{V_k\}$  are constants dependent on the fitting parameters, we have

$$(x^2 + 4x + 4)f'' + (1-m^2)\frac{f}{x^2} + \frac{(x+2)}{x}f \sum_{k=0}^N V_k x^k + \epsilon_g(x+2)\frac{f}{x} = 0 \quad (\text{A.3})$$

We seek a series solution of the form,

$$f(x; R) = x^c \sum_{r=0}^{\infty} a_r x^r, \quad \text{with } a_0 \neq 0. \quad (\text{A.4})$$

Using (A.4) in (A.3) we have,

$$\begin{aligned} & \sum_{r=0}^{\infty} [(c+r)(c+r-1) + \epsilon_g] a_r x^{c+r} + \sum_{r=0}^{\infty} [4(c+r)(c+r-1) + 2\epsilon_g] a_r x^{c+r-1} \\ & + \sum_{r=0}^{\infty} [4(c+r)(c+r-1) + (1-m^2)] a_r x^{c+r-2} \\ & + \sum_{r=0}^{\infty} a_r x^{c+r} \sum_{k=0}^N V_k x^k + 2 \sum_{r=0}^{\infty} a_r x^{c+r-1} \sum_{k=0}^N V_k x^k = 0 \end{aligned} \quad (\text{A.5})$$

Equating the coefficient of the term  $x^{c-2}$  in (A.5) to zero, we obtain the indicial equation;

$$4c^2 - 4c + 1 - m^2 = 0, \quad (\text{A.6})$$

with the solutions,

$$c_1 = \frac{1}{2} + \frac{m}{2}. \quad (\text{A.7a})$$

$$c_2 = \frac{1}{2} - \frac{m}{2}. \quad (\text{A.7b})$$

Therefore, one solution of the differential equation (A.3) will be given by,

$$f_1(x; R) = x^{1/2+m/2} \sum_{r=0}^{\infty} a_r x^r \quad (\text{A.8})$$

To find the recursion relations among the  $\{a_i\}$ , we equate the coefficient of  $x^{c+r-2}$  term in (A.5) to zero:

$$\begin{aligned} & \frac{1}{4}[(2r+m-3)(2r+m-5) + 4\epsilon_g]a_{r-2} + [(2r+m-1)(2r+m-3) + 2\epsilon_g]a_{r-1} \\ & + [(2r+m+1)(2r+m-1) + (1-m^2)]a_r + \sum_{k=0}^N V_k(2a_{r-k-1} + a_{r-k-2}) = 0 \quad (\text{A.9}) \end{aligned}$$

And (A.9) defines all  $\{a_i; i = 1, \infty\}$  provided that we specify  $a_j = 0$  for all  $j < 0$ .  $a_0 (\neq 0)$  will remain undefined for the time being.

The second series solution (linearly independent of  $f_1(x; R)$ ) of the differential equation will be given by,

$$f_2(x; R) = K f_1(x; R) \ln x + x^{1/2-m/2} \sum_{r=0}^{\infty} b_r x^r \quad (\text{A.10})$$

where  $K$  is some constant (to be determined later), and  $b_0 \neq 0$ . Using (A.10) and (A.8) in (A.3) we obtain;

$$\begin{aligned}
& \sum_{r=0}^{\infty} \frac{1}{4} [(2r-m)^2 - 1 + 4\epsilon_g] b_r x^r + \sum_r [(2r-m)^2 - 1 + 2\epsilon_g] b_r x^{r-1} \\
& + \sum_r 4r(r-m) b_r x^{r-2} + \sum_r b_r x^r \sum_{k=0}^N V_k x^k + \sum_r 2b_r x^{r-1} \sum_{k=0}^N V_k x^k \\
& + \sum_r K(2r+m) a_r x^{r+m} + \sum_r 4K(2r+m) a_r x^{r+m-1} \\
& + \sum_r 4K(2r+m) a_r x^{r+m-2} = 0 \tag{A.11}
\end{aligned}$$

Case (1) :  $m = 0$

Consider the Wronskian of  $f_1$  and  $f_2$ ,

$$W(f_1, f_2) = f_1' f_2 - f_1 f_2' \tag{A.12}$$

Since  $f_1$  and  $f_2$  are linearly independent,  $W$  is a non-zero constant. Evaluating  $W$  at  $x = 0$  for the  $m = 0$  case,

$$W = -K a_0^2 \tag{A.13}$$

Impose the condition that

$$W(f_1, f_2) = 1 \tag{A.14}$$

Then,  $-K a_0^2 = 1$ .

In order to satisfy the above relationship, we set

$$K = -1, \tag{A.15}$$

$$\text{and } a_0 = 1 \tag{A.16}$$

$$\text{We also set the constant } b_0 = 1 \tag{A.17}$$

In order to obtain the recursion relations among the  $\{b_i\}$ , equate the coefficient of  $x^{r-2}$  in (A.11) to zero:



$$\begin{aligned}
& \frac{1}{4}[(2r-4)^2 - 1 + 4\epsilon_g]b_{r-2} + [(2r-2)^2 - 1 + 2\epsilon_g]b_{r-1} \\
& + 4r^2b_r + \sum_{k=0}^N V_k(2b_{r-k-1} + b_{r-k-2}) + K(2r-4)a_{r-2} + 4K(2r-2)a_{r-1} \\
& + 4K(2r)a_r = 0 \quad (A.18)
\end{aligned}$$

(A.12) defines all  $\{b_j; j = 1, \infty\}$  with  $K = -1$ ,  $b_0 = 1$ ,  $a_0 = 1$ , and  $\{a_j; j = 1, \infty\}$  given by (A.9).

**Case (2) :  $m > 0$**

Again computing the Wronskian of  $f_1$  and  $f_2$  at  $x = 0$ ,

$$W = ma_0b_0 \quad (A.19)$$

We impose once again the condition

$$W(f_1, f_2) = 1 \quad (A.20)$$

Therefore,  $ma_0b_0 = 1.$   $\int$

To satisfy above relation, we select

$$a_0 = 1 \quad (A.21)$$

$$\text{and} \quad b_0 = 1/m. \quad (A.22)$$

And equating the coefficient of  $x^{r-2}$  in (A.11) to zero,

$$\begin{aligned}
& \frac{1}{4}[(2r - m - 4)^2 - 1 + 4\epsilon_g]b_{r-2} + [(2r - m - 2)^2 - 1 + 2\epsilon_g]b_{r-1} + 4r(r - m)b_r \\
& + \sum_{k=0}^N V_k(2b_{r-k-1} + b_{r-k-2}) + K(2r - m - 4)a_{r-m-2} + 4K(2r - m - 2)a_{r-m-1} \\
& \qquad \qquad \qquad + 4K(2r - m)a_{r-m} = 0
\end{aligned} \tag{A.23}$$

(A.23) defines all  $\{b_i; i = 1, \infty\}$  (except for  $b_m$ ), with the  $\{a_i\}$  being given by (A.9), and  $a_j, b_j = 0$  for  $j < 0$ .

$$\text{We choose} \qquad \qquad \qquad b_m = 0 \qquad (m > 0) \tag{A.24}$$

And finally, to fix the value of  $K$ , put  $r = m$  in (A.23);

$$\begin{aligned}
& \frac{1}{4}[(m - 4)^2 - 1 + 4\epsilon_g]b_{m-2} + [(m - 2)^2 - 1 + 2\epsilon_g]b_{m-1} \\
& \qquad \qquad \qquad + \sum_{k=0}^N (2b_{m-k-1} + b_{m-k-2})V_k = -(4m)K
\end{aligned} \tag{A.25}$$

Thus, for a given set of potential constants  $\{V_k\}$ , the two linearly independent series solutions of the differential equation (A.1),  $f_1(x; R)$  and  $f_2(x; R)$  are completely defined. They have a theoretical radius of convergence of 2, within an annulus centered at the origin,  $x = 0$ .

It is easily seen that  $\lim_{x \rightarrow 0} f_1(x; R) \cdot (\xi^2 - 1)^{-1/2} = \text{finite constant}$  while  $\lim_{x \rightarrow 0} f_2(x; R) \cdot (\xi^2 - 1)^{-1/2} = \infty$ ; so that the regular (at  $x = 0$ ) solution is  $f_1(x; R)$  while  $f_2(x; R)$  corresponds to the irregular solution. With these forms of the series solutions the limiting properties (at  $x = 0$ ) of functions such as Milne's function, quantal momentum, phase function, etc may be determined using the definitions given in Chapter 4.